Numerical estimation of wave loads on crest walls on top of rubble mound breakwaters using OpenFOAM

Marisol Irías Mata

5014166

Thesis committee:

Chairman:

Dr. ir. Antonini, A.
Delft University of Technology
Hydraulic Engineering
Coastal Engineering

Supervisors:

Dr. ir. Van Gent, M.
Delft University of Technology
Hydraulic Engineering
Coastal Engineering

Dr. ir. Zijlema, M.
Delft University of Technology
Hydraulic Engineering
Environmental Fluid Mechanics

Ir. van der Lem, C.
Royal HaskoningDHV
Water & Maritime
Senior Port Engineer

Ir. drs. Boersen, S.
Royal HaskoningDHV
Water & Maritime
Hydraulic & Coastal Engineer

Dr. ir. Jansen, B.
DHI Group
Ports and Offshore Technology
Senior Hydraulic Engineer

Preface

This research project marks the final step to obtain my master in Civil Engineering at the Delft University of Technology, in the field of Hydraulic Engineering. It was an exciting and challenging experience to develop a CFD model to gain better insights into the wave-structure interaction.

This thesis was carried out in collaboration with the Water & Maritime department at Royal HaskoningDHV and the department of Ports and Offshore Technology at DHI Group. I would like to thank Royal HaskoningDHV for giving me the opportunity, resources and internal knowledge to develop this research topic in their Rotterdam office. Also, I would like to thank DHI Group for providing the data from the small scale physical modelling campaign of the Holyhead breakwater and for willingly taking the time to clarify any questions regarding the experimental data. I take this opportunity to express my gratitude to all the persons who had an impact on this final work.

My special thanks to Alessandro Antonini for his constant and valuable guidance. His support since the moment I was searching for my graduation project is highly appreciated. The knowledge on OpenFOAM model and numerical modelling provided during our meetings help me deeply to develop the numerical model of this study. I express deep gratitude to Marcel van Gent, whose inputs along my project, in the topics of turbulence model and modelling of flow porous media, increased highly the quality of my research. I would also like to acknowledge the support given by Marcel Zijlema, who was willing to take the time in every progress meeting to discuss in detail the findings from my research. His collaboration certainly has helped to gain more insight into the results of the numerical model.

I would like to express my deep gratitude to Cock van der Lem and Stef Boersen, my supervisors from Royal HaskoningDHV. Without their continuous support and guidance throughout all my project, the thesis process would not have been so successful. Their knowledge on numerical wave-structure interaction helped on solving the many challenges faced during this research project.

I am profoundly grateful for the support given by Bjarne Jansen. His knowledge in the numerical modelling of porous media was essential and highly appreciated.

Finally, my deep and sincere gratitude to my family and friends for their continuous and unparalleled love, help and support. Their encouragement made this master experience, an enjoyable journey.

Marisol Irías Mata
September 22, 2021
Delft, NL

Abstract

The design of hydraulic structures like breakwaters and crest walls is often based on empirical formulations, physical models test, numerical models and a fair amount of expert judgement. Each technique has its own pros and cons. The main limitation of the empirical formulas is that often they have to be applied outside their range of validity. Physical modelling also has its own shortcomings. When breaking waves hit the structure, the location of the maximum pressures is still not well known due to the high spatial variability. By using an array with low spatial resolution, the forces estimated in the physical flume will usually underestimate to some extent the actual forces experienced by the wall (Ramachandran et al., 2013). In the last decades, numerical modelling has become an attractive alternative in simulating wave-structure interactions. Nevertheless, estimating loads on crest walls in the numerical flume is still at its early stages. On that account, the present work validates the prediction of wave induced forces on the front face of crest walls on top of rubble mound breakwaters in CoastalFOAM. A scale model of the Holyhead breakwater, located in Wales, is used.

The key validation topics are the reproduction of wave-structure interaction when heavily breaking waves reached the wall, the evaluation of the ventilated boundary condition implemented by Jacobsen et al. (2018), the porous flow inside the armour layer formed by Tetrapods units and whether the simplication of not using a turbulence model, as done by Jensen et al. (2014) and Jacobsen et al. (2018), is also valid under heavily breaking waves.

Four validation cases were used to test the capabilities of the numerical flume. The results confirm that it is possible to accurately reproduce the wave conditions and the wave induced forces from a physical modelling campaign. Overall, the CoastalFOAM model is able to capture the shape and the order of magnitude of the force events. A calibrated model predicts the highest wave induced forces (forces with an exceedance probability of 0.4% and 0.1%) with errors lower than 20%. Moreover, the results indicate that for practical applications it is not essential to include a turbulence model in the numerical flume to obtain reliable forces on the front face of crest walls for different wave conditions. Another outcome of this study is that the implementation of the ventilated boundary condition is required in the interface between water surface and structural elements to mimic accordingly the air-water mixture when the structure is subjected to a heavy wave attack. Nonetheless, there is still room for improvement in this area, where a better understanding of this boundary condition and of the air entrapment during wave-structure interaction needs further research.

Despite the large computational time required by the numerical flume when large wave trains must be simulated, a CFD model during design stages of breakwaters and crest walls provides higher spatial and temporal resolution of the wave induced pressures exerted on the wall than a physical test. Therefore, a better picture of the forces and pressure distribution in the front face can be obtained.

Table of content

List of Figures

List of Tables

List of symbols

α	Linear calibration coefficient of van Gent (1995) parametrisation
α_R	Relaxation function
β	Nonlinear calibration coefficient of van Gent (1995) parametrisation
β_d	Slope angle in degrees
γ	Scalar field used to track the free surface
γ_J	Peak enhancement factor of the standard JONSWAP wave spectrum
γ_p	Empirical coefficient used to estimate the added mass coefficient (takes value of 0.34)
Δt	Time step
Δx	Space step
η	Position of the free surface relative to the still water level
κ_{gamma}	Surface curvature
μ	Dynamic molecular viscosity
μ_a	Air viscosity
μ_s	Friction coefficient
μ_t	Kinematic eddy viscosity
μ_w	Water viscosity
ν_t	Eddy viscosity
ξ_f	Loss coefficient based on $u^{\perp}$
ξ_p	Loss coefficient
ξ_0	Dimensionless Irribaren number or surf similarity parameter
ρ	Fluid density
ρ_a	Air density
ρ_w	Water density
σ_T	Surface tension coefficient
τ	Specific Reynolds stress tensor
Φ	Velocity potential function
Φ_R	Velocity or indicator function in relaxation function
χ_R	Relaxation function parameter
∇	Operator: $\frac{\partial}{\partial x} + \frac{\partial}{\partial y} + \frac{\partial}{\partial z}$
a	Linear resistance coefficient of the Darcy-Forchheimer equation
b	Nonlinear resistance coefficient of the Darcy-Forchheimer equation
C_m	Added mass coefficient
C_0	Courant number
d_{n50}	Median grain diameter of the porous structure
e_p	Degree of openness of the structure
F_G	Buoyancy-reduced weight of the crest wall
$F_{H,max}$	Wave induced horizontal force
F_p	Resistance force due to the presence of the porous media
$F_{V,max}$	Wave induced vertical force
g	Gravitational acceleration constant
h	Water depth at the toe of the structure
h_b	Water depth at breaking
H_i	Incident wave height
H_{max}	Maximum wave height during the simulation time
H_{m0}	Significant wave height
H_r	Reflected wave height
$H_{s,b}$	Incipient breaking significant wave height
$H_{1\%}$	Wave height exceeded by 1% of the waves
$H_{0.1\%}$	Wave height exceeded by 0.1% of the waves
$\boldsymbol{I}$	Kronecker delta
k	Turbulent kinetic energy per unit mass
K_r	Reflection coefficient
KC	Keulegan-Carpenter number
L_0	Deepwater wavelength

L_{0p}	Deep water wavelength estimated from the peak period
M_{cw}	Mass of the crest wall
M_G	Stabilising moment due to mass of the crest wall
M_H	Wave generated moment due to the horizontal forces
M_U	Wave generated moment due to uplift pressures
n_p	Porosity of the permeable structure
N_{Ursell}	Ursell number
N_{waves}	Number of waves
P	Exceedance probability
p^*	Excess pressure
p_b^*	Pressure at the boundary between water surface and structural elements
p_{ref}^*	Pressure in the imaginary reservoir on the backside of the structural element
r	Rank of the sample, once ordered from largest to smallest
s	Bottom slope
$\boldsymbol{S}$	Strain rate tensor
SWL	Still Water level
t	Time
T	Period of the oscillation used for the KC estimation
$T_{m-1,0}$	Spectral wave period
T_p	Peak period
$\boldsymbol{u}$	Mean velocity in Cartesian coordinates
u	Mean velocity in the x direction
$\bar{u}$	Mean velocity
u'	Fluctuating velocity due to turbulent motion
$u^{\perp}$	Filter velocity normal to the structural element
$\boldsymbol{u}_f$	Filter velocity vector in Cartesian coordinates
u_m	Maximum oscillating velocity used for the KC estimation
u_{max}	Maximum particle velocity during the simulation time
u_p	Velocity of the wave paddle
$u_p^{\perp}$	Pore velocity of the fluid in the gap(s) through the structural element
u_r	Compression term that limits the smearing of the interface in the VOF approach
v	Mean velocity in the y direction
V_{cw}	Volume of the crest wall
w	Mean velocity in the z direction
WG	Wave gauge
WL	Water level
$\boldsymbol{x}$	Cartesian coordinate vector
x	Cartesian coordinate in the x direction
y	Cartesian coordinate in the y direction
z	Cartesian coordinate in the z direction
EVA	Extreme Value Analysis
FFT	Fast Fourier Transform
GPD	Generalized Pareto Distribution
IFFT	Inverse Fast Fourier Transform
OCW3D	OceanWave3D
OpenFOAM	Open Field Operation and Manipulation
POT	Peak Over Threshold
RANS	Reynolds Averaged Navier-Stokes Equation
RMSE	Root Mean Square Error
VARANS	Volume Averaged/Reynolds Averaged Navies-Stokes equations
VOF	Volume of Fluid

Chapter 1

Introduction

1.1 Relevance

Coastal areas have large economic benefits such as ocean navigation, fisheries, tourism and recreation. Therefore, the majority of the human settlements are located in these zones. Approximately 40% of the world's population (around 2.4 billion people) lives within a 100 km from the coast and nearly 10% (more than 600 million people) lives in coastal areas that are less than 10 m above mean sea level (United Nations, 2017). As time goes by, the investments in the coastal zones increases as well as the threads against these areas: global warming leads to stronger storms and sea level rise.

To protect these coastal areas, soft and hard measures such as beach nourishments, revetments and breakwaters, just to name a few, have been applied worldwide. Breakwaters are coastal structures designed to protect ports and shores against the incoming wave attack. Often, these structures are used to protect port facilities, allowing vessels to enter the ports safely. Further they reduce the wave motion inside the harbours, avoiding moored ships to move. Sometimes, they are used to reduce beach erosion and to protect valuable habitats that are threatened by wave attack. Additional functionalities are preventing or reducing siltation of navigation channels, guiding the currents and providing quay facilities (van den Bos & Verhagen, 2018).

On the crest of the rubble mound breakwaters, crest walls, also known as crown walls, can be placed. Their main function is to reduce the overtopping volumes at the lee side of the structure. Other purposes are providing access for maintenance, port activities or tourism (CUR et al., 2007). From an economical point of view, when placing a crest wall on top of a rubble mound breakwater, the size of the rubble mound can be reduced, resulting in less quarried material. Hence, the implementation of crown walls has become a very attractive design solution. It can even be decided to build a very high wall; nonetheless, the higher the protruding section of the wall, the greater are the forces that the structure will experience during its lifetime and the more robust the concrete structure must be.

Pedersen (1996) stated that a failure of the crown wall can lead to a failure of the whole breakwater. To emphasize this fact, the failure of two rubble mound breakwaters are mentioned in Pedersen (1996). The first one is the total breakdown of the Antalya harbour breakwater in Antalya, Turkey in 1971. After the crown wall was destroyed, the unprotected crest was rapidly destroyed by the direct wave action. The second one is the Tripoli Harbour North West breakwater in Tripoli, Libya in 1981. After severe storms, several sections of the crest wall failed, leading to excessive erosion of the reclamation area behind it. Since these failures, many efforts have been made on understanding the loading against crown walls and in deriving reliable design formulas for these concrete structures (Irribaren & Nogales, 1964, Bradbury et al., 1988, Pedersen, 1996, Martin et al., 1999, Nørgaard et al., 2013).

With the existing knowledge, available tools and site information, coastal engineers must come up with reliable cost effective coastal structures. Specifically, for the correct design of crest walls on top of rubble mound breakwaters, an accurate estimation of the wave loads and of the forces faced by the crest walls is of major importance.

1.2 Problem description

Recent studies (van Heemst, 2014, Bekker, 2017, Jacobsen et al., 2018, Sigalas, 2019) found that existing empirical formulas overestimate the forces experienced by the crown walls when the freeboard is increased, i.e. empirical methods result in an overdesign of crown walls. This is reflected in unnecessary heavy structures and higher construction costs. Another problem of using empirical formulas is that often they must be applied outside their range of validity because the coastal structures include new breakwater layouts, new materials or stronger boundary conditions. Both limitations often require that the designed breakwater is to be included in a physical flume. However, physical model testing of different configurations of such breakwater involves more resources and may become costly and time consuming.

With the increase capabilities of the computers, numerical modelling has become an attractive alternative in simulating wave-structure interactions. These models are known as Computational Fluid Dynamics (CFD) models. Depending on the governing equations, different types of CFD models have been developed and commonly can be separated in two branches: the nonlinear shallow water models (NLSW) and the Navier-Stokes equations models (NS). The NLSW models have the abilities of modelling large wave trains quite rapidly. Suzuki et al. (2017) applied SWASH (Zijlema et al., 2011) to simulate wave overtopping on impermeable coastal structures. The results were promising but limitations can be encountered when complex structural layouts need to be modelled. The NS models describe the flow in three dimensions but solving for pressure and for the complete velocity field in time and space becomes computationally expensive. The Reynolds Averaged Navier-Stokes (RANS) models with a surface tracking technique have being widely used in the last decades. The existing tracking surface techniques are volume of fluid (VOF) and Smooth particle hydrodynamics (SPH). In this research, the RANS/VOF model implemented in OpenFOAM is applied.

OpenFOAM combined with the `waves2foam` toolbox (explained in detailed in Chapter 4) is being used extensively to simulate wave-structure interactions. Nonetheless, numerical models are only valuable if they can represent adequately the physical processes. Therefore, many validation cases and aspects must be undertaken to achieve a level where the CFD models can be trusted to simulate wave-structure interactions at design stages. Wave overtopping has been validated in OpenFOAM for different situations (impermeable structures, porous breakwater, crest walls on top of rubble mound breakwaters, low-crested structures) by Jensen et al. (2014), Karagiannis et al. (2015), Patil (2019), Boersen et al. (2019), Moretto (2020), Jonker (2020) and Chen et al. (2021). More specific, Moretto (2020) evaluated the wave overtopping of rubble mound breakwaters with promising results, using as base case the OpenFOAM model set up by Jacobsen et al. (2018). A calibration procedure was undertaken for medium overtopping conditions with protruding and non-protruding walls by analysing the incoming and reflected wave conditions. Van Melis (2019) used the OpenFOAM solver to evaluate the wave overtopping over a breakwater under construction to define a safe working level based on tolerable flow depths and velocities. Recently, Chen et al. (2021) predicted wave overtopping at dikes with complex geometries, including configurations with berms and roughness elements. All results show the capabilities of OpenFOAM on reproducing the incident wave field and on estimating the overtopping volumes. Patil (2019) concluded from his research that the process of wave breaking has high influence on the run-up and overtopping values.

The wave interaction with porous structures and open filters was further analysed in the studies conducted by Jensen et al. (2014), Jacobsen et al. (2015), Jacobsen et al. (2017) and van Gent et al. (2018), respectively. Jensen et al. (2014) implemented the modelling of flow through porous media by volume averaging the RANS equations and by applying porosity models that rely on empirical coefficients. The model was validated under regular and irregular wave attack. In a later work, Jacobsen et al. (2015) computed the wave damping through a permeable breakwater, finding good agreement between the numerical and experimental data. Both studies focused on rock composed structures. So far, very little attention has been paid to the wave-structure interaction for structures with layers composed of artificial blocks. To this author's knowledge, only the works carried out by Hsu et al. (2002), Neves et al. (2011) and Lee et al. (2019) analysed the porous media drag coefficients for Tetrapods numerically. Solely Lee et al. (2019) performed their simulations in OpenFOAM, obtaining good predictions of wave pressures on the caisson exerted by regular waves once the empirical porous media coefficients were calibrated.

Wave breaking, on the other hand, was studied more in detail in the numerical flume by Brown et al. (2016), Devolder (2018) and Larsen and Fuhrman (2018). Brown et al. (2016) concluded that for spilling and plunging breakers, the nonlinear $k-\epsilon$ model (Lin & Liu, 1998a, Lin & Liu, 1998b) provided good results in terms of accuracy and numerical efficiency. They also found that including no turbulence model lead to good results for spilling breakers since the turbulence models over-predict the Turbulent Kinetic Energy (TKE). Devolder

(2018) and Larsen and Fuhrman (2018) propose modifications to the $k-\omega\,SST$ and $k\omega$ (Wilcox, 2006) models respectively, that avoid the overestimation of the turbulence levels. Their results showed the capability of the modified turbulence closure model in replicating pre- and post-breaking surface elevations.

Despite all the validation cases using CFD models involving wave-structure interactions, estimating loads on crest walls is still at its early stages. Jacobsen et al. (2018) validated a model where an implementation into the `waves2foam` toolbox was undertaken to obtain better results: the ventilated boundary condition (more details in Chapter 4, Section 4.2). For the validation cases, surging waves reaching a conventional rubble mound breakwater (a breakwater with an armour layer, a filter layer, a core and a protruding crest wall) were used. During the tests, as the main dissipation of energy occurred inside the porous structure, no turbulence closure model was included in the numerical flume. At the end, they conducted a sensitivity analysis of the ventilated boundary condition based on the wave induced forces. From this analysis, they recommended settings for this newly developed condition. Afterwards, Sigalas (2019) applied this boundary condition on the assessment of pressures on crown walls caused by swell waves breaking on the front wall on top of rubble mound breakwaters. He also performed a sensitivity analysis of the ventilated boundary condition with no realistic results. Thereby, the same settings recommended by Jacobsen et al. (2018) were included in his final simulations. Moretto (2020) and Jonker (2020) also included this boundary condition. Nonetheless, they did not study its effect on the forces but in their overtopping volume estimations subjected to irregular wave attack. In both cases, their conclusions imply that it has an influence in the average overtopping estimations. The studies including the ventilated boundary condition have in common the modelling of waves where wave breaking played little or no role. Moreover, when the prediction of forces is the aim of the research, only conventional rubble mound breakwaters have been included in the numerical flume and solely Jacobsen et al. (2018) have studied properly the influence of the ventilated boundary condition in the wave induced forces.

Therefore, the estimation of crest wall loads placed on top of non conventional breakwaters (specifically breakwaters with a wide foreshore and a layer conformed by artificial concrete units placed in front of the crest wall) under heavily breaking waves is still not researched. Even more, whether it is beneficial to include a turbulence model or if assuming no turbulence under heavily breaking waves already provides good force estimations is still unknown. The development of the present project seeks to approach these not researched factors and to provide a new insight into this important topic.

1.3 Objective and research questions

The aim of this study is to assess the capability of the OpenFOAM model to accurately estimate the forces on the front face of crest walls on top of impermeable and partly-permeable breakwaters subjected to non-breaking and heavily breaking waves. The assessment uses a real life case study, the Holyhead breakwater located in Wales, and evaluates as permeable media a Tetrapods layer placed in front of the crest wall.

Hence, the main objective is formulated as:

> **To investigate and improve the capacity of OpenFOAM to model accurately the wave loads on crest walls on rubble mound breakwaters under heavily breaking waves.**

Based on the outlined problem and the aim of the project, this study focuses on answering the following research question and sub-questions:

> **How accurate is OpenFOAM to predict the wave loads against the front face of crest walls on top of impermeable and partly-permeable breakwaters under heavily breaking waves?**.
>
> 1. How accurate is OpenFOAM in predicting forces on the front face of crest walls subjected to non-breaking and heavily breaking waves in case of an impermeable structure/foreshore?
>
> 2. How accurate is OpenFOAM in predicting forces on the front face of crest walls subjected to non-breaking and heavily breaking waves in case of an permeable structure/foreshore including Tetrapods?
>
> 3. What is the effect of applying the ventilated boundary condition and varying the degree of openness of the ventilated boundary condition it in the estimation of forces in the front face of crest walls on top of impermeable breakwaters subjected to non-breaking and heavily breaking waves?
>
> 4. How essential is the usage of a turbulence model in OpenFOAM to get reliable forces on the front face

of crest walls on top of impermeable and partly-permeable breakwaters subjected to non-breaking and heavily breaking waves?

1.4 Methodology

Figure 1.1 shows the methodology followed along this research project. First, an extensive literature review was conducted to understand the design process of crest walls on top of rubble mound breakwaters, the wave loads on crest walls and the numerical models OpenFOAM and Ocean Wave3D. Next, the case study is presented, followed by a description of the first physical modelling campaign of the Holyhead breakwater. The existing experimental data allowed to elaborate the aim of the research project and the research question and sub-questions further. Then, the literature review deepened in numerical implementations to accurately predict the forces on the wall and in the estimation of the empirical porous media coefficients for Tetrapods units. Following the methodology, the models were set-up in the numerical flume. The decision was made of using only one mesh resolution for all the validation cases to avoid the bias caused by different grid sizes in the results analysis. It also eased the model setup process. Finally, OpenFOAM was validated testing four cases, where different cross-sections and hydraulic conditions were modelled. Based on the results from the validation cases and the sensitivity analysis conclusions and recommendations were formulated.

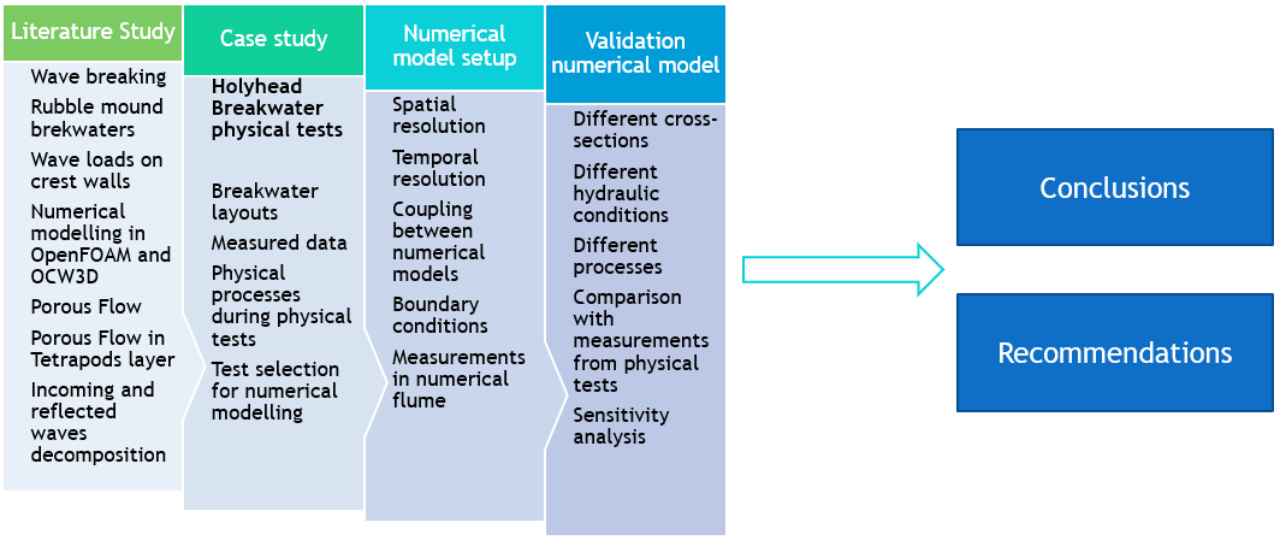

Figure 1.1: Research Methodology

1.5 Thesis outline

The structure of this report is as follows:

- Chapter 1 begins with the problem description and its relevance to the engineering community, including the current state of the art. Subsequently, the goal of the study, the research question and sub-questions and the methodology are outlined.
- Chapter 2 starts with a characterization of the rubble mound breakwaters and its advantages. Then, the chapter focuses on the crest walls and the determination of forces acting on the vertical wall elements. It ends with an outlined of the current design process for the crest walls on top of rubble mound breakwaters.
- Chapter 3 provides an overview of the case study: Holyhead breakwater in Wales. It includes a summary of the small scale 2D physical tests: breakwater layouts, hydraulic conditions and available data. The chapter concludes with a selection of test cases used to validate OpenFOAM.

- Chapter 4 briefly describes the numerical framework and the mathematical equations. Aspects related to wave-structure interaction in the numerical flume are addressed as well as coupling between different numerical models.
- Chapter 5 presents the numerical model set-up for the selected cases. Special attention is paid to the definition of the boundary conditions and to the force estimation methods available in OpenFOAM.
- Chapter 6 shows the capabilities of OpenFOAM in predicting the water surface elevation and the forces on crest walls by presenting and the comparing the results of the numerical model for the different validation cases against the experimental data. Sensitivity analysis for the degree of openness of the ventilated boundary condition and for the empirical porous media coefficients for Tetrapods units are included.
- Chapter 7 discusses in depth the results included in Chapter 6 for the four validation cases, by mentioning the advantages and shortcomings of numerical modelling.
- Finally, in Chapter 8, conclusions are drawn based on the validation results. This chapter ends with recommendations for future research.

Chapter 2

Concept of breakwater design

2.1 Introduction

This chapter begins with a characterization of rubble mound breakwaters. Here, the advantages of different types of rubble mound breakwaters are outlined. Then, the focus changes towards the crest walls and how a failure of the wall can lead to a failure of the whole breakwater. The pressure distribution along the front face of the crest wall in relation to the behaviour of the waves reaching the wall is presented. Finally, details of the available tools for the design process of breakwaters, with special emphasis on the crest walls placed on top of rubble mound breakwaters are given.

2.2 Breakwaters

2.2.1 Rubble mound breakwaters

Rubble mound breakwaters are structures consisting mainly of quarried rock, protected by a cover layer of heavy armour stones or concrete armour units. The core is usually built from quarry run. Between the armour layer and the core, one or more filter or underlayers must be placed to prevent the washing away of the finer material. Figure 2.1 shows a typical cross-section of a rubble mound breakwater. This type of breakwaters have several advantages in projects because the outer slope force storm waves to break, dissipating their energy and thus, causing partial reflection. Moreover, the materials needed are usually available in local quarries and even with limited equipment and expertise, the structures built performed successfully (CUR et al., 2007).

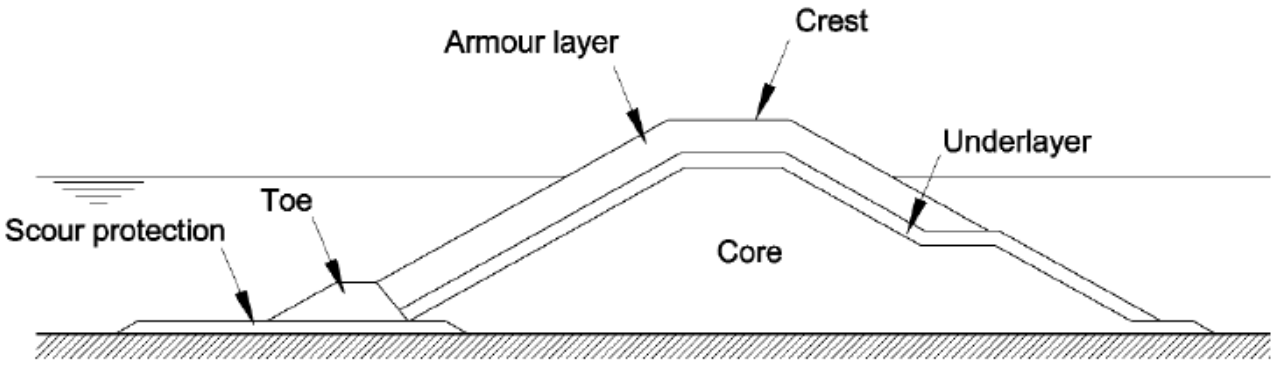

Figure 2.1: Typical cross-section of a rubble mound breakwater
Copied from Figure 6.2 in CUR et al., 2007

There are different types of rubble mound breakwaters depending on their purpose (see Figure 2.2). The conventional rubble mound is typically used to provide shelter to other structures as jetties or berths. The conventional rubble mound with crown wall is mainly used for port protections. In the berm breakwater the outer armour layer is not sufficient to guarantee stability under all conditions; hence, some extra quantity of material is provided so that the slope can reshape between given limits. Low crested breakwaters are submerged structures that only limit wave heights effectively for a narrow variation in water levels. These structures may be used as beach control structures and are often applied in areas where wave conditions need to be modified, where overtopping is acceptable or where horizontal visibility is a requirement. Finally, the vertically and horizontally

composite breakwater are a combination of a rubble mound with a caisson and are generally constructed for port protection (CUR et al., 2007). The Holyhead breakwater lies in the last category.

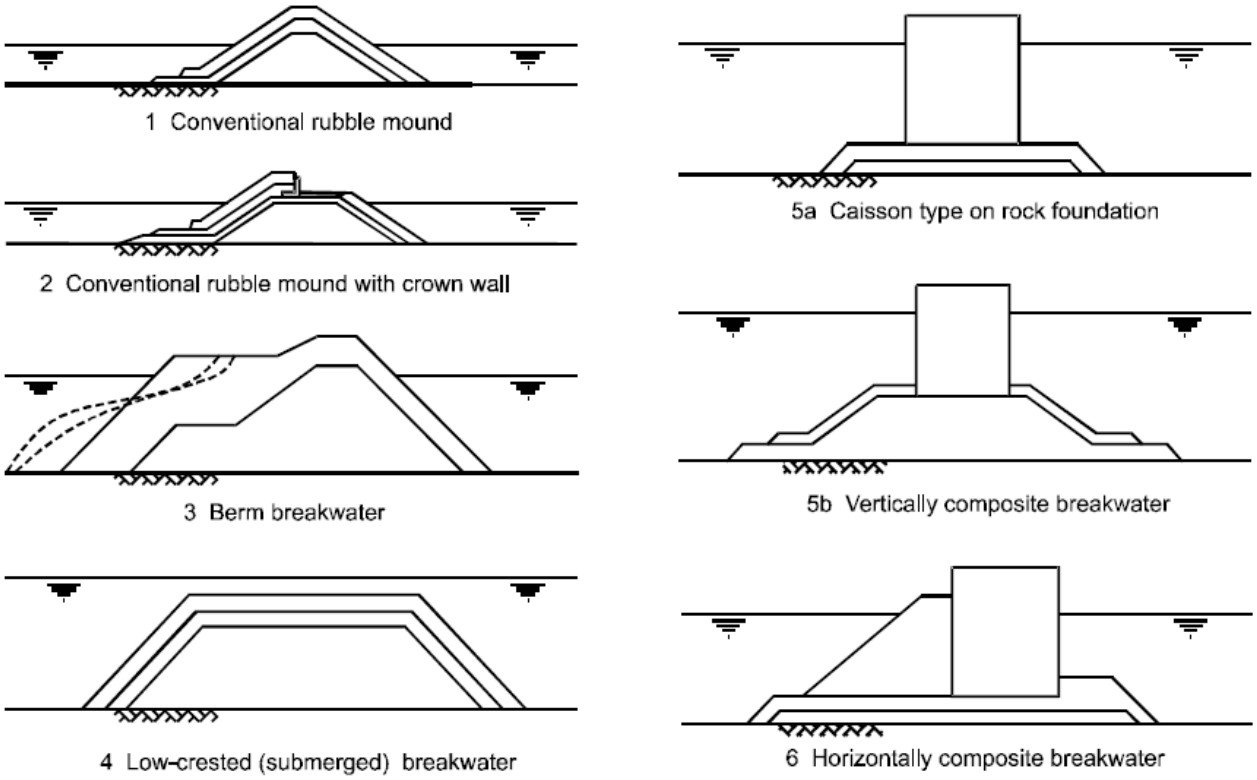

Figure 2.2: Types of rubble mound breakwaters
Copied from Figure 6.3 in CUR et al., 2007

2.2.2 Crest walls

To reduce the overtopping volumes without increasing the height and amount of material of the rubble mound, a crest wall or crown wall on top of the breakwater is recommended. These L-shaped concrete elements besides improving the overtopping performance of the breakwater, also provide access, a working platform and can be used to carry pipelines or conveyors (CUR et al., 2007).

Crest wall loads

Crest walls are subjected to severe wave attack. The forces against the wall happen in two ways. The primary action occurs at the vertical front face resulting in large horizontal forces and overturning moments. The second action is the wave penetration into the core, which leads to an increase pore pressure in the rubble mound. If the water reach the location under the wall, a vertical force defined as an uplift force is exerted on the slab, reducing the resistance forces. Figure 2.3 gives a simplification of the wave loads caused by wave impact.

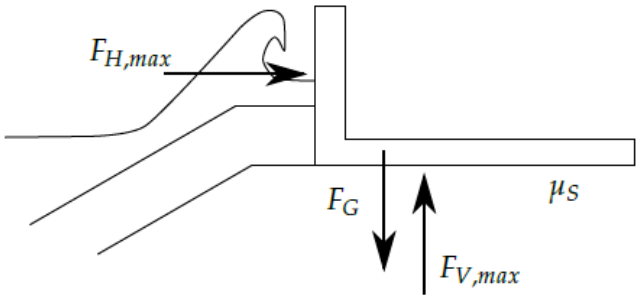

Figure 2.3: Simplification of wave loads on a crest wall
Copied from Figure 2.12 in Bekker, 2017

Where $F_{H,max}$ is the wave induced horizontal force, $F_{V,max}$ is the wave induced uplift force, μ_s is the friction coefficient and F_G is the buoyancy-reduced weight of the crest wall estimated as $F_G = (M_{cw} - V_{cw}\rho_w)g$ being M_{cw} and V_{cw} the mass and volume of the crest wall.

The stability against sliding and overturning can be assessed with the following equations:

$$\mu_s(F_G - F_{V,max}) \geq F_{H,max} \tag{2.1}$$

$$M_G - M_U \geq M_H \tag{2.2}$$

Here, M_G is the stabilising moment due to mass of the concrete element, M_U is the wave generated moment due to uplift pressures and M_H is the wave generated moment due to the horizontal forces (CUR et al., 2007).

Crest wall failure mechanisms

When the wave loads exerted on the crest wall surpass a certain threshold, they can lead to the crest wall failure mechanisms depicted in Figure 2.4.

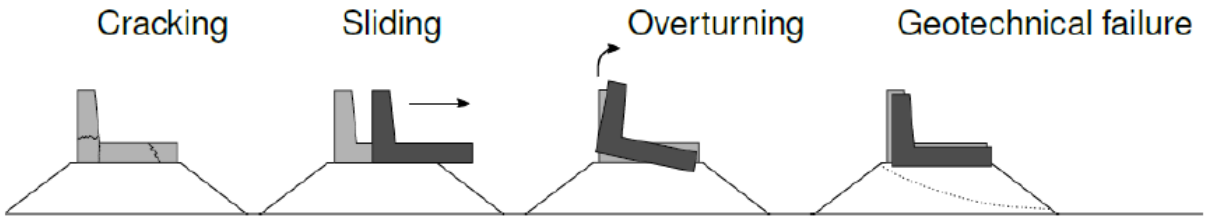

Figure 2.4: Crest wall failure mechanisms
Adapted from Figure 1.3 in Pedersen, 1996

The crest wall failure modes can be separated in two groups, the first related to the strength of the superstructure, e.g. breakage and the second group where the strength depends on the interaction between the structure and the underlaying material, such as sliding, overturning and geotechnical failure (CUR et al., 2007). According to Pedersen (1996), sliding is the most common failure mechanism.

Crest wall pressure distribution

Losada et al. (1995) showed the time evolution of wave pressure on a vertical wall, under increasing wave steepness (see Figure 2.5). For low steepness waves acting almost as standing waves, the pressure-time series

displays a sinusoidal shape. When a slight increase in wave steepness occurs, the peak pressure at the bottom of the wall fluctuates with twice the wave frequency (Figure 2.5 a). If the steepness increases further, the fluctuation reaches the water surface and a symmetrical double peak pressure-time series can be distinguished (Figure 2.5 b). Near breaking conditions, the double peak signal becomes asymmetric being the first peak shorter and higher (Figure 2.5 c). The asymmetry marks the separation between a standing and a breaking wave character. When a wave breaks on the wall, the first peak increases drastically and may even be divided into two peaks of very short duration (Figure 2.5 d). The subsequent peak with larger duration and smaller amplitude is known as reflecting pressure. Sometimes, the wave breaks before reaching the wall. In these cases, the two peak behaviour remains (Figure 2.5 e) but the magnitude and duration depends on the distance between the breaking point and the wall (Losada et al., 1995).

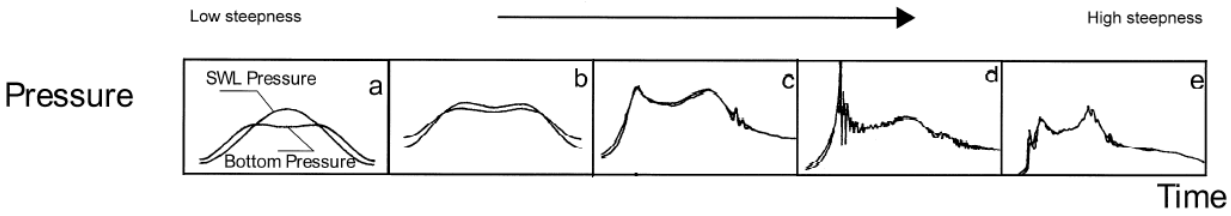

Figure 2.5: Time evolution of wave pressure distribution on a vertical wall under increasing wave steepness
Adapted from Losada et al., 1995

The experimental results from Martin (1995) and Losada et al. (1995) showed that after breaking, when the wave impinges the crest wall, the first peak is the result of the abrupt change of direction of the bore due to the presence of the structure (referred in Martin (1995) as dynamic pressure but referred hereafter as impulse pressure). The second peak happens after the instant of maximum wave run-up and is related to the water mass down rushing the wall. Figure 2.6 exemplifies this double-peak behaviour. Peak A represents the dynamic pressure where 2 regions can be distinguished. The upper one is the unprotected wall zone while the lower one is protected by the armour layer. Peak B, also called reflecting pressure, increases linearly downwards displaying a more quasi-static behaviour. For the reflecting pressure, the presence of the armour layer is less influential.

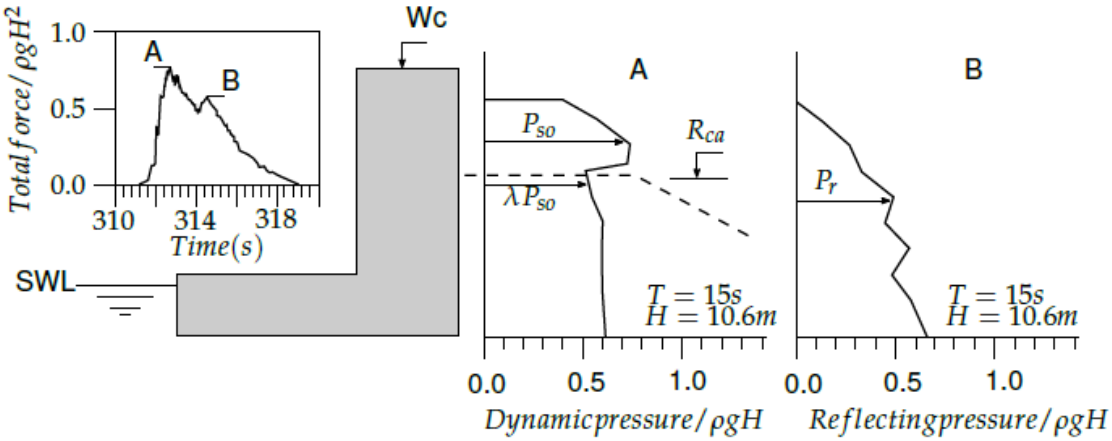

Figure 2.6: Dynamic and reflecting pressure for broken waves
Copied from Figure 4 in Martin et al., 1999

Additionally, Pedersen (1996) indicated that the forces experienced by the wall depend on the wave characteristics and the geometry of the structure, including permeability and roughness of the breakwater layers. Determining a formulation for the pressure distribution in the front face of crest walls is quite complex due to the random character of the waves and the fact that the crown wall is partially protected by the armour layer, which consists of non uniform placed rocks or concrete blocks.

2.3 Design process

The design process of a coastal structure should produce a concept that is functional, technical and economically feasible, and that meets the social and legal requirements. Depending on the type and complexity of the structure, different design guidelines should be followed.

Figure 2.7 illustrates the design process of rubble mound breakwaters. In an idealized situation, a designer could make the design based on design formulas, rules of thumb, physical and numerical model tests. However, depending on the design phase, the time, the budget and the complexity of the project, a combination of the above mentioned tools is often applied. The upper part in Figure 2.7, i.e. the design formulas, are usually semi-empirical or empirical methods based on field measurements or model tests. These formulas are often applied outside their range of validity.

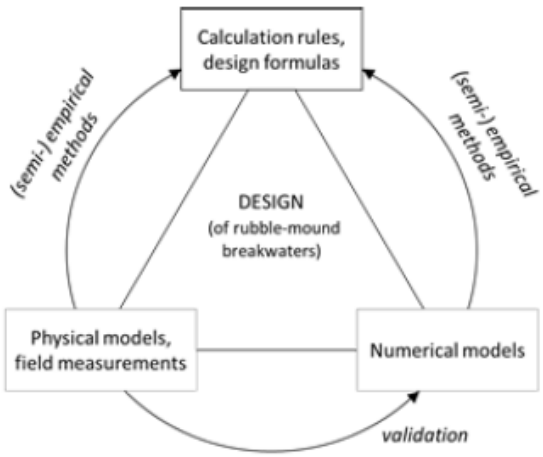

Figure 2.7: Current approach for breakwater design
Copied from Figure 1 in van den Bos, Verhagen, & Kuiper, 2015

Therefore, designers often resort to the additional tools included in the lower part of Figure 2.7: physical and numerical tests. Traditionally, wave induced forces have been measured in the physical flume by placing pressure transducers in the middle of the crest wall, where the maximum pressures are expected to happened. Then, the force is obtained by spatial integration of the point measurements. A limitation of this methodology is that when breaking waves hit the structure, the location of the maximum pressures is still not well known due to the high spatial variability. By using an array with low spatial resolution, the forces estimated with the physical models will always underestimate a little the actual forces experienced by the wall (Ramachandran et al., 2013).

The goal of this work is to make a contribution towards the lower right part of Figure 2.7; i.e. towards a wider applicability of numerical modelling during the design stages of a project. This is done by presenting a validation of impermeable and partly-permeable breakwaters subjected to non-breaking and heavily breaking waves. The results from this study will show the benefits and limitations of the numerical flume in the estimation of wave induced forces and pressure distribution along the wall.

Chapter 3

Case Study: Holyhead breakwater

3.1 Introduction

This chapter defines the real life case study used to assess the capability of OpenFOAM to model accurately the wave induced forces on the front face of crest walls on top of impermeable and partly-permeable breakwaters. The chapter begins with a small characterization of the the Holyhead breakwater located in Wales. Then, it gives an overview of the first small scale 2D physical model tests campaign performed by DHI during the development of the refurbishment studies. These physical tests are used to develop and validate the numerical models. The description includes the breakwater layouts, the measuring devices deployed along the physical flume and the available information generated for each test. At the end of the chapter, a selection from all the physical tests is made and explained based on the objectives of this research project.

3.2 Holyhead breakwater

The Holyhead breakwater protecting the Holyhead Port on the west coast of Anglesey in Wales, United Kingdom (see Figure 3.1) is used as the real life case study to answer the research question.

Figure 3.1: Location Holyhead breakwater
Source: Google Earth, 2021

The Holyhead breakwater is a rubble mound breakwater of 2.4 km long. It is considered a historic grade II listed structure, built in 1875. The rubble mound has a width larger than a 100 m and is generally submerged

in normal operational conditions. This structure was built by end-tipping from the shore and allowing waves to reshape the rock into a stable profile. On top of the rubble mound, there is a vertical structure formed from blockwork walls containing rocky fill (HASKONING DHV UK LTD, 2020). Figure 3.2 shows a top view and a close view of the breakwater.

Figure 3.2: Holyhead breakwater
Left: top view. Right: vertical wall view.
Source: Google

Over its operational time, the breakwater has experienced some damages that may jeopardize the safety of the port. It was identified that the structure is at risk of breaching due to undermining of the vertical walls, impulsive loading on the vertical wall and excessive overtopping. Therefore, a refurbishment project for the Holyhead breakwater was set in motion. The expected outcome was to provide a structure that can protect the Holyhead Port against the incoming wave attack for years to come.

The refurbishment of the breakwater includes stabilizing the toe of the vertical wall. To assess different solutions and designs, three physical model test campaigns were undertaken in a wave flume at DHI, Denmark. The first campaign evaluated two alternative solutions: a solution with Tetrapods and a solution with Xblocs as armour units in a 2D physical model. The results showed that the Tetrapods option was better but still needed further improvement. Therefore, a second round of 2D model tests was carried out where the friction between the armour layers and the mound was included. Moreover, different ways to stabilize the toe were covered within these tests. The conclusion was to add a double row of 60t chevrons (see Figure 3.3). To finalize the design, a final campaign with 3D model tests was undertaken to evaluate the performance of the design at the roundhead (HASKONING DHV UK LTD, 2020).

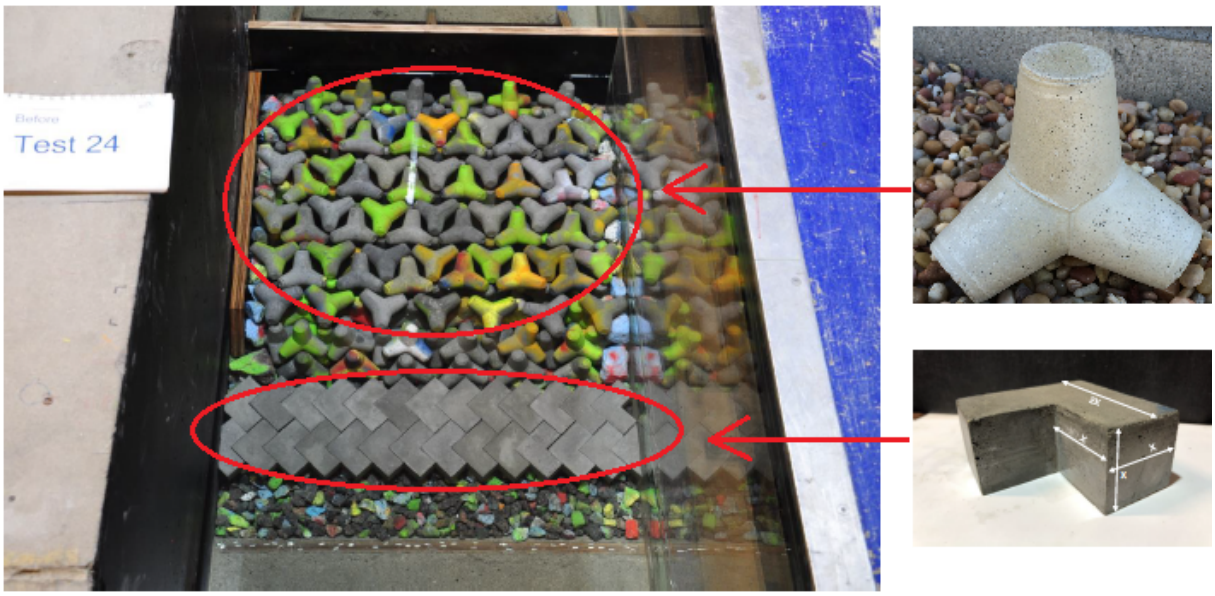

Figure 3.3: Tetrapods as armour layer and Chevrons for toe stabilization
Adapted from DHI, 2019

3.3 Physical modelling campaign

The first 2D modelling campaign was conducted in June and July 2019, for a cross-section of the Holyhead breakwater. In the modelling campaign, a length scale factor of 1:52.2 is used. From this factor follows a time scale factor of 1:7.22 and a volume scale factor of 1:142,327 (DHI, 2019). Froude's model law was applied for conversion between model measures and prototype measures because the important physical properties related to the present study are inertia and gravitational forces.

A total of 16 tests were carried out during this campaign, including 3 different geometries: Baseline layout, Tetrapods as armour layer and Xblocs as armour layer (exemplified in Figure 3.4) and 4 different hydraulic conditions: operational conditions with high water level, 100-year extreme conditions with high water level, 100-year extreme conditions with low water level and overload conditions (see wave characteristics in prototype and model scale in Table 3.1 and Table 3.2, respectively). Additionally, 4 calibration tests were performed using the Baseline layout.

The Baseline layout consists of the rubble mound and the caisson, also referred in this report as wall, as illustrated in the left panel of Figure 3.4a. For the physical modelling, the rubble mound is assumed as impermeable. The right panel of Figure 3.4a includes the model set up in the laboratory. Figure 3.4b includes the Tetrapods layout where a Tetrapods layer of 30 m wide and 5.2 m thick was added in front of the crest wall. Finally, Figure 3.4c includes the Xbloc layout. In this case, a trench is made in the existing rubble mound where a single layer of $6\,m^3$ Xbloc units is placed on a 4:3 slope followed by a 15 m wide horizontal berm. In front of the Xbloc, a toe built from 10-15 ton rock is placed (measures in prototype scale).

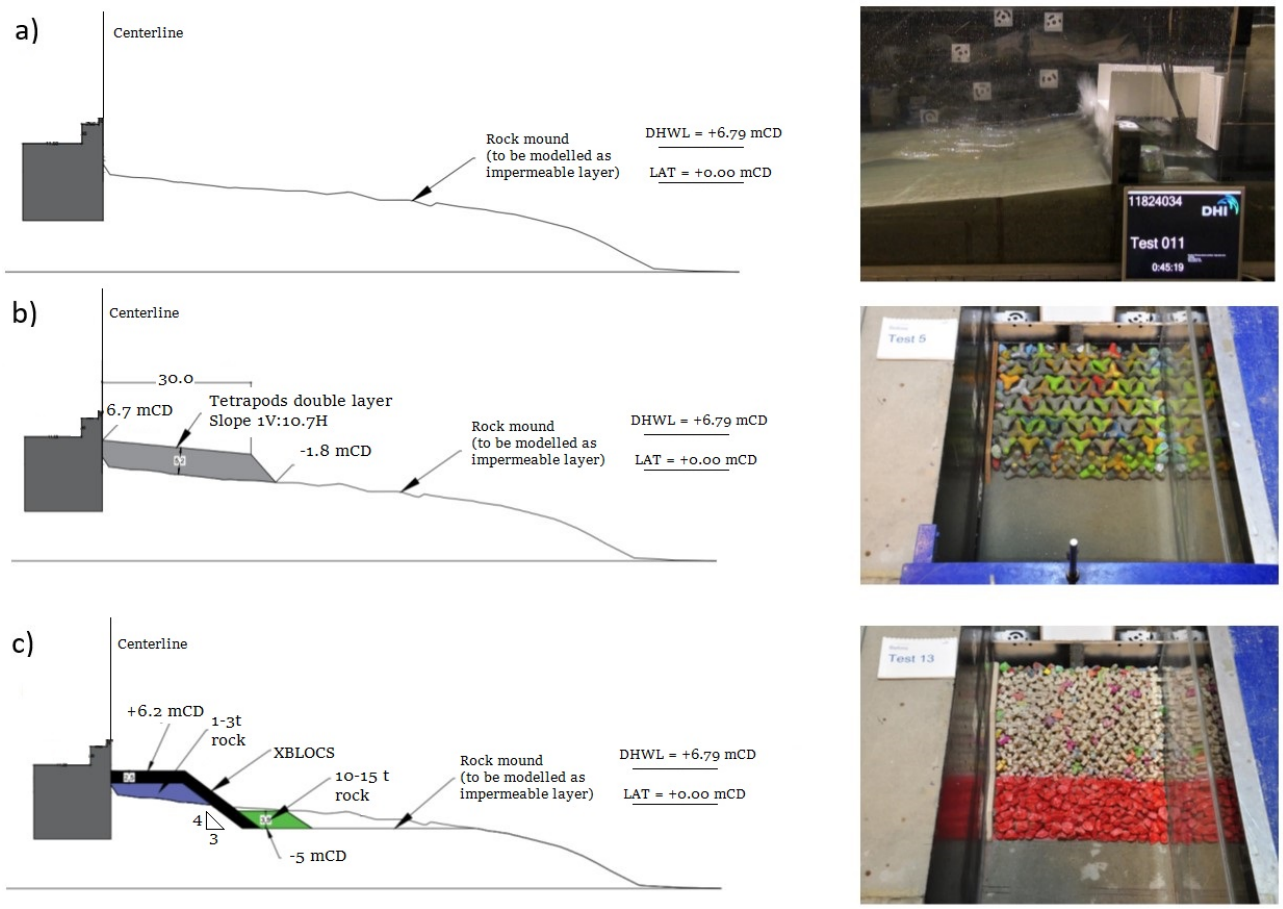

Figure 3.4: Model tests layouts
a) Baseline layout: rubble mound and vertical wall, b) Option 1: Tetrapods as armour layer and c) Option 2: Xblocs as armour layer. Left panel: profile and measurements in prototype scale. Right panel: model set up in the laboratory. Adapted from DHI, 2019

Table 3.1: Test conditions applied during the tests – prototype conditions

Hydraulic Conditions	WL $[m]$	Duration $[h]$	H_{m0} $[m]$	T_p $[s]$	WL $[mCD]$
Operational conditions - high water	+26.78	6	2.28	7.4	+6.79
100-year extreme conditions - high water	+26.78	6	5.39	10.6	+6.79
100-year extreme conditions - low water	+19.99	6	5.39	10.6	+0.00
Overload conditions (120% of 100-year extreme conditions)	+26.78	6	6.47	12.7	+6.79

Source: DHI, 2019

Table 3.2: Test conditions applied during the tests – model conditions

Hydraulic Conditions	WL (1) $[m]$	H_{m0} $[m]$	T_p $[s]$
Operational conditions - high water	0.513	0.044	1.025
100-year extreme conditions - high water	0.513	0.103	1.468
100-year extreme conditions - low water	0.383	0.103	1.468
Overload conditions (120% of 100-year extreme conditions)	0.513	0.124	1.759

(1) Relative to flume bottom
Source: DHI, 2019

The waves in the flume were generated by an electric wave generator controlled by DHI's Wave Synthesizer software. For all tests, a standard JONSWAP wave spectrum with a peak enhancement factor of $\gamma_J = 3.3$ was applied. The wave generating system has a wave reflection compensation module able to absorb the reflected waves, reducing the undesired re-reflection at the wavemaker (DHI, 2019).

During the tests, the surface elevation, the overtopping and the wave pressures at the wall were measured. Figure 3.5 shows a diagram of the flume and the measurement devices. The surface elevation was recorded by 11 wave gauges – 5 located offshore, 5 located just before the rubble mound and 1 placed before the toe of the new armour layers to measure the wave height in front of the new structures (see location of each gauge in Table 3.3). The wave overtopping was collected by a tray situated behind the vertical wall. The mean overtopping was estimated by dividing the total volume by the width of the tray (31 cm) and the duration of the test. Then, the values were converted into prototype scale. There is no information about the overtopping time-series. Finally, the wave loads on the wall were measured by pressure transducers located in the centre of the front side of the wall at 5 different heights (see position of each transducer in Table 3.4).

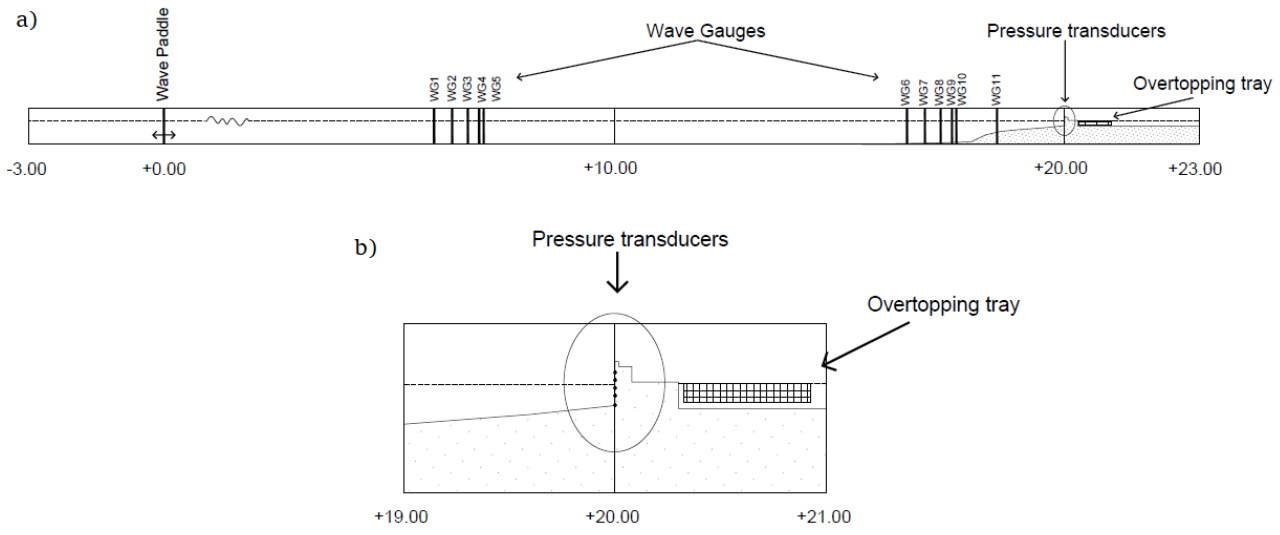

Figure 3.5: Location of wave gauges, pressure transducers and overtopping tray during the tests
a) Total length of physical flume, b) zoom in at crown wall. All distances in model scale

Table 3.3: Location of wave gauges in the flume in model scale

Wave gauge number	Distance from wave paddle [m]	Distance from vertical wall [m]
WG1	6	14
WG2	6.4	13.6
WG3	6.75	13.25
WG4	7	13
WG5	7.1	12.9
WG6	16.5	3.5
WG7	16.9	3.1
WG8	17.25	2.75
WG9	17.5	2.5
WG10	17.6	2.4
WG11	18.5	1.5

Table 3.4: Location of pressure transducers along the vertical wall

Pressure transducers	Height above model bathymetry to centre of pressure transducers [mm]	Chart datum in prototype [mCD]
1	10	2.09
2	46.5	3.99
3	83	5.90
4	119.5	7.81
5	156	9.71

The available information used in this research project is:

- Paddle position
- Water level at 11 wave gauges
- Dynamic pressure readings at 5 pressure transducers located in the front side of the wall

The paddle data and the measurements from the gauges and the pressure transducers are not synchronized. There is a warm up period from the wave maker until the waves hit the structure. The delay for all tests is approximately $20\,s \pm 1\,s$ and it varies per test.

3.4 Selection of physical tests

To answer the research question and sub-questions of this research project, a selection from the 16 physical tests was made. Figures 3.6 and 3.7 show the wave conditions present for each hydraulic condition. During operational conditions with high water levels, the waves show more a standing wave behaviour whereas for the other 3 cases, the waves break at the rubble mound. To validate the model for non-breaking and breaking waves, the operational conditions with high water level and the 100-year extreme condition with high water level were selected. In this way, the work done by Jacobsen et al. (2018) is further validated for non-breaking waves and even expanded by including the simulation of heavily breaking waves. The hydraulic condition with low water level is not of interest for this project because the waves do not reach the vertical wall that often. The overload case is also neglected since the first two conditions already include non-breaking and heavily breaking wave conditions reaching the vertical wall.

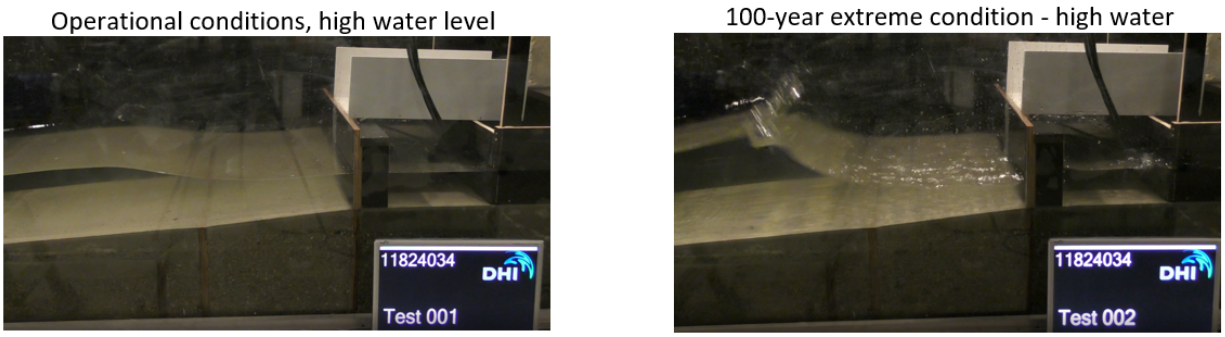

Figure 3.6: Pictures from calibration tests from DHI, 2019, for operational conditions with high water level and 100-year extreme conditions with high water level

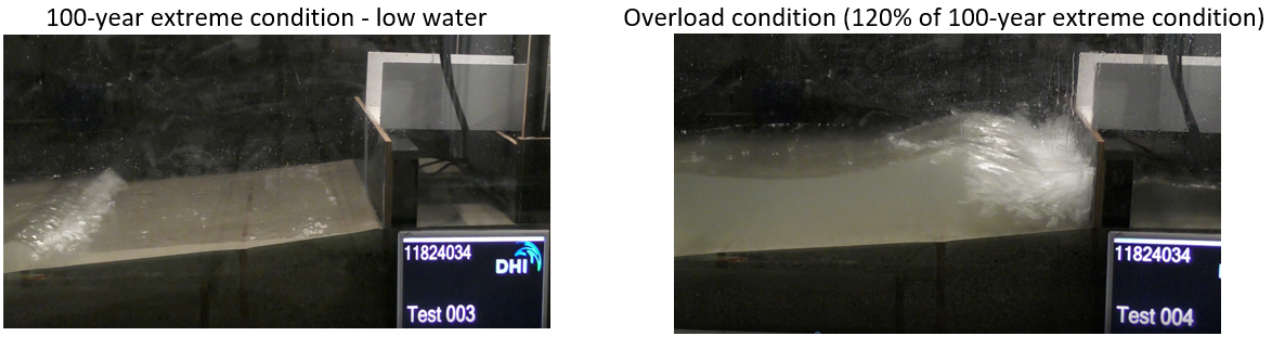

Figure 3.7: Pictures from calibration tests from DHI, 2019, for 100-year extreme conditions with low water level and overload conditions

Another target is to model different breakwater layouts in the numerical flume to assess the performance of the numerical model for impermeable and partly-permeable structures. The baseline case represents an impermeable rubble mound with a vertical wall on top. This case will be simulated because it has a non-typical breakwater layout. It also represents an impermeable rubble mound with high wave reflection. By including this case, the focus of the validation is set on the ventilated boundary condition and how this can be tuned to reproduce the forces at the wall when non-breaking and heavily breaking waves are present. Moreover, these simulations will allow to assess the performance of the current breakwater layout. The second layout that will be simulated includes the Tetrapods as armour layer. The results from the 2D physical tests indicated that using these concrete blocks as armour for the refurbishment works was the best option. By adding an armour layer, there is porous flow inside this layer. This includes another set of parameters that affect the reflection caused by the breakwater. Table 3.5 summarizes the cases that were simulated in OpenFOAM. By modelling these cases, the porous flow inside the armour layer, the ventilated boundary condition and the wave-structure interaction under non-breaking and heavily breaking waves is studied in more detail to fairly reproduce the water levels inside the flume and the pressure forces at the front face of the wall. The different cases show the strength and weaknesses of the numerical model.

Table 3.5: Cases simulated in the numerical flume

Geometry	**Hydraulic Conditions**
Baseline	Operational conditions, high water level
Baseline	100-year extreme condition - high water
Tetrapods	Operational conditions, high water level
Tetrapods	100-year extreme condition - high water

Chapter 4

Numerical modelling

4.1 Introduction

During this research project, two numerical frameworks were used to simulate the free surface flows: a CFD model named OpenFOAM (Weller et al., 1998) and the fully nonlinear potential flow solver OceanWave3D (Engsig-Karup et al., 2009).

This chapter begins with an explanation of the mathematical model. The Reynolds Averaged Navier-Stokes equations, the porous media resistance forces, the volume of fluid method, the relaxation zones technique and the turbulence modelling are mentioned. Implementations in OpenFOAM to solve wave-structure interactions such as the ventilated boundary condition are also defined. In the end, a brief description of both numerical frameworks is included, as well as an explanation of the coupling between OpenFOAM and OceanWave3D developed by Paulsen et al. (2013).

4.2 Mathematical framework

4.2.1 Reynolds Averaged Navier-Stokes Equation

The equations presented in this sections are being solved for two immiscible fluids simultaneously: water and air. Thus, the hydrodynamic model is based on the two phase Navier-Stokes equations. In order to solve the equations, a simplification is made by applying Reynolds decomposition. This substitutes the velocity by a mean motion and a fluctuating part : $u = \bar{u} + u'$. After averaging the equations over the turbulent motion (the fluctuating part), the so-called Reynolds Averaged Navier-Stokes Equations (RANS) are derived:

$$\nabla \boldsymbol{u} = 0 \tag{4.1}$$

$$\frac{\partial \rho \boldsymbol{u}}{\partial t} + \nabla \left[\rho \boldsymbol{u}\boldsymbol{u}^T\right] = -\nabla p^* - g\boldsymbol{x}\nabla\rho + \nabla\left[\mu\nabla\boldsymbol{u} + \rho\boldsymbol{\tau}\right] + \sigma_T\kappa_\gamma\nabla\gamma \tag{4.2}$$

Where $\nabla = \frac{\partial}{\partial x} + \frac{\partial}{\partial y} + \frac{\partial}{\partial z}$, $\boldsymbol{u} = (u, v, w)$ is the mean velocity in Cartesian coordinates, ρ is the fluid density, t is time, p^* is an excess pressure, g is the gravity acceleration, $\boldsymbol{x} = [x, y, z]$ is the Cartesian coordinate vector, μ is the dynamic molecular viscosity and $\boldsymbol{\tau}$ is the specific Reynolds stress tensor:

$$\boldsymbol{\tau} = \frac{2}{\rho}\mu_t\boldsymbol{S} - \frac{2}{3}k\boldsymbol{I} \tag{4.3}$$

Here, μ_t is the kinematic eddy viscosity (the eddy viscosity ν_t is denoted as μ_t/ρ), $\boldsymbol{S}$ is the strain rate tensor, k is the turbulent kinetic energy per unit mass and $\boldsymbol{I}$ is the Kronecker delta. The last term in Equation 4.2 is the effect of the surface tension. σ_T is the surface tension coefficient, κ_γ is the surface curvature and γ is the scalar field used to track the free surface. This term appears because the equations are being solved for two immiscible fluids simultaneously. Further details about the surface tracking are given in Section 4.2.3. .

The RANS equations describe the dynamics of the mean flow; not of the fluctuations (smaller time scale). The consequence of Reynolds-averaging is that new terms appear in the Navier-Stokes equations. Therefore, additional equations are needed to approximate the Reynolds stresses, also known as turbulence closure models.

According to dimensional analysis, the eddy viscosity ν_t is proportional to a characteristic velocity and a characteristic length scale. More details about turbulence modelling are given in Section 4.2.6.

The design and assessment of many coastal structures includes the interaction between flow and waves with porous media. Jensen et al. (2014) applied the volume averaging procedure on the RANS equations to obtain the Volume Averaged/Reynolds Averaged Navies-Stokes equations (VARANS) to account for permeable structures by including the effect of the porosity. In their version of the Navier-Stokes equations, the velocity was defined as the filter velocity. Thus, the momentum conservation equation is written as:

$$(1 + C_m)\frac{\partial}{\partial t}\frac{\rho \boldsymbol{u}_f}{n_p} + \frac{1}{n_p}\nabla\frac{\rho}{n_p}\boldsymbol{u}_f\boldsymbol{u}_f^T = -\nabla p^* + \boldsymbol{g}\boldsymbol{x}\nabla\rho + \frac{1}{n_p}\nabla\mu\nabla\boldsymbol{u}_f - \boldsymbol{F}_p \tag{4.4}$$

Where C_m is the added mass coefficient that accounts for the transient interaction between grains and water, $\boldsymbol{u}_f$ is the filter velocity vector in Cartesian coordinates, n_p is the porosity of the permeable structure and F_p accounts for the resistance force due to the presence of the porous media (more details in Section 4.2.2). This implementation uses a version of the Navier-Stokes equations which does not account for the eddy viscosity; thus, a turbulence closure model is not necessary. This assumption was validated by Jensen et al. (2014) and Jacobsen et al. (2015), when there is little energy dissipation caused by wave breaking and large energy dissipation caused by the structure. For the case study of the Holyhead breakwater, this simplification may not be valid due to the presence of an impermeable breakwater subjected to extreme wave attack. The results of this thesis will shed some light on this topic.

4.2.2 Porous media resistance forces

By volume averaging the RANS equations to account for the presence of the porous media, new terms arose: the added mass coefficient (C_m) and the resistance term (F_p). To resolve these terms, the extended Darcy-Forchheimer equation is applied as a closure model:

$$\boldsymbol{F}_p = a\rho\boldsymbol{u}_f + b\rho\|\boldsymbol{u}_f\|_2\boldsymbol{u}_f \tag{4.5}$$

The extended Darcy-Forchheimer equation includes linear, non-linear and inertia forces to account for accelerations. When the first term dominates in Equation 4.5, the flow behaves as laminar while if the second term dominates, the flow is turbulent. The parameters a and b are resistance coefficients that must be determined empirically.

Jensen et al. (2014) used the parametrisation derived by van Gent (1995) where the effect of the oscillatory flows was included by means of the KC number (Keulegan-Carpenter number):

$$a = \alpha\frac{(1-n_p)^2}{n_p^3}\frac{\nu}{\rho d_{n50}^2} \tag{4.6}$$

$$b = \beta\left(1 + \frac{7.5}{KC}\right)\frac{1-n_p}{n_p^3}\frac{1}{d_{n50}} \tag{4.7}$$

α and β are calibration coefficients depending on grading and shape of the grains, ν is the kinematic molecular viscosity, d_{n50} is the median grain diameter of the porous structure and $KC = u_m T/nd_{50}$ where u_m is the maximum oscillating velocity and T is the period of the oscillation. Since estimating the KC number is rather complicated, Jacobsen et al. (2015) resorted to a pragmatic approach where this number was determined based on incident wave field and shallow water wave theory:

$$KC = \frac{H_{m0}}{2}\sqrt{\frac{g}{h}}\frac{1.1T_{m-1,0}}{d_{50}} \tag{4.8}$$

Here, H_{m0} is the significant wave height, $T_{m-1,0}$ is a spectral wave period defined as $\frac{m_{-1}}{m_0}$ and h is the water depth taken at the toe of the structure. The spectral wave period may also be approximated as $T_{m-1,0} \approx T_p/1.1$.

By following this approach two effects were neglected. First, the gradual increase in the nonlinear resistance coefficient b with the decrease of the orbital velocities, due to the dampening experienced by the waves inside the porous media. The dampening of the quadratic velocity goes faster to zero than the linear increase of KC; therefore, the nonlinear resistance becomes less important across the width of the structure. Second, there is a probability distribution of KC given the irregular wave field. By using the significant wave height, a representative KC is applied along the simulation. (Jacobsen et al., 2015).

The inertia term in the extended Forchheimer-Darcy equation was already included in Equation 4.4 by means of C_m. Also, van Gent (1995) gave a formulation to estimate this parameter as:

$$C_m = \gamma_p \frac{1 - n_p}{n_p} \tag{4.9}$$

Where γ_p is an empirical coefficient which takes the value of 0.34.

The calibration coefficients α and β and the KC number included in van Gent (1995) parametrisation are discussed in more detail in the following paragraphs.

α and β

Traditionally, the closure coefficients - α and β - are determined by three different methods: using laboratory measurements, basing them on analytical considerations or performing a best fit to experimental data when the drag forces are obtained numerically (Losada et al., 2016). For stones, van Gent (1995) found from experimental data, that α lies between 0-2780 and β, between 0.36-1.33. The final recommendation, despite the grading, shape, aspect ratio and orientation of the stones, was to use values of 1,000 and 1.1 for α and β, respectively. Losada et al. (2008) carried out a sensitivity analysis by comparing the free surface, pressure time series and spectra under regular and irregular waves hitting a rubble mound breakwater against experimental data. The best-fit parameters were $\alpha = 200$ and $\beta = 0.8$ for the breakwater core; $\alpha = 200$ and $\beta = 1.1$ for the small gravel external layer and $\alpha = 200$ and $\beta = 0.7$ for the big gravel external layer. Given the large variation for these two coefficients, Losada et al. (2016) performed an extensive literature study where they found an ample range of values for the porous media drag coefficients depending on the coastal application; clearly indicating there is still the need for improvement in determining the empirical coefficients and how they are related to different flow conditions. Their review pointed out that the influence of material grading, shape or packing density on the damping inside the porous media is not completely understood. Additionally, the effect of the shape and nature of natural and artificial blocks on the drag forces is not yet studied.

For artificial concrete blocks, the available data is even scarcer. There is not sufficient indication in literature on which α and β values to use for layers composed by Tetrapods units. To this author's knowledge, these coefficients have only been estimated by calibrating numerical models (Hsu et al., 2002, Neves et al., 2011 and Lee et al., 2019).

Hsu et al. (2002) developed a mathematical model to describe the flow both inside and outside the porous media by volume-averaging the RANS and the $k - \epsilon$ equations. The performance of the model was validated by comparing the numerical results with the outcomes from the experiments conducted by Sakakiyama and Liu (2001) on a caisson breakwater covered with Tetrapods. The value of the resistance coefficients were set to be $\alpha = 200$, $\beta = 1.1$ and $n_p = 0.5$. Neves et al. (2011) modelled the waves interacting with the breakwaters of Leixões harbour in Portugal. They applied the numerical models: AMAZON (Hu, 2000) and IH-2VOF developed at University of Cantabria. This breakwater consists of four different porous media: one is composed by small rocks, two correspond to concrete cubes and the last one is conformed by Tetrapods. In their work, they conducted a sensitivity analysis for the porous media parameters of the artificial blocks based on the free surface elevation. Table 4.1 shows the values tested for the Tetrapods layer. No final recommendation on which set of values to used was found from their work.

Table 4.1: Porous media parameters values used in the calibration tests of the breakwaters of Leixões harbour in Portugal

Parameters	n_p [-]	α [-]	β [-]
Tetrapods Layer	0.4, 0.5, 0.6	100, 200, 1000	0.5, 0.8, 1.1

Source: Neves et al., 2011

On a more recent work, Lee et al. (2019) estimated the empirical coefficients for permeable layers of Tetrapod-covered caisson breakwaters by simulating the wave-structure interaction in CoastalFOAM. No turbulence closure model was included in the numerical simulations. After a calibration process based on representing as accurately as possible the wave pressures on the caisson, an optimal combination of the coefficients α and β to use in the Van Gent parametrisation (see Equations 4.6 and 4.7) was found. For a D_{50} of 0.075 m, the recommended values are: $\alpha = 200$, $\beta = 0.7$ and $n_p = 0.33$.

Keulegan-Carpenter number

The KC number incorporates the effect of the non-stationary flow (oscillatory movement caused by the waves hitting the porous structure) in the nonlinear resistance coefficient b in the Darcy-Forchheimer equation. Under oscillatory wave motions, the drag forces are higher than under stationary flows due to additional turbulence inside the porous media (more details in van Gent, 1995).

Studies as the ones conducted by Jensen et al. (2014) and Jacobsen et al. (2017) include the contribution of the KC number in the estimation of the porous media drag coefficients. Other investigations also exclude this contribution by setting a high value for the KC number. Jacobsen et al. (2018) and Lee et al. (2019) used a default value of 10,000, obtaining good agreements between the experimental and the numerical results. However, they don't indicate a reason to leave out the dependency on the KC number in the estimation of the nonlinear resistance coefficient.

4.2.3 Volume of Fluid method

The tracking of the free surface between the air and water interface is performed by the Volume of Fluid approach (VOF). By following this approach, many coastal processes are well captured by the numerical model, e.g. wave breaking, overturning waves, overtopping, wave set-up, among others. This method captures the free surface by adding an advection equation:

$$\frac{\partial \gamma}{\partial t} + \frac{1}{n_p}\left[\nabla \boldsymbol{u}_f \gamma + \nabla \boldsymbol{u}_r \left(1-\gamma\right)\gamma\right] = 0 \tag{4.10}$$

As stated in Section 4.2.1, γ is the indicator function of the VOF field. The indicator function takes values between 0 and 1, with values of zero when the cell is filled with air, values of 1 when is filled with water and intermediate values when the two phases are present inside the cell. The factor $1/n_p$ was introduced by Jensen et al. (2014) to ensure the mass conservation when the fluid passes through porous media. This factor accounts for the fact that a given volume is emptied or filled faster when sediment grains are also included inside that volume. OpenFOAM uses an explicit advection algorithm named MULES (Multidimensional Universal Limiter for Explicit Solution) to determine the advection of the indicator field. Using MULES ensures a non-diffusive solution. The last term on the left hand side of Equation 4.10 is a compression term that limits the smearing of the interface. The strength of the interface compression is ruled by u_r, which efficiently keeps a sharp interface.

The indicator function is used to estimate the fluids densities and viscosities:

$$\rho = \gamma \rho_w + \rho_a \left(1-\gamma\right) \tag{4.11}$$

$$\mu = \gamma \mu_w + \mu_a \left(1-\gamma\right) \tag{4.12}$$

The subscripts a and w represent air and water, respectively. The fluids densities and viscosities are weighted average based on the distribution of water and air in each control volume, i.e. in each cell. After computation, the fluid properties at each grid cell are used in the RANS/VARANS equations. A more detailed explanation of the VOF method can be found in Berberović et al. (2009).

4.2.4 Relaxation zones

The relaxation zones avoid reflection of waves from outlet boundaries. They also avoid that the internal reflected waves interfere with the wave maker boundaries (Jacobsen et al., 2012). Relaxation zones work by weighing the computed and target solutions. A relaxation function as the one exemplified in Equation 4.13 is applied inside the relaxation zone as shown in Equation 4.14 and in Figure 4.1.

$$\alpha_R\left(\chi_R\right) = 1 - \frac{exp\left(\chi_R^{3.5}\right) - 1}{exp(1) - 1} \; for \; \chi_R \in [0\ 1] \tag{4.13}$$

$$\phi_R = \alpha_R \phi_{computed} + \left(1 - \alpha_R\right) \phi_{target} \tag{4.14}$$

Where ϕ_R is the velocity $\boldsymbol{u}_f$ or the indicator function γ. The term χ_R works in a way that causes that α_R is always 1 at the interface between the non-relaxed part of the computational domain and the relaxation zone, i.e. the computed solution remains. On the other side, χ_R becomes 1 and α_R equals zero, causing the target solution to persist (Jacobsen et al., 2012).

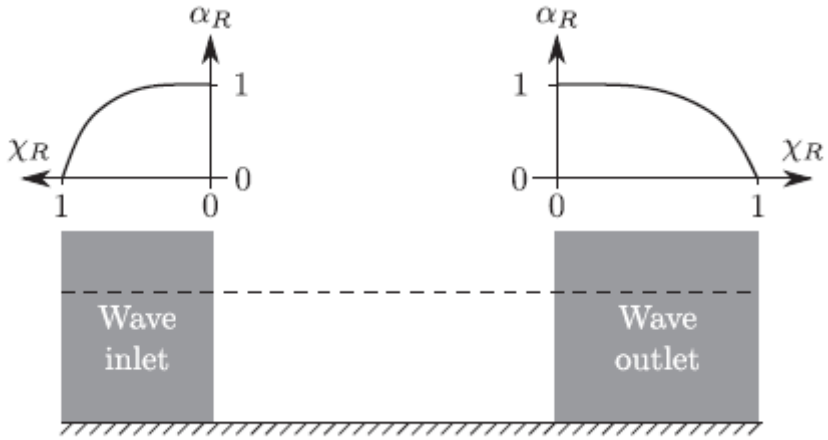

Figure 4.1: Variation of $\alpha_R\left(\chi_R\right)$ for inlet and outlet relaxation zones
Copied from Figure 3 in Jacobsen et al., 2012

4.2.5 Ventilated Boundary Condition

Jacobsen et al. (2018) propose a technique to solve the spurious entrapment of air between water surface and structural elements. The phenomena where the waves in air-filled cavities exert large forces on structures was seen experimentally and numerically, resulting in inaccurate predictions of wave loads on crest walls. At the moment of their research, the existing techniques involve introducing small tubes through a structure to allow air ventilation (see Figure 4.2A). However, this lead to highly time-consuming numerical simulations because all the volume of air was transported through the thin tube causing high air velocities, thus, limiting the time-step of the numerical model. The proposed solution by Jacobsen et al. (2018) is the use of a permeable boundary condition at the structure that allows for air ventilation without restricting the time-step (see Figure 4.2B), also known as the ventilated boundary condition (see Equation 4.15).

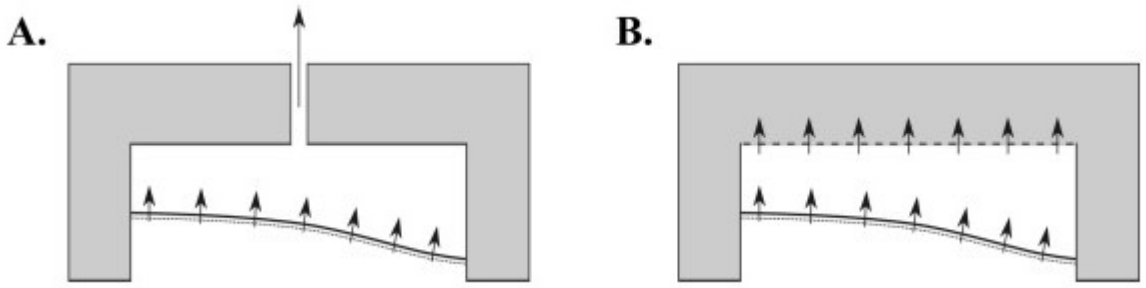

Figure 4.2: Sketch of two methods to model ventilation through a structural element
A: The use of a meshed tube to ventilate the cavity. B: The use of a permeable boundary to ventilate the cavity (dashed line). Copied from Figure 1 in Jacobsen et al., 2018.

$$p_b^* = p_{ref}^* + \frac{\rho}{2}\xi_p |u_p^\perp| u_p^\perp \tag{4.15}$$

Here, p_b^* is the pressure at the boundary (dotted line in Figure 4.2), p_{ref}^* is the pressure in the imaginary reservoir on the backside of the structural element, $u_p^\perp$ is the pore velocity of the fluid in the gap(s) through the structural element and ξ_p is a loss coefficient. As the mathematical framework uses filter velocities as stated in Section 4.2.1, the ventilated boundary condition must also be expressed in the same way:

$$p_b^* = p_{ref}^* + \frac{\rho}{2}\frac{\xi_f}{e_p^2} |u^\perp| u^\perp \tag{4.16}$$

Where $u^\perp$ is the filter velocity normal to the structural element, e_p is the degree of openness of the element and ξ_f is the loss coefficient based on $u^\perp$. Theoretically, the degree of openness can take values between 100% and 0%. However, for mathematical reasons, a very small value for the degree of openness must be used when low ventilation needs to be modelled. Jacobsen et al. (2018) found that a 3% degree of openness and a loss coefficient of 1.5 provided good results for the prediction of forces on crest walls.

4.2.6 Turbulence modelling

Turbulence is a three-dimensional, time-dependent and nonlinear phenomenon. This complex fluid motion involves different length scales, energy cascades, horizontal and vertical mixing. During this process, there is a transfer or energy from the larger eddies to the smaller ones until the energy is transformed into heat.

The RANS equations are transport equations for the mean variables in a turbulent flow. These equations contain net fluxes due to turbulent fluctuations. In order to solve the RANS equations – specifically the Reynolds Stresses terms, turbulence models - also called closure models - are applied.

Many turbulence models (constant eddy viscosity, $k-\epsilon$, $k-\omega$, $k-\omega\,SST$, $RNG\,k-\epsilon$, among others) with different degree of complexity and limitations have been developed overtime. Some models provide expressions for the Reynolds stresses based on an effective 'eddy viscosity', as is the case of the constant eddy viscosity model, while others account for the production, dissipation and transport of the turbulent quantities in their formulations.

Turbulence is an important process in coastal waters. Wave breaking results in a large amount of turbulence which converts the organized wave motion into a random, chaotic fluid motion. Jensen et al. (2014) used a version of the Navier-Stokes equations where no turbulence model was introduced. In their research, the results from the validation cases were not affected by not including a turbulence closure model. In their specific case, wave breaking played little or no role; i.e, the turbulence levels outside the structure were of minor importance while the production of turbulence inside the porous media were of interest and accounted by solving the Darcy-Forchheimer equation (Equation 4.5). As stated by Jensen et al. (2014), when the resistance coefficients α and β are obtained from experimental measurements, they already include the turbulence effects. Hence, if a turbulence model is added to the numerical flume, these resistance coefficients must be modified to avoid double quantification of turbulence.

Jacobsen et al. (2015) and Jacobsen et al. (2018) followed the same approach showing the possibility of modelling correctly the bulk hydrodynamics (free surface elevation, wave transformation and wave reflection) and the forces on the crest walls. Just as before, little or no wave breaking happened during the tests.

In this research, operational and extreme conditions are simulated in the numerical flume, where, for the latter conditions, a lot of wave breaking occurred during the tests. Besides, when the baseline layout is modelled, no porous media is present in the flume. Two approaches were followed in this case, the exclusion of a turbulence closure model and the inclusion of a simple turbulence model: the constant eddy viscosity model.

4.3 Numerical framework

4.3.1 OpenFOAM

OpenFOAM (for Open Field Operation and Manipulation), version foam-extended-3.1 is used as one of the numerical frameworks in the present research. OpenFOAM is an open-source object-oriented C++ class library able to solve CFD problems using the finite volume method (Weller et al., 1998). It contains a method for solving free surface Reynolds Averaged Navier-stokes (RANS) equations coupled with a volume of fluid method (VOF) (e.g. van Gent, 1995; Losada et al., 2016; Jensen et al., 2014).

In the last decade, many efforts have been made to extend the applications of OpenFOAM into the coastal field by adding the capability of modelling wave-structure interactions. The `waves2foam` library enables to generate and absorb waves in the numerical flume using the relaxation zone technique (Jacobsen et al., 2012). Afterwards, an addition was made to the `waves2foam` library by including the flow in porous media (Jensen et al., 2014). The coupling between the CFD toolbox (OpenFOAM) and the fully nonlinear potential flow solver OceanWave3D was developed by Paulsen et al. (2013). Lastly, during the JIP CoastalFOAM (2015-2019) several tools and processing utilities were added into the `waves2foam` toolbox. One of them is the ventilated boundary condition implemented by Jacobsen et al. (2018) to solve the numerical time constraints caused by air-entrapment between the water surface and the structural elements (see details in Section 4.2.5). These packages are compiled together and for simplicity are referred in this report as CoastalFOAM (see Figure 4.3)

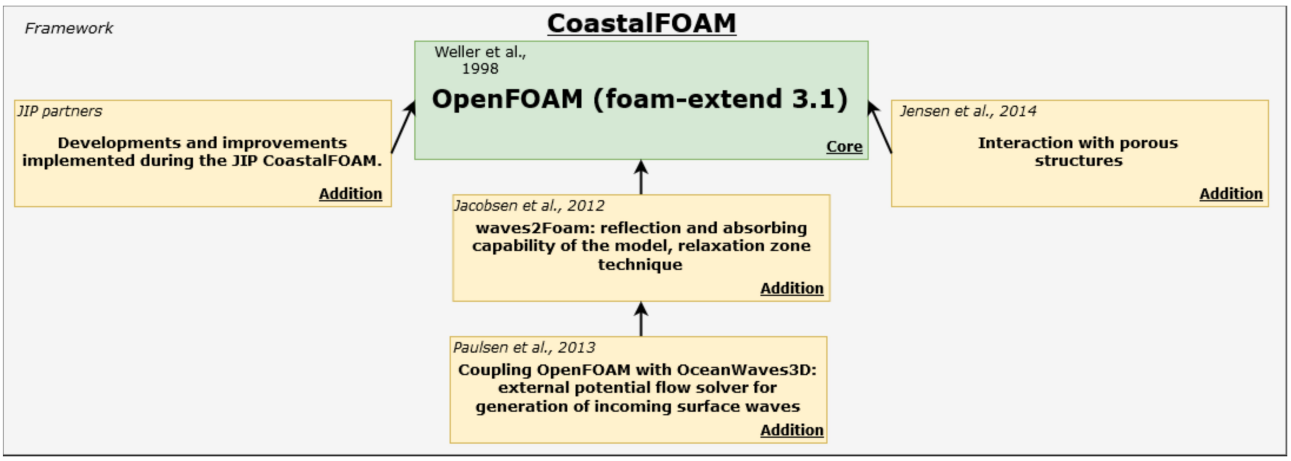

Figure 4.3: CoastalFOAM model
OpenFOAM model including the additional packages: `waves2foam` library, coupling with OceanWaves3D and JIP CoastalFOAM developments and improvements

4.3.2 OceanWave3D

OceanWave3D (OCW3D) is a finite difference model based on nonlinear and dispersive potential flow. This model can simulate free surface waves in varying bathymetries ranging from deep to shallow water until the breaking point. For the free surface time integration, the explicit four-stage, fourth-order Runge Kutta scheme was applied, implying a time-step limitation defined by the Courant number.

A potential flow problem is fully characterized by means of the velocity potential function ϕ, which represents

the particles velocities in the water, and the position of the free surface η, expressed relative to the still water level. Using the velocity potential function requires that the particles motion is irrotational, i.e. $\nabla u = 0$. This assumption is valid when the viscous terms are not dominant in the fluid. For many engineering problems, the viscous effects are only important very close to solid boundaries or in regions where strong wave breaking occurs (Engsig-Karup et al., 2009).

OCW3D uses the relaxation zone technique for the wave generation and absorption. Also, an inhomogeneous time varying Newmann boundary condition was implemented at the inlet boundary, which enables wave generation without using relaxation zones. Thus, the boundary condition of the Laplace equation can be expressed as:

$$\frac{\partial \phi}{\partial x} = u_p \tag{4.17}$$

This type of wave generation allows to reproduce physical experiments because u_p can be defined as the velocity of the wave paddle (Paulsen et al., 2013). In fact, steering files including the time series of the wave paddle velocities can be used as input in OCW3D to reproduce the desired wave conditions.

More details about the mathematical framework of the potential flow solver OCW3D can be found in Engsig-Karup et al. (2009).

4.3.3 Coupling OceanWave3D and OpenFOAM

Modelling large spatial domains can be optimized by coupling two different numerical models. On the one hand, a CFD solver is preferred in areas where resolving wave-breaking and associated physics is important. In these regions, explicit resolution of the wave dynamics and kinematics becomes crucial. However, applying a CFD model like OpenFOAM along the entire simulation domain implies high computational times resulting in a non-efficient and non-attractive model. Potential flow solvers are, on the other hand, much faster. Nonetheless, in the surf zone where turbulence is a dominant process, the potential flow assumption is no longer valid. Therefore, by using the capabilities of both numerical models, an accurate and efficient model can be obtained. The offshore wave conditions from the wave paddle until the vicinities of the breakwater, before the point of wave breaking are simulated in OCW3D. The wave breaking and the wave-structure interaction is computed by OpenFOAM.

The coupling between OpenFOAM and OceanWave3D is achieved by a relaxation zone. This relaxation zone transfers the hydraulic conditions from the OCW3D model to the OpenFOAM solver (see details of the relaxation zone technique in Section 4.2.4). In this case, the target solution is given by the potential flow solver OCW3D. Moreover, the re-reflected fields from the OpenFOAM domain are gradually damped towards the OCW3D domain avoiding the re-reflection from the inner domain towards the potential flow domain. An advantage of this methodology is the high numerical efficiency since only one iteration per time-step is required. Nonetheless, the application of the coupled model also has its drawbacks. Moretto (2020) evidenced that when steeper waves are propagated in the coupled model, high resolution in the the x-axis of the OCW3D domain must be incorporated. This increases the computational time by a factor of 2.

Chapter 5

Model set-up

5.1 Introduction

This chapter focuses on setting-up the numerical flume. This step is explained for the four validation cases: Baseline layout under operational and extreme conditions and Tetrapods layout under operational and extreme conditions. Topics as relaxation zones, temporal and spatial resolution, measuring devices in the numerical flume and definition of the boundary conditions are addressed. For the validation cases including a Tetrapods layer, the definition of the porous media parameters is presented. The chapter includes a summary of the settings applied in this research project for all the validation cases.

5.2 Numerical flume

The 2DV numerical flume consists of an OpenFOAM model coupled with an OCW3D model (see details in Chapter 4, Section 4.3.3). The numerical flume illustrated in Figures 5.1 and 5.2 (for operational and extreme conditions, respectively) was defined with a total length of 26.4 m and a height of 0.8 m, to mimic the physical flume shown in Figure 3.5. Eleven wave gauges were positioned along the numerical flume at the same locations as in the physical flume to capture the water surface elevation (see locations in model scale in Chapter 3, Table 3.3). The breakwater and the crown wall were located 15.5 m and 20 m from the inlet boundary. This is the same distance between the wave maker and the structures in the laboratory.

Relaxation zones were used to generate and absorb waves (see more details in Chapter 4, Section 4.2.4). The first relaxation zone (left region in the OpenFOAM domain), also known as coupling zone, transferred the hydraulic conditions from OCW3D domain to the OpenFOAM domain (more details can be found in Section 5.2.2). The length of the relaxation zones was defined based on the deep water wave length (estimated for the peak period). This was adapted depending on the simulated wave climate. For operational conditions, the length of the inlet relaxation zone was set at 1.64 m, which is about one deep water wave length. Behind the structure, the relaxation zone was defined at 0.82 m, corresponding to half the deep water wave length (see Figure 5.1). Following the same approach, the length of the relaxation zones for the extreme conditions were 3.36 m and 1.68 m (see Figure 5.2).

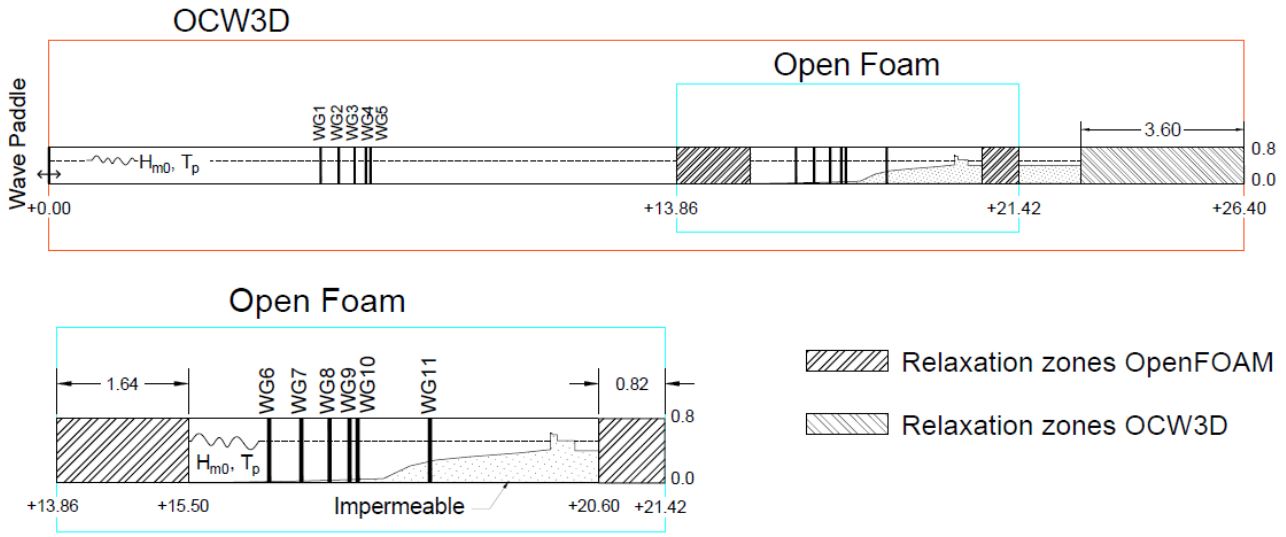

Figure 5.1: Numerical flume for operational wave conditions for the baseline layout
In orange the extension of the OCW3D model; in light blue the extension of the OpenFOAM domain. All units are in model scale. Upper figure: OCW3D model coupled with OpenFOAM. Lower figure: zoom in to OpenFOAM domain.

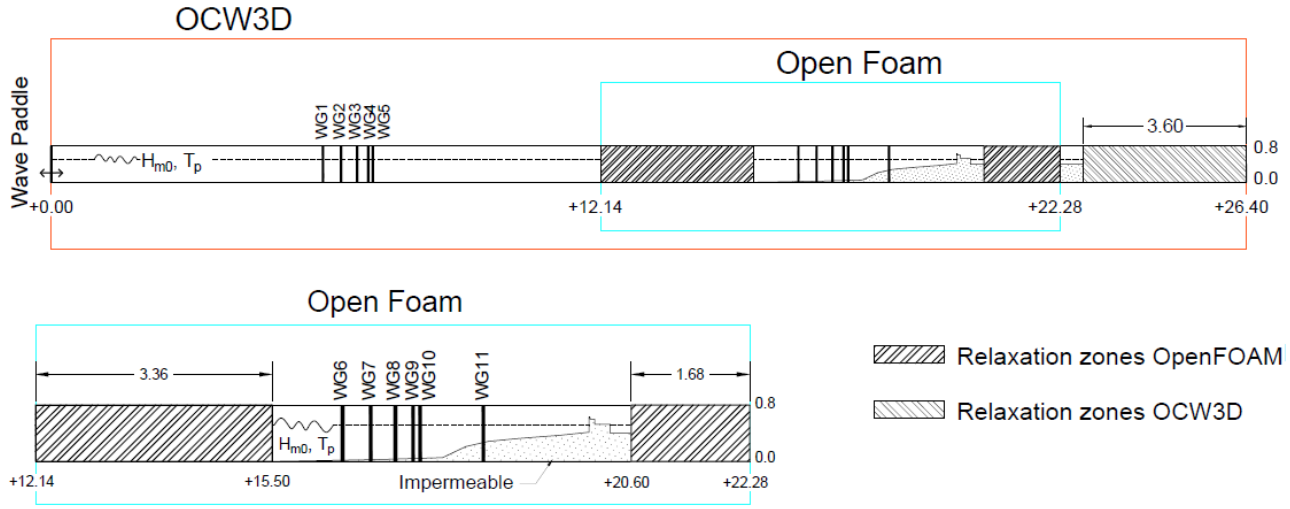

Figure 5.2: Numerical flume for extreme wave conditions for the baseline layout
In orange the extension of the OCW3D model; in light blue the extension of the OpenFOAM domain. All units are in model scale. Upper figure: OCW3D model coupled with OpenFOAM. Lower figure: zoom in to OpenFOAM domain.

5.2.1 Model coupling

The coupling between OCW3D and OpenFOAM influences the accuracy and efficiency of the numerical model. To determine where the potential flow is still valid, the possible breaking point was defined. First, the waves were propagated up to the crest wall by accounting for the shoaling effect induced by the change in water depth. Then, the incipient breaker index of the significant wave was estimated by applying the following equation:

$$\left(\frac{H_{s,b}}{h_b}\right)_{incipient} = \frac{0.12}{h_b/L_0}\left\{1 - exp\left[-1.5\pi\frac{(h_b)_{incipient}}{L_0}(1+11s^{4/3})\right]\right\} \tag{5.1}$$

Here, $H_{s,b}$ corresponds to the incipient breaking significant wave height, h_b is the water depth at breaking, L_0 is the deepwater wavelength and s is the bottom slope (Goda, 2010). The breaker index uses the significant wave

height at breaking (i.e., the incipient breaking significant wave height) because it was derived for an irregular wave field.

Finally, to account for the effect of the shallow foreshore, a Composite Weibull distribution proposed by Battjes and Groenendijk (2000) was applied to define the $H_{1\%}$ and the $H_{0.1\%}$ for each location along the flume, allowing a rough estimation of where the waves may start breaking. This information was necessary due to the irregular wave attack generated by the wave maker during the experiments.

Figure 5.3 and Figure 5.4 illustrate the procedure for operational and extreme conditions, respectively. The still water level is 0.513 m for both wave climates. For the first case, the results indicate that the waves break at the crest wall. For the extreme conditions, wave breaking starts approximately 18 m from the wave paddle. Thus, the OCW3D domain could be extended until 18 m. Nonetheless, to include the wave gauges 6 to 11 in the OpenFOAM domain for reflection analysis and experimental comparison, the OCW3D domain was set back a few meters. Under these considerations, the end of the coupling zone was defined at 15.5 m from the wave paddle, for both operational and extreme conditions (see Figures 5.1 and 5.2).

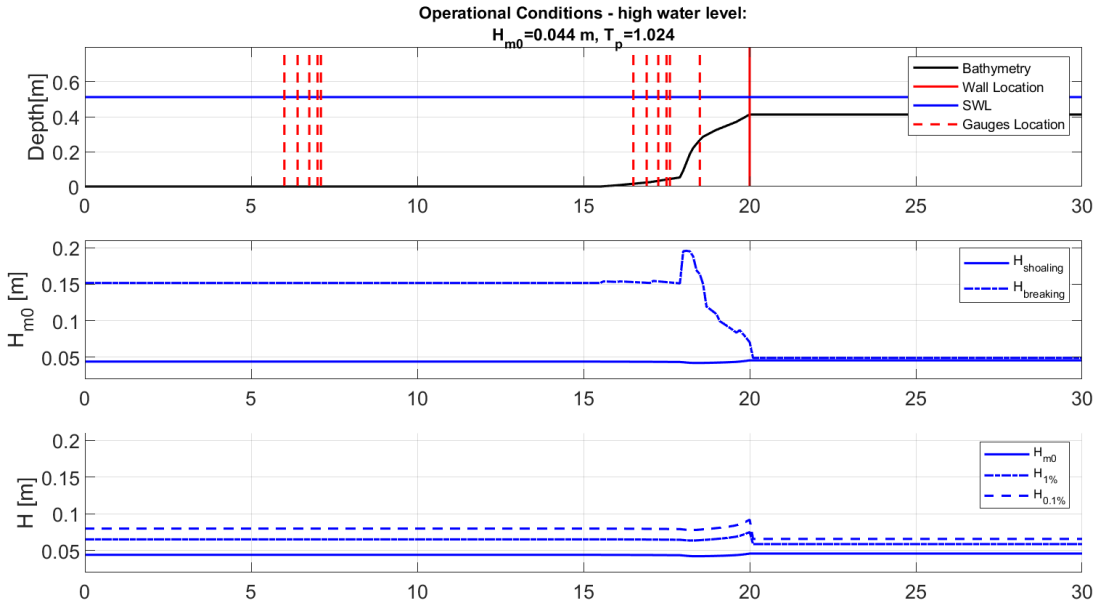

Figure 5.3: Determination of breaking point for operational conditions
All units are in model scale. The initial station is set at the location of the paddle. Upper panel: position of breakwater, crest wall, wave gauges and SWL (for Still Water Level) in the physical and numerical flume. The red line represents the location of the front face of the wall. The SWL is defined at 0.513 m. Middle panel: definition of shoaling wave and breaking wave based on the significant wave height. At the point where the lines intersect, the waves start to break. Lower panel: propagation of significant wave height (dashed line), $H_{1\%}$ (dashed line with smaller gaps) and $H_{0.1\%}$ (continuous line).

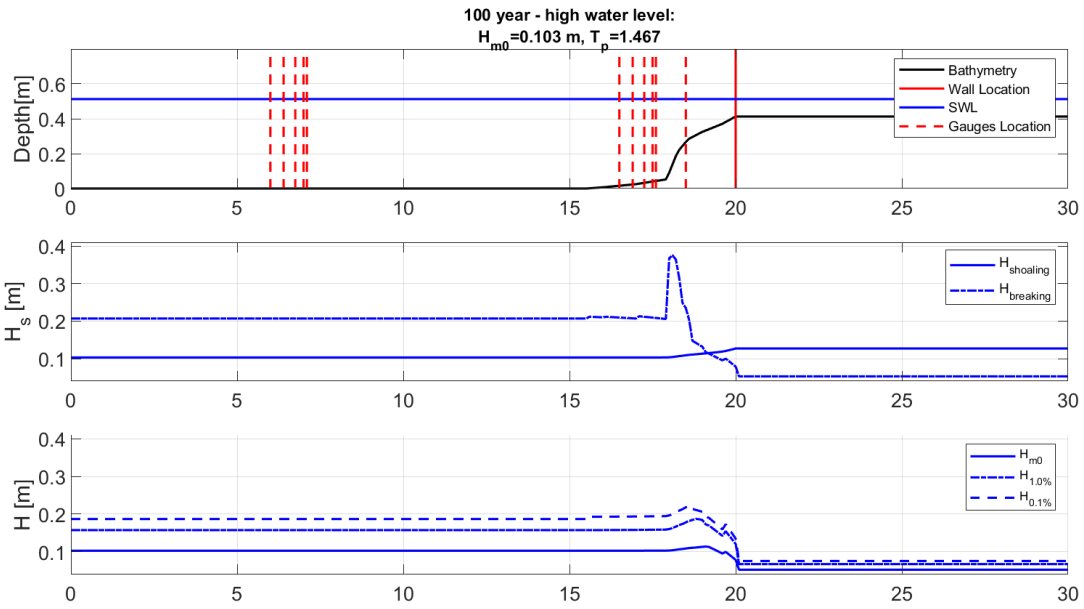

Figure 5.4: Wave characteristics for extreme conditions
All units are in model scale. The initial station is set at the location of the paddle. Upper panel: position of breakwater, crest wall, wave gauges and SWL (for Still Water Level) in the physical and numerical flume. The red line represents the location of the front face of the wall. The SWL is defined at 0.513 m. Middle panel: definition of shoaling wave and breaking wave based on the significant wave height. At the point where the lines intersect, the waves start to break. Lower panel: propagation of significant wave height (dashed line), $H_{1\%}$ (dashed line with smaller gaps) and $H_{0.1\%}$ (continuous line).

5.2.2 Wave generation

In the numerical flume, the waves were generated in OCW3D by inputting the wave paddle velocity signal measured during the physical experiments. Then, through the coupling zone (first relaxation zone in Figures 5.1 and 5.2) the target solution from OCW3D was provided to the OpenFOAM model.

Since only the paddle position time signal was recorded during the experiments, the wave paddle velocity signal was calculated as:

$$u_p(t) = \frac{dx(t)}{dt} \tag{5.2}$$

Central differences was used to obtain the wave paddle velocity signal given its higher order of accuracy as done by Patil (2019). Afterwards, the signal was interpolated to a smaller Δt by using FFT (Fast Fourier Transform) signal reconstruction. This step was necessary due to the fact that the paddle data was too coarse (recorded every 0.2 s). The interpolation procedure is outlined in the following two steps:

1. Apply FFT to the paddle position time series to obtain phases and frequencies.
2. Apply IFFT (Inverse Fast Fourier Transform) to reconstruct the time signal with a smaller Δt by using the already estimated phases and frequencies.

In this case, FFT signal reconstruction of the wave paddle data was used rather than linear interpolation of this data because the later method was not sufficient. Applying linear interpolation led to inaccurate results associated with large underestimations of the incoming wave conditions (exemplified in Figures 5.5 and 5.6).

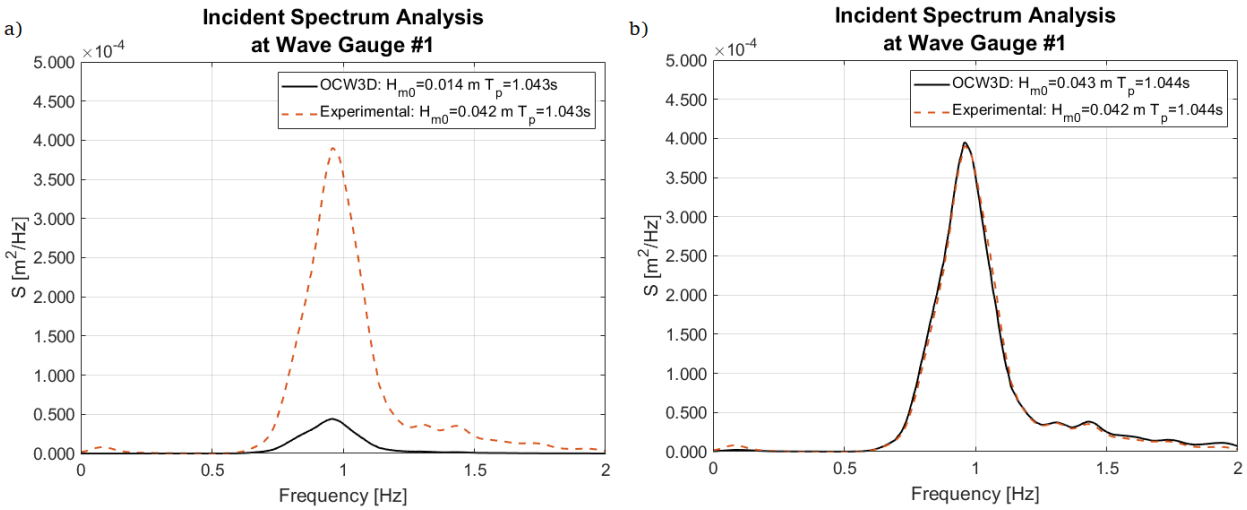

Figure 5.5: Comparison of incident Spectrum Analysis at Wave Gauge 1 for operational conditions a) Linear interpolation of the wave paddle data, b) FFT signal reconstruction of the wave paddle data. The numerical results are extracted from OCW3D domain.

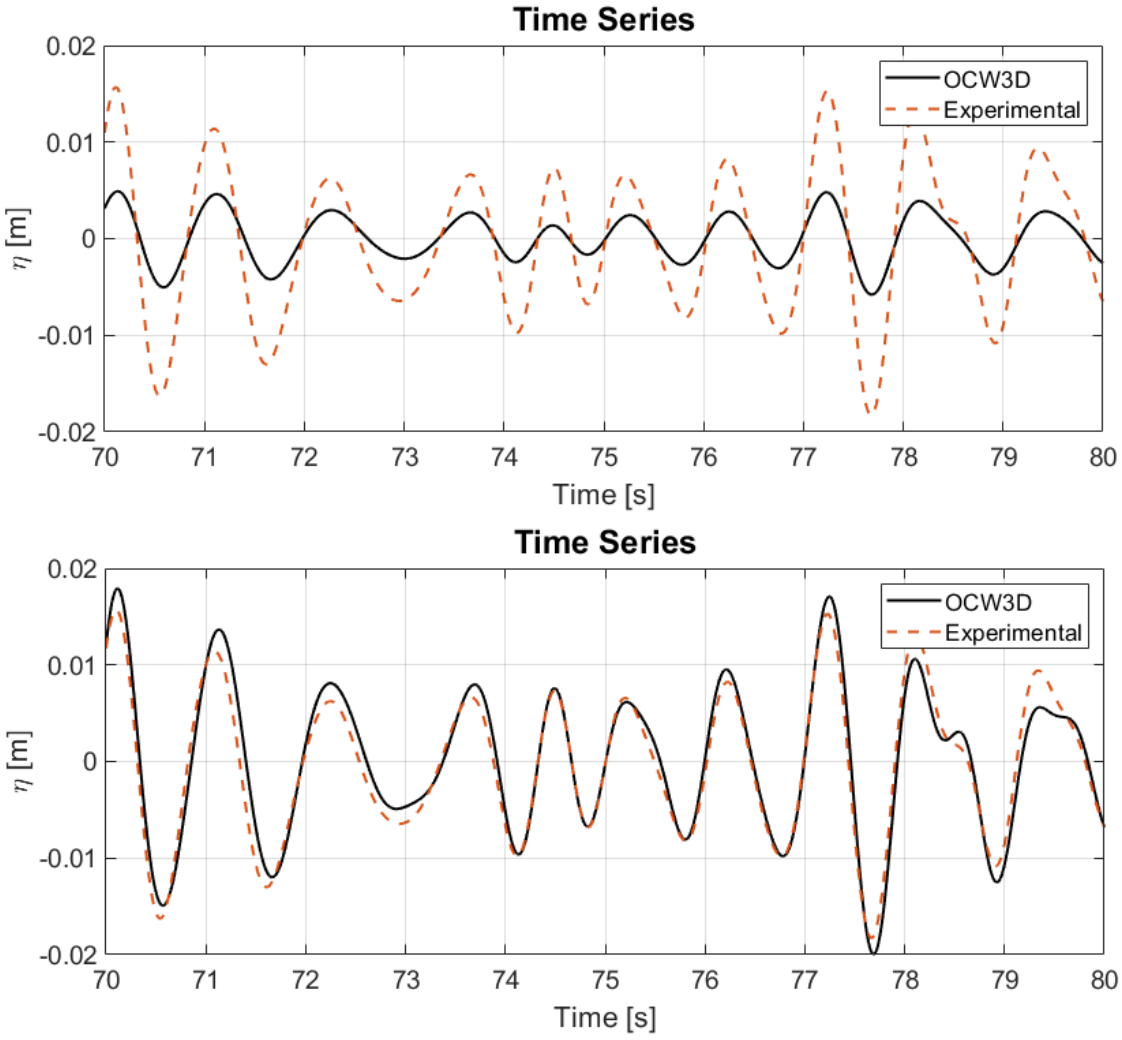

Figure 5.6: Comparison of incident water surface elevation at Wave Gauge 1 for operational conditions a) Linear interpolation of the wave paddle data, b) FFT signal reconstruction of the wave paddle data. The numerical results are extracted from OCW3D domain.

To emphasize the differences between the two methodologies, Figure 5.7 presents the paddle position time signal estimated by the two interpolation approaches. It is evident that the signal characteristic that varies between both methodologies is the smoothness of the paddle position.

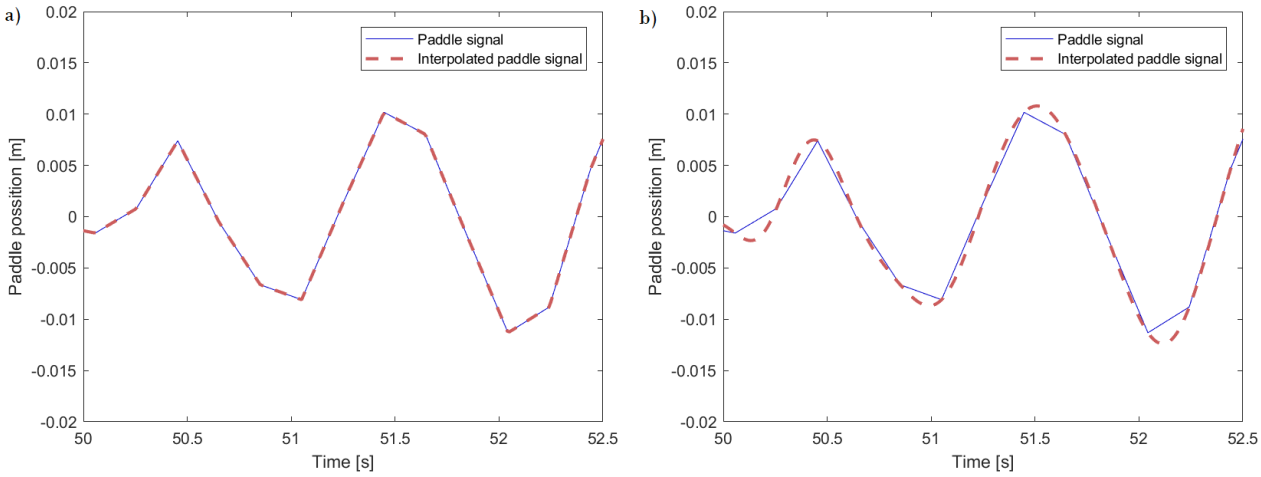

Figure 5.7: Paddle signal interpolation methods
a) Linear interpolation, b) FFT signal reconstruction.

5.2.3 Spatial resolution

To obtain accurate results without increasing significantly the computational time, an appropriate computational grid was defined. First, details of recommended grid dimensions are presented. Taking into account these recommendations and by performing sensitivity analysis, a mesh resolution is selected for the current numerical flume. The spatial resolution is detailed for both numerical solvers: OCW3D and OpenFOAM.

OceanWave3D

OCW3D uses a cartesian grid in horizontal and vertical direction. For the horizontal direction the grid is defined by Δx while in vertical direction it is defined by the number of layers. An increased resolution in the vertical direction towards the surface was set up by selecting vertical stretching, which enhances the accuracy of the propagating waves.

Paulsen et al. (2013) recommended 10 layers along the vertical domain, which was adopted by Jonker (2020) in his research project after finding no differences in the results when varying the number of vertical layers between 7 and 20. Jacobsen et al. (2018) used for his research, 12 vertical layers with good outcomes.

For the horizontal resolution, the JIP CoastalFOAM program recommends more than 10 cells per leading order wave length. Jacobsen et al. (2018) used 80 grid points per peak wave length in the horizontal direction and Van Melis (2019) used 20 grid cells per smallest wave length expected. Jonker (2020) used 40 grid cells per peak wave length for the smallest expected wave length during the simulations after performing a sensitivity analysis. He concluded that the horizontal resolution is normative for the performance of OCW3D and becomes even more important when modelling steeper nonlinear waves. Moretto (2020), on the other hand, recommends 165 cells/wave length according to his research project.

Following the recommendations from other researchers and after performing a grid sensitivity analysis (see Appendix A), for the vertical axis 11 layers were selected for modelling operational conditions and 16 layers, for extreme conditions. In the horizontal direction, the study revealed the need of 96 cells/wave length under operational conditions and 186 cells/wave length under extreme conditions.

OpenFOAM

The JIP CoastalFOAM program recommends 100-150 cells per wave length based on the peak period for the horizontal resolution and a minimum of 5-10 cells over the wave height for the vertical resolution. Moretto (2020) used 635 points per wave length (although no specification of which wave length can be derived from his work) and 20 points per significant wave height. Jonker (2020) found that 10 grid cells per representative (i.e. significant) wave height provided good results; similar outcome was found by Chen et al. (2021), who used in their research nearly 12 cells per wave height.

Usually, the number of grid cells per wave height results normative in defining the mesh resolution in OpenFOAM. Defining a representative wave height depends on which processes should be accurately simulated in the numerical flume. As this research project focuses on determining wave forces on the wall, modelling properly the higher waves is important. Therefore, the representative wave height used is the significant wave height for each wave climate; i.e., $H_{m0} = 0.044\,m$ for operational conditions and $H_{m0} = 0.103\,m$ for extreme conditions.

In this research project, only one grid size for both wave climates was defined to ease the model set-up and avoid bias in the results, when comparing the performance of OpenFOAM for different wave conditions. Thus, a mesh sensitivity analysis was conducted under operational conditions (see- details in Appendix B). It was found that a cell size around the free surface of 0.005 m, corresponding to nearly 9 cells/wave height for operational conditions and to nearly 21 cells/wave height for extreme conditions already provided accurate results. Table 5.1 shows the number of cells per wave height and wave length for both wave climates.

Table 5.1: Grid resolution near the water surface

Hydraulic Conditions	**Grid size near the water surface [cm]**	$\boldsymbol{H_{m0}\,[m]}$	$\boldsymbol{Cells/H_{m0}}$	$\boldsymbol{L_p\,[m]}$ (1)	$\boldsymbol{Cells/L_p}$
Operational conditions	0.5 X 0.5	0.044	8.8	1.582	316
100-year extreme condition	0.5 X 0.5	0.103	20.6	2.7653	553

(1) Peak period wavelength at water depth of 0.513 m

The grid in OpenFOAM was generated by applying the utilities blockMesh and snappyHexMesh. Square cells were used as recommended by Jacobsen et al. (2012) since they give better solutions when modelling non-linear waves. A base mesh of 0.01 m in X and Y direction was created using the blockMesh utility. The base mesh is coarser than the requirements specified in the previous paragraph to enhance computational time. In this way, the mesh is only refined in the necessary regions where a good estimation of the physical processes is vital. The refinements, defined with the snappyHexMesh utility, satisfy the recommendations and allow the model to return accurate results. They were prescribed near the water surface, at the shoaling area, near the slope surface and around the crest wall. For the later region, two levels of refinement were used since high resolution close to the wall is desired for obtaining better prediction of the forces. For the other refinement regions, one refinement level was used. The refinement around the water surface and the shoaling area was included to have the required number of cells per significant wave height. Moreover, the wave propagation and wave breaking processes must be modelled as accurate as possible since they have a direct impact on the forces exerted on the wall. Finally, the refinement near the slope surface was added due to the presence of the boundary layer. A summary and a visualization of the final grid size per region is shown in Table 5.2 and Figure 5.8, respectively.

Table 5.2: Mesh resolution for different regions

Mesh region	**Grid size $\boldsymbol{\Delta x X \Delta y}$ $\boldsymbol{[cm X cm]}$**
Base Mesh	1 X 1
Mesh near the water surface	0.5 X 0.5
Mesh at shoaling area	0.5 X 0.5
Mesh near the slope surface	0.5 X 0.5
Mesh around the crest wall	0.25 X 0.25

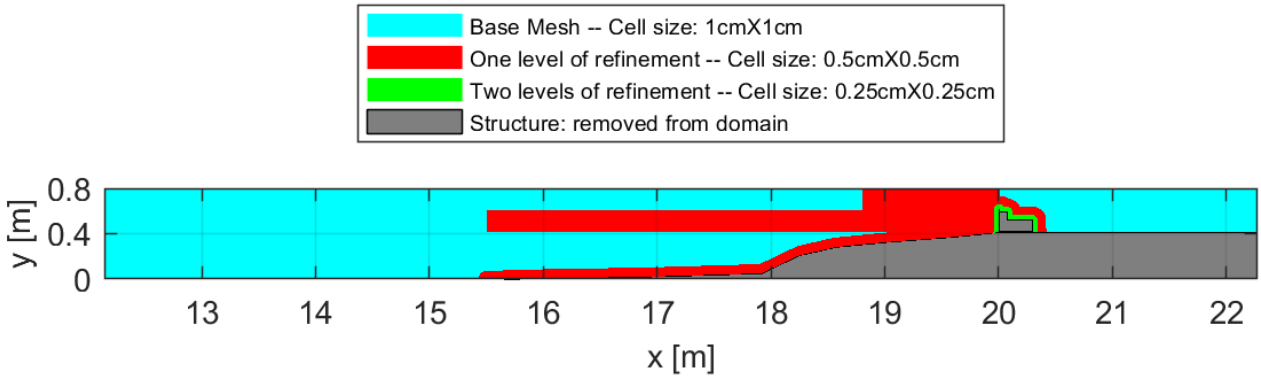

Figure 5.8: Mesh refinements near water surface, at shoaling area, near the slope surface and around the wall

The impermeable structures (e.g. the crest wall and the existing rubble mound as shown in Figure 5.9) were removed from the numerical domain by applying the snappyHexMesh utility. In total, the operational conditions domain consists of approximately 96,652 cells and the extreme conditions domain, of 113,717 cells.

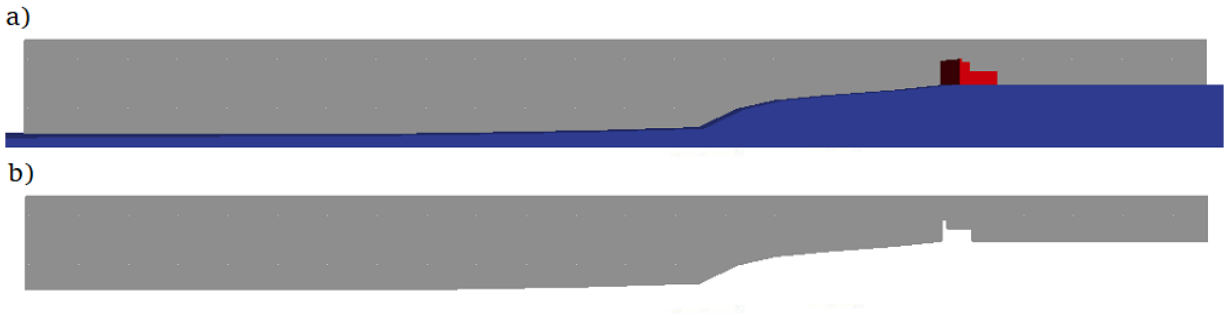

Figure 5.9: OpenFOAM domain showing the impermeable structures removed from the numerical flume a) Base mesh in grey and impermebale structures in blue and red, representing the rubble mound and the crest wall, respectively. b) Final mesh after applying snappyHexMesh for surface removal.

5.2.4 Temporal resolution

The CFL (Courant–Friedrichs–Lewy) condition is used to evaluate the convergence of numerical schemes. The CFL condition states that the full numerical domain of dependence must contain the analytical domain of dependence, i.e. the information must not travel faster than the distance between mesh elements. The CFL condition is a necessary condition for the numerical stability of a model and is defined by the Courant Number:

$$C_0 = \frac{u\Delta t}{\Delta x} \tag{5.3}$$

Here, C_0 is the Courant Number, u is the velocity, Δt is the time step and Δx is the space step. In OpenFoam a prescribed maximum Courant value of 0.35 was applied. Since the grid is predefined and the wave celerity cannot be modified, an adaptive time step approach is followed, i.e. for every time step, the time step is defined in such a way that corresponds to the prescribed maximum Courant number. This method seeks computational efficiency while keeping numerical stability. Another reason to keep low the maximum Courant number is to avoid smearing of the interface. On the other hand, in OceanWave3D, the maximum Courant Number is defined at 0.8. When coupled with OpenFoam, the latter adjusts the time step of OCW3D. Due to the larger Courant restrictions of OpenFoam, the numerical stability of OCW3D is not compromised by the coupling.

To select the time step of OCW3D when used as a standalone software, Equation 5.4 was applied.

$$\Delta t = \frac{C_0\,\Delta x}{u_{max}} = \frac{C_0\,\Delta x}{\sqrt{\frac{g}{h}}H_{max}}, H_{max} \approx H_{0.1\%} = 1.86H_{m0} \tag{5.4}$$

Where u_{max} is the maximum particle velocity during the simulation time, h is the water depth, H_{max} is the maximum wave height and H_{m0} is the significant wave height. Using linear wave theory, this velocity can be defined as $\sqrt{\frac{g}{h}}H_{max}$, where the maximum wave height can be defined as the $H_{0.1\%}$.

Additionally, a sensitivity analysis was conducted to define the proper time discretization of the paddle signal (see details in Appendix A). Finally, a time step of 0.01 s was selected for the operational conditions and a time step of 0.002 s, for the extreme conditions.

5.2.5 Porous media layer: Tetrapods

The validation cases of partly-permeable breakwaters subjected to non-breaking and heavily breaking waves include a Tetrapods layer placed just in front of the crest wall. In Figure 5.10, the OpenFOAM domain in the numerical flume for operational and extreme conditions is illustrated. For the Tetrapods layout numerical flume, the same settings explained so far are applied. Only the settings related to the additional porous media layer are addressed in this section.

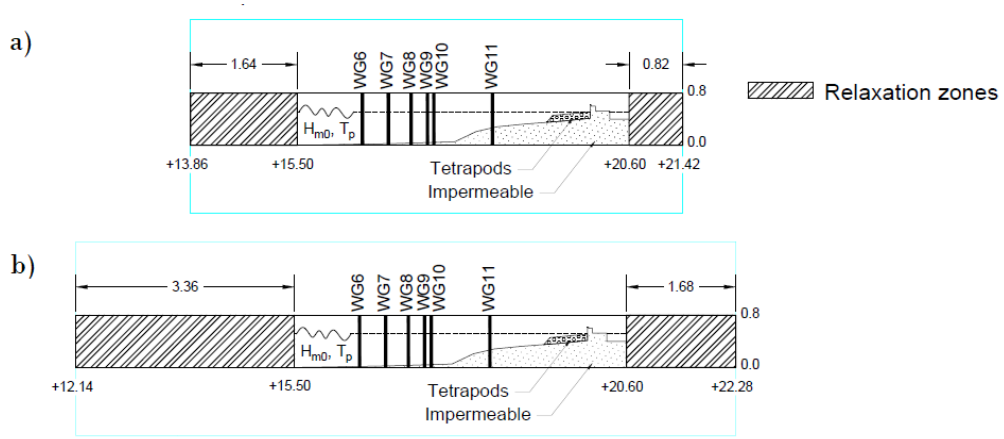

Figure 5.10: Tetrapods layout in OpenFOAM
a) Operational Conditions, b) Extreme conditions

In the numerical flume, the Tetrapods are not modelled by individual pods but by adding a porous layer with specific properties (see details in Chapter 4, Section 4.2.2). In the following paragraphs, the median grain diameter, the porosity, the closure coefficients α and β and the KC number for the Tetrapods layer are defined.

Nominal diameter

The Tetrapod units used in the physical flume corresponded to a volume of 18.1 m^3 and a weight of 43.4 tons in prototype scale and to a volume of 142.8 cm^3 and a weight of 327 g in model scale (DHI, 2019). The corresponding value is converted into nominal diameter; i.e.:

$$d_n = (3.57\,V)^{1/3} \tag{5.5}$$

Here, d_n is the nominal diameter, V is the volume of the concrete block and 3.57 corresponds to the inverse of the shape coefficient recommended by the Rock Manual (CUR et al., 2007). It results in a nominal diameter of 0.08 m.

Porosity

During the physical modelling campaign of the Holyhead breakwater, the Tetrapods layer porosity was not measured. To have a valid and adequate estimation of the porosity, the suggestions from the Rock Manual

(CUR et al., 2007) were followed. Therefore, a constant porosity value of 0.5 is selected for the estimation of the resistance coefficients.

α and β

The existing investigations related to numerical modelling of Tetrapods units, already summarized in Chapter 4, Section 4.2.2, provide a valid starting point for the definition of the porous media drag coefficients for this type of concrete blocks. Due to the fact that numerical modelling of Tetrapods units is a topic with little available research, different combinations of closure coefficients are tested in CoastalFOAM (see Table 5.3).

Table 5.3: Porous media parameters values used in the calibration tests

Parameters	α [-]	β [-]
Tetrapods Layer	200 - 500 - 1,000	0.8 - 1.1 - 1.8

Keulegan-Carpenter number

As explained in Chapter 4, Section 4.2.2, the KC number incorporates the effect of the non-stationary flow in the nonlinear resistance coefficient b in the Darcy-Forcheimer equation. By applying Equation 4.8 and using as water depth the depth at the toe of the porous structure; i.e., 0.16 m, the KC number was calculated as 2.19 for operational conditions and 7.41 for extreme conditions.

Since a few researchers have obtained valid results by excluding the influence of the oscillating flow in the estimation of the nonlinear drag coefficient, a simulation with a KC value of 10,000 is also run in the numerical flume.

5.2.6 Final settings

The numerical settings used in OCW3D and OpenFOAM for all the validation cases are summarized in Tables 5.4, 5.5, 5.6 and 5.7. In OCW3D, the settings vary per wave climate. In OpenFOAM, almost all settings remain the same for all the validation cases. The extension of the relaxation zones differs depending on the simulated wave climate and the porous media parameters are added for the Tetrapods layout validation cases.

Table 5.4: OCW3D settings based on the simulated wave conditions

Hydraulic Conditions	Number of vertical layers	Number of horizontal grid points	$\Delta t\,[s]$
Operational conditions - high water	11	1600	0.01
Extreme conditions - high water	16	1800	0.002

Table 5.5: OpenFOAM general settings

General Settings	**Value**
Base mesh	1 cm X 1 cm
Mesh near the water surface	0.5 cm X 0.5 cm
Mesh at shoaling area	0.5 cm X 0.5 cm
Mesh near the slope surface	0.5 cm X 0.5 cm
Mesh around the crest wall	0.25 cm X 0.25 cm
Courant number	0.35
Gauges	11 (see locations in Table 3.3, Chapter 3)
Pressure transducers	5 along the wall (see locations in Table 3.4, Chapter 3)

Table 5.6: OpenFOAM specific settings based on the simulated wave conditions

Specific settings	**Operational conditions**	**Extreme conditions**
Inlet relaxation zone	Length = 1.64 (13.86 m to 15.50 m) (1)	Length = 3.36 (12.14 m to 15.50 m) (1)
Outlet relaxation zone	Length = 0.82 (20.60 m to 21.42 m) (1)	Length = 1.68 (20.60 m to 22.28 m) (1)

(1) Distances from wave maker

Table 5.7: Tetrapods layer porous media settings based on the simulated wave conditions

Wave conditions	d_{n50} [m]	n_p [-]	α [-]	β [-]	KC [-]
Operational	0.08	0.5	200	1.1	2.19
Extreme	0.08	0.5	200 - 500 - 1,000	0.8 - 1.1 - 1.8	7.41 - 10,000

The wave conditions and numerical settings applied for each CoastalFOAM simulation are summarized in Appendix C.

5.3 Force measuring

The forces exerted on the front wall were recorded in two different ways in CoastalFOAM. First, a patch was created in the front wall (see blue sheet in Figure 5.11) to store the forces and moments experienced by the front face of the wall. These forces and moments are already integrated along the whole area. The second way of measuring the force at the wall is to follow the procedure performed in the physical modelling campaign; i.e. to place probes along the vertical axis of the wall to measure the pressure. Figure 5.12 shows the location of the probes in the numerical flume, which resembles as much as possible the placement in the physical tests (see Chapter 3, Table 3.4). The available information is only pressures recorded at five locations. Hence, the force results from the integration of these point data.

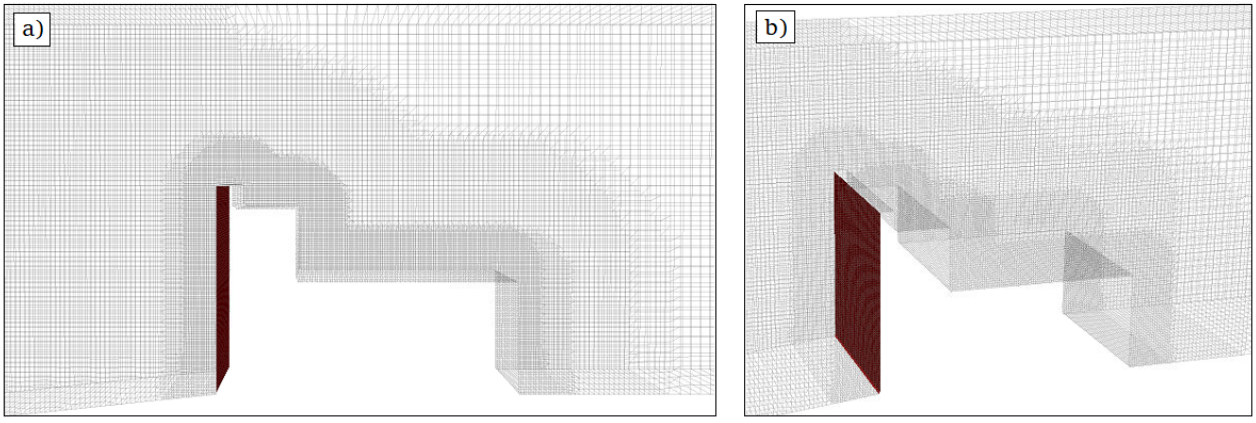

Figure 5.11: Measuring devices in the numerical flume: force patch integration in red
a) Front view, b) 3D view

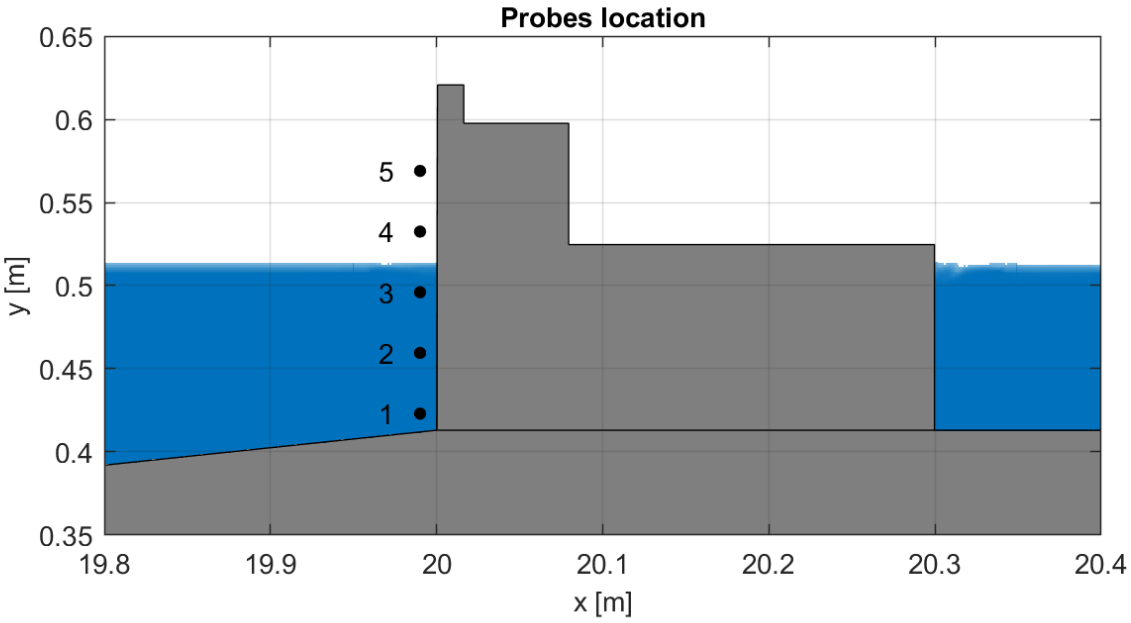

Figure 5.12: Measuring devices in the numerical flume: probes plotted as black dots in front of the wall
Numbering based on the physical test settings

Depending on the method used to calculate the forces in the numerical flume, different results were obtained. Figure 5.13 compares the forces between the experimental measurements and the two numerical force estimation methods. The comparison is made for operational and extreme conditions. In both cases, the probes integration approach mirrors better the experimental forces. The reason is that the patch integration method is based on the pressures recorded at each grid cell while the probes integration depends on only 5 pressure values, same as the experimental force. For the sake of comparison against the physical flume results, the probes integration method is selected. Nevertheless, the patch integration provides a better picture of the actual forces experienced by the wall under wave attack.

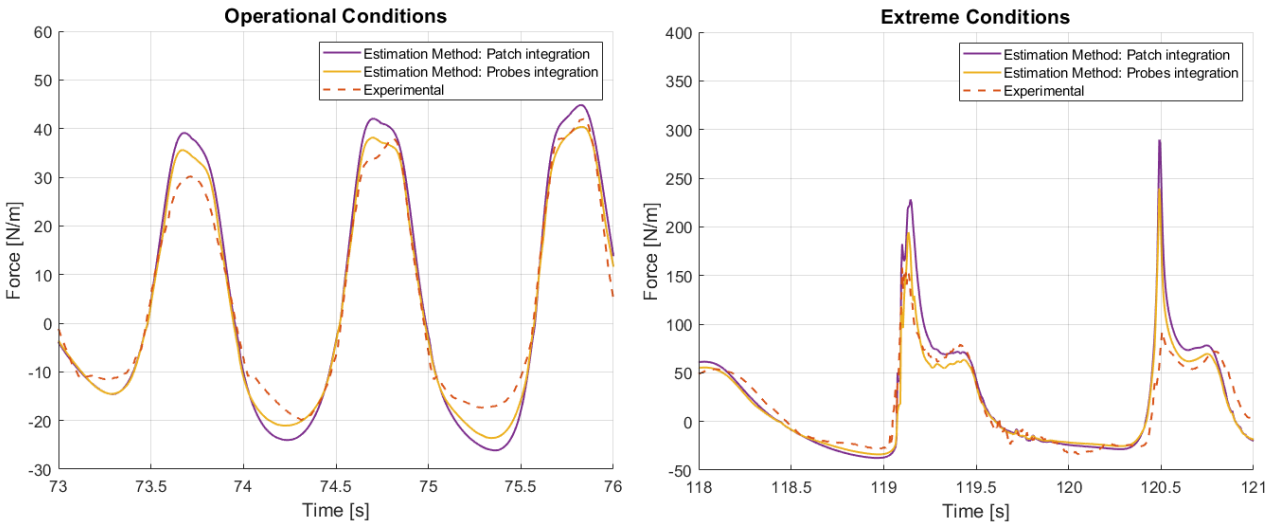

Figure 5.13: Comparison of force estimation methods available in OpenFOAM
Left panel: operational conditions time series from 73 to 76 seconds. Right panel: extreme conditions time series from 118 to 121 seconds. The experimental forces are obtained from pressure transducers integration.

Chapter 6

Model validation

6.1 Introduction

This chapter applies the numerical model, described in Chapter 5, for the four cases: baseline layout under operational and extreme conditions and Tetrapods layout under operational and extreme conditions. For each case, a detailed analysis of the water surface elevation close to the structure and of the dynamic forces experienced by the crown wall is included. All the simulations are compared against the physical modelling results, showing the capabilities of the numerical flume.

At first, the procedure followed to validate and calibrate the CoastalFOAM model is outlined. Followed by the results for the 4 cases. Two special settings are analysed in more detail. For the baseline layout under operational and extreme conditions, the influence of the ventilated boundary condition is studied by varying the degree of openness. For the Tetrapods layout subjected to extreme conditions, a sensitivity analysis of the porous media parameters is carried out. Additionally, the effect of including a simple turbulence model is considered for the baseline layout under extreme conditions.

6.2 Validation and calibration procedure

6.2.1 Validation procedure

The numerical model is validated by comparing the modelled surface elevation and pressures exerted on the wall against the measured time series in the physical model.

The validation procedure consists of the following steps:

Step 1: Alignment of the modelled and measured surface elevation and dynamic pressure time signals. This step is required because of the warm up period of $20s \pm 1s$ in the physical flume for the measuring devices (wave gauges and pressure transducers) from the wave maker starting time until the moment the waves reached the structure.

Step 2: Reflection analysis applying the method of Zelt and Skjelbreia (1993). 5 gauges (gauges 6-10 located just before the steep slope of the breakwater) were used to decompose the surface elevation in incoming and reflecting waves at the location of gauge 10 (2.4 m from the crown wall).

Step 3: Comparison of incoming surface elevation at gauge 10 in bulk wave statistics (H_{m0}, T_p), time domain and frequency spectrum.

Step 4: Time domain comparison of pressures and forces exerted on the wall (excluding the hydrostatic pressure). The probes integration approach was followed to calculate the forces in the numerical flume as explained in Chapter 5, Section 5.3. No filtering was applied in the numerical and experimental results. For comparison, the pressures and forces obtained numerically were resampled to the time step of the experimental data ($\Delta t = 0.005s$) to have the same sampling frequency in the experimental and numerical time series.

Step 5: Comparison of the pressure distribution (excluding the hydrostatic pressure) across the front face of the crest wall for different wave steepness, and for the impulse and reflecting pressures. This step is followed to evaluate if the numerical flume is able to capture the different pressure distributions according to the type of waves reaching the wall.

Step 6: Comparison of the force events. In step 4, the time signal of the wave induced forces were investigated. In this step, the force events are analyzed rather than the full time signal. The force events comparison is done event by event and in terms of exceedance probability curves (see detail explanation in Section 6.2.2).

6.2.2 Force event analysis

A force event is a pressure increase experienced by the wall as a result of the impact of a wave or a group of waves (see more details in in Chapter 2, section 2.2.2). In step 6 of the validation procedure, wave induced force events are analysed rather than the full time signals. In the design of the structure it is more important that the force events and even more that the maximum forces are correct rather than the full time signal.

To compare the physical and numerical results, the maximum forces exerted on the crest wall during each force event are selected. First, a peak over threshold (POT) method is followed to select the maximum forces. In this way, the force events are identified and only the highest value is sort out for each event. This procedure was carried out for the numerical and the experimental force time signals. Only the events captured by both models were kept for the event by event comparison and for the extreme value analysis (EVA), where the experimental and numerical data was fitted following an analytical distribution: the Generalized Pareto Distribution (GPD).

For the POT method, different threshold values were selected depending on the validation case. For the baseline layout and Tetrapods layout under operational conditions, the threshold was set at 3 N/m. For the baseline layout under extreme conditions, the threshold was defined at 20 N/m and for the Tetrapods layout under extreme conditions, at 10 N/m. The selection procedure followed in this research is considered valid because only the smaller force events are sometimes neglected depending on the numerical settings; thus, the more relevant information for the design process of the crown wall is always included in the extreme value analysis.

The number of force events is not only dependent on the duration of the test but also on the structure itself. To be able to compare different structures (or different numerical settings), the exceedance probabilities are based on the number of waves (N_{waves}) reaching the structure during the simulated time frame:

$$P = \frac{r}{N_{waves} + 1} \tag{6.1}$$

Here, r is the rank of the sample, once ordered from largest to smallest. The number of incident waves were defined at gauge 10, located 2.4 m from the crest wall just before the steep slope of the breakwater. Gauge 10 was selected because the wave decomposition method is limited to non-sloping bottom profiles.

6.2.3 Calibration procedure

The calibration process resorted to vary specific settings in the numerical flume. For the baseline layout cases, the model calibration was based on modifying the degree of openness of the ventilated boundary condition. For the Tetrapods layout cases, the model calibration involved testing different combination of porous media parameters. For this research, the wave paddle signal was not calibrated. It was only necessary to apply the FFT signal reconstruction method, as explained in Chapter 5, section 5.2.2.

The selection of optimal settings was then determined by comparing the force events (in terms of exceedance probabilities, procedure detailed in Section 6.2.2).

6.3 Validation case: Baseline layout

This section studies the wave climate characteristics and the wave-structure interaction under operational and extreme conditions for the impermeable breakwater. For each validation case, Steps 3 to 6 of the validation procedure outline in Section 6.2.1 are presented. Steps 1 and 2 are not included in this section but were performed for each validation case.

The results of the numerical model under breaking and non-breaking waves shown in Sections 6.3.1 and 6.3.2 were obtained using the following settings:

Table 6.1: Case specific settings for Baseline layout under operational and extreme conditions

Simulation	Wave climate	Turbulence model	Degree of openness	Loss coefficient
BO03	Operational	No	3%	1.5
BE05	Extreme	No	3%	1.5

More information about the numerical settings can be found in Appendix C.

6.3.1 Hydraulic conditions: Operational

For the operational conditions with high water level (water depth of 0.513 in model scale), the waves present a behaviour closer to a partially standing wave pattern. The high reflection is induced by the impermeable structures and the non-breaking nature of the waves (exemplified in Figure 6.1).

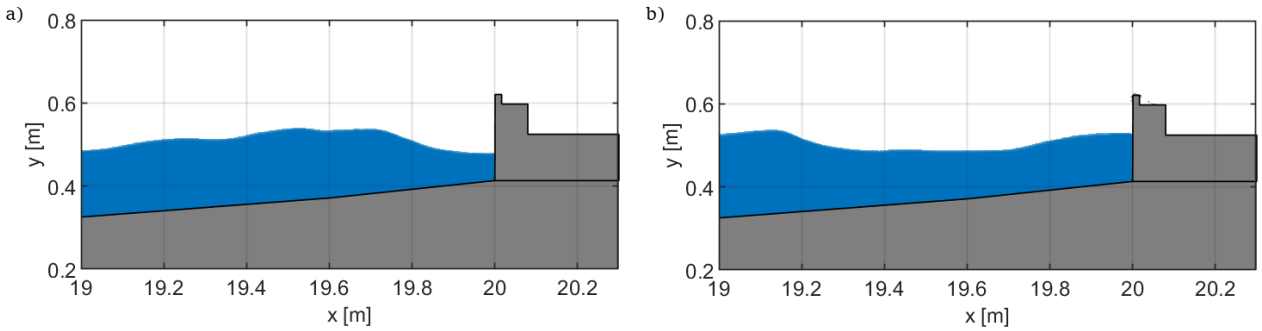

Figure 6.1: Wave reflection under operational conditions
a) Wave set-down. b) Wave set-up

Figure 6.2 shows the incident water surface elevation, recorded in the physical and numerical flume at wave gauge 10, in frequency and time domain. A close look to the spectrum analysis indicates that the wave energy at gauge 10 for all frequencies is fairly captured by the numerical flume. Differences of less than 5.0% and 1.5% were found between the modelled and measured significant wave height and peak period, respectively. A comparison of the time signal of incident surface elevation measured in both models shows that the CoastalFOAM model is able to reproduce the wave conditions generated during the physical modelling campaign for a mild wave climate. The Pearson correlation coefficient was estimated to express the accuracy of the model in terms of shape. For this specific simulation, a correlation of 0.91 verifies that the behaviour of the signal overall the simulation time is well captured by CoastalFOAM model.

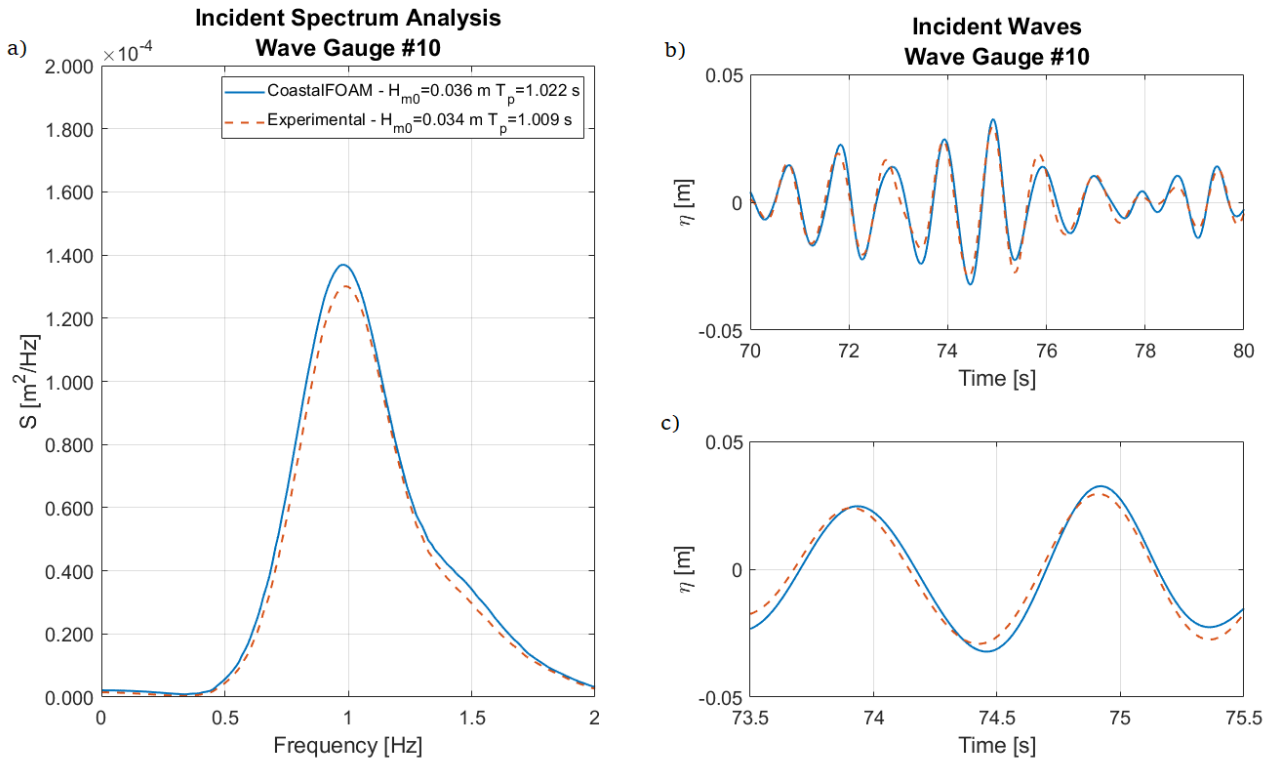

Figure 6.2: Incident water surface measured at wave gauge 10 located 2.4 m from the front face of the crest wall for the baseline layout under operational conditions
a) Smooth energy spectrum including the significant wave height and peak period, b) time series of incident waves captured between 20-30 s and c) zoom in of time series of incident waves between 26-30 s.

Figure 6.3 presents the time signals of the wave induced pressures and forces for the physical and numerical flume. In general, the same behaviour is shown. When the pressure sensors are analysed in more detail (see density scatter plot in Figure 6.4), it is noted that the first 3 pressure transducers have a smaller difference between the experimental and numerical measurements than the other pressure sensors. This is because the first 3 pressure sensors are located below the still water level while the fourth and fifth sensors are located above the still water level (see sensors placement in Chapter 5, Figure 5.12). Around the water level the simulation of the water movement is much more complex because complex processes like air entrapment become more important. This explains the increase in error. Since the main pressures exerted by the waves happened below and at the still water level, the overall behaviour of the dynamic forces is well predicted by the numerical model. This is portrayed by a Pearson correlation coefficient of 0.91. Figures 6.3 and 6.4 also indicate that along the same numerical simulation; underpredictions and overpredictions of wave induced pressures are displayed depending on the pressure sensor and on the force event.

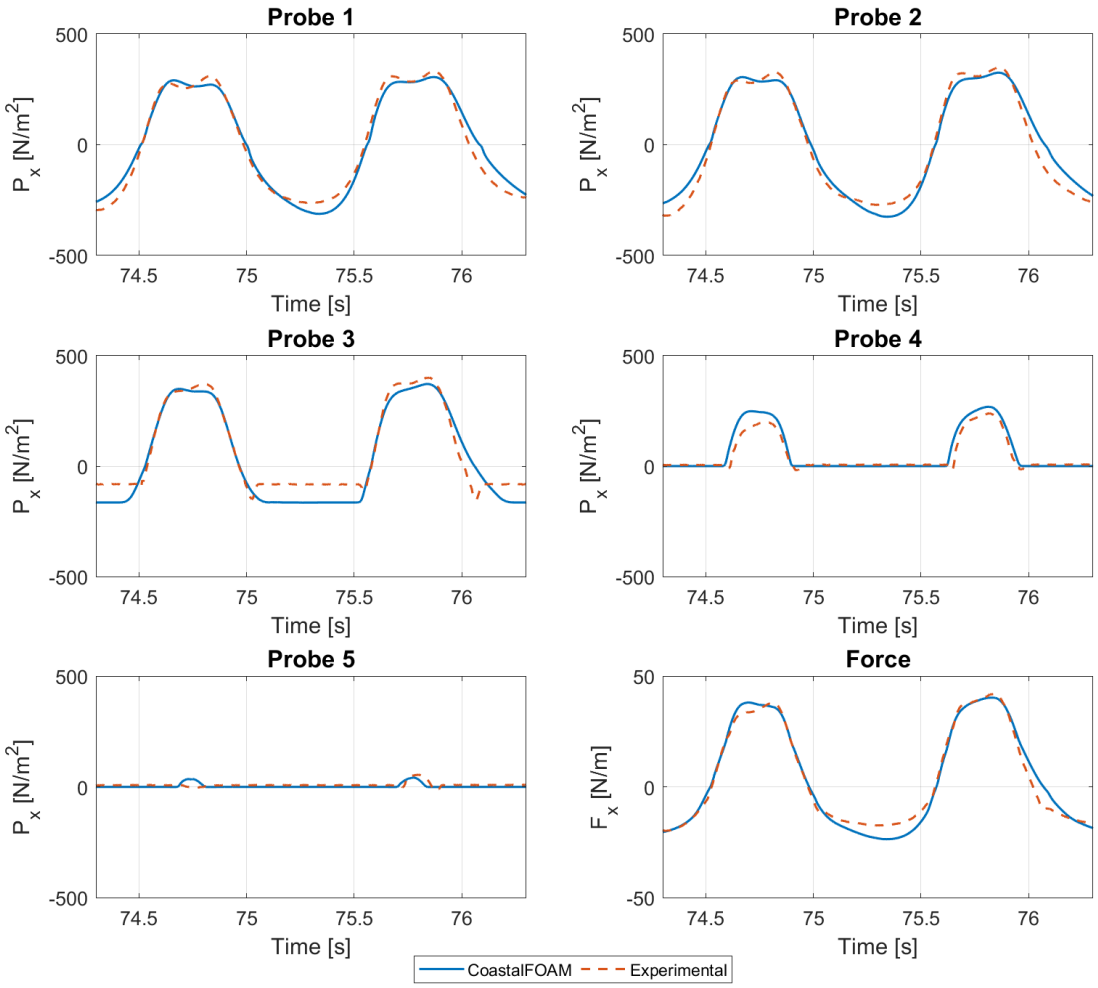

Figure 6.3: Comparison of the simulated and experimental pressure and force time series for baseline layout under operational conditions

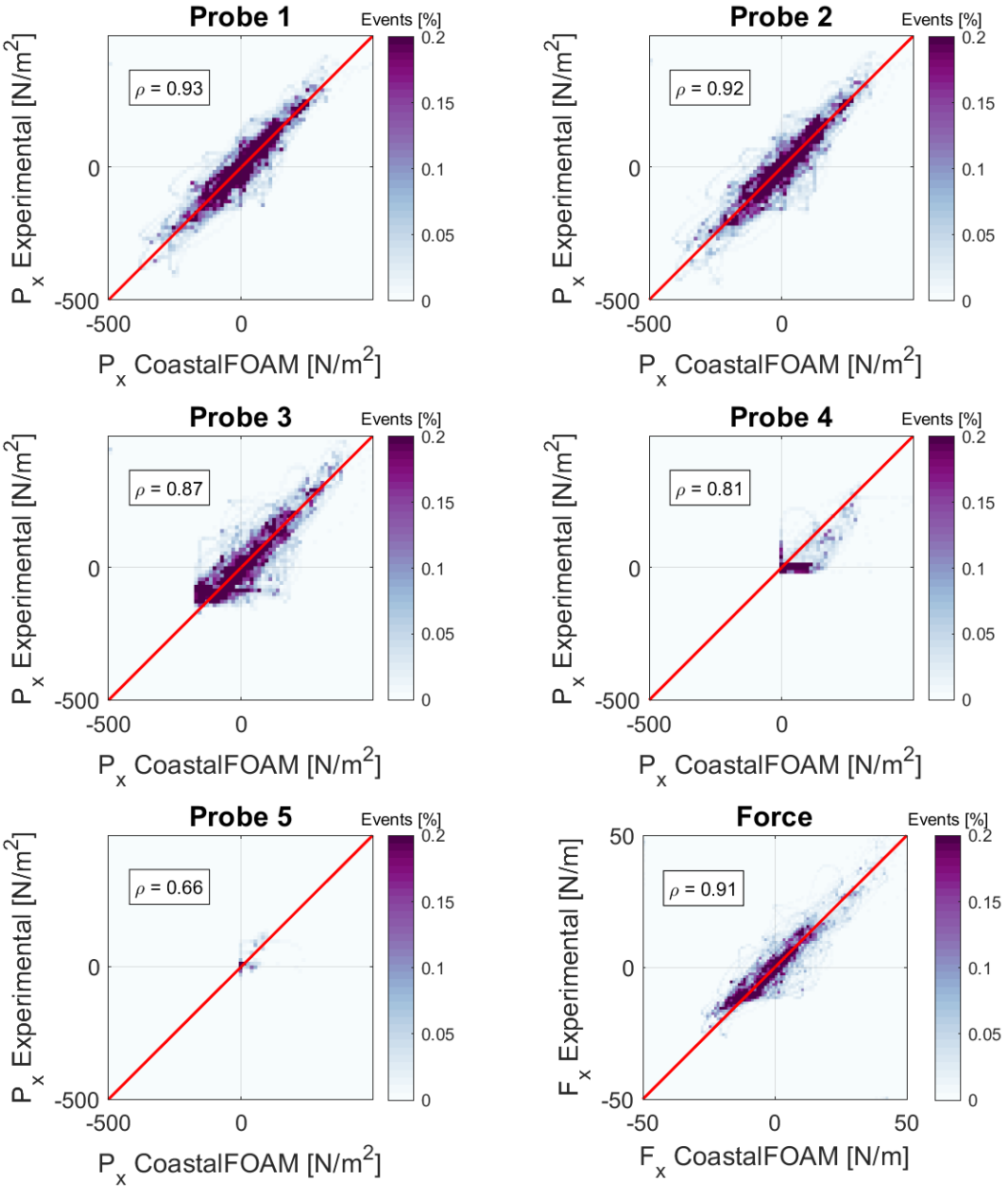

Figure 6.4: Density scatter plot comparing the simulated and experimental time series of pressure and force exerted on the vertical face of the crown wall for the baseline layout under operational conditions The Pearson correlation coefficient is displayed for each pressure transducer and for the dynamic force integration. Negative and zeros values appeared because the hydrostatic pressure is removed from the signal. The color scale represents the percentage of events falling in each grid point.

To verify that not only the temporal distribution but also the spatial distribution of the pressures across the front face of the wall are fairly reproduced, the pressure distribution measured during two different force events is presented in Figure 6.5. The comparison between the experimental and numerical pressures shows that the numerical model is in good agreement with the experimental measurements, displaying the same shape for the pressure distribution for different wave impacts. For the specific cases shown in Figure 6.5, the numerical model underpredicts the pressures in the pressure sensors located below still water level.

The spatial distribution of the pressure is important for the evaluation of overturning stability during design stages. From the pressure distribution along the vertical wall, the application point of the force can be obtained.

For the both cases displayed in this report, the force is applied 0.48 m from the base of the wall.

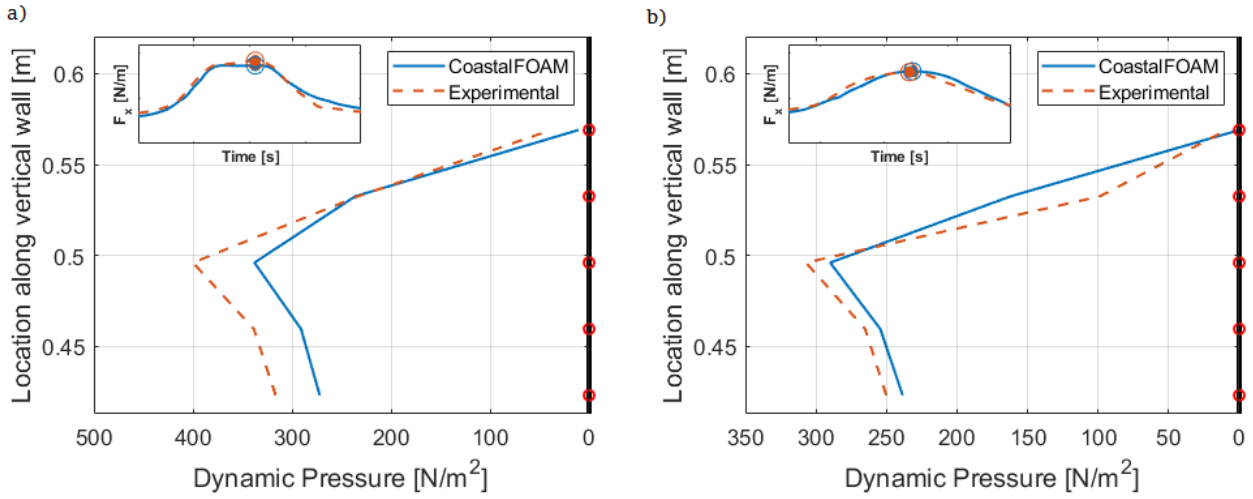

Figure 6.5: Distribution of pressure along the vertical wall for two different force events denoted as a) and b), for the baseline layout under operational conditions
The red circles are the pressure sensors and the black line is the front face of the wall. In the graph located in the upper left corner, the force event in the time domain is illustrated. The orange and blue circles represent the moment in time where the pressure distribution is extracted

The correlation between the pressures and integrated forces is good to get the overall behaviour. However, it is influenced by two factors: the alignment of the modelled and measured time signals and the zero and negative values recorded at each pressure sensor. Dynamic pressures of zero are recorded by the pressure sensors located above the still water level, where the wave attack impacts that location not that often. Negative pressures are recorded because the hydrostatic pressure is removed from the time signal. The zero and negative pressures are also associated to times where no waves are hitting the structure. Thus, to have an insight into the maximum wave induced pressures and forces, the force events are studied. In this way, the above effects are neglected. Furthermore, an accurate prediction of the force events is interesting for the design process.

A comparison between the modelled and measured force events resulted in a RMSE (Root Mean Square Error) of 4.9 N/m and a Pearson correlation coefficient of 0.91. For these specific settings, 4 force events were not included in the force event analysis because they were not captured by the numerical flume. The magnitude of 3 of those events is lower than 4.5 N/m while the fourth event has a magnitude of approximately 7.6 N/m. As stated in section 6.2.2, only small force events are neglected, thus, the more relevant information for the force event analysis is always considered.

Figure 6.6 compares statistically the force events captured by the physical and numerical model. In this case, the numerical flume overpredicts the highest wave induced forces because the GPD fit is influenced by the maximum force event. In general, the predictions lay inside the 50% error band.

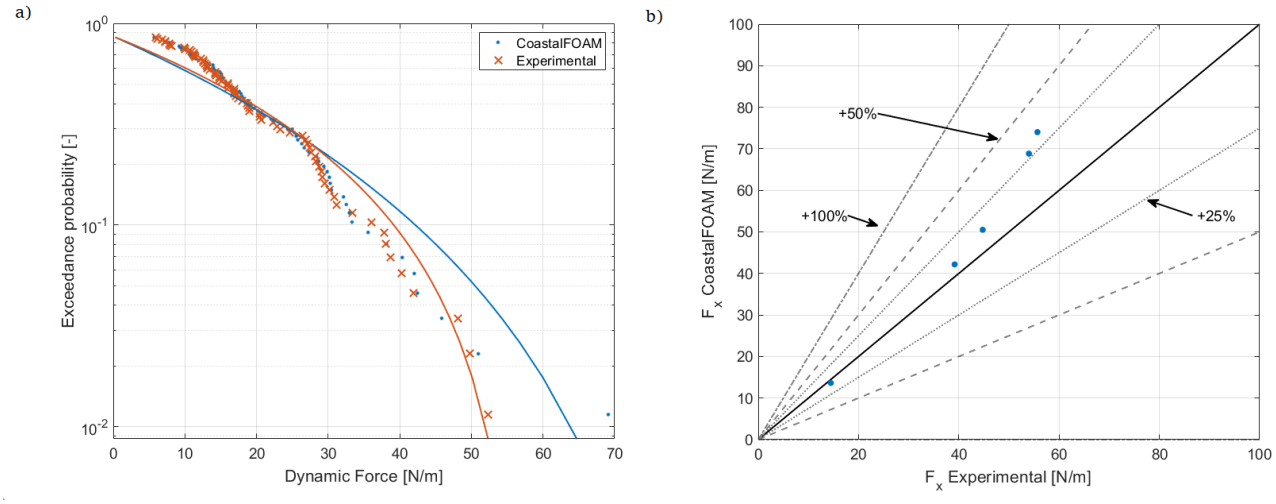

Figure 6.6: Experimental and numerical force events comparison for the baseline layout under operational conditions
a) GPD fitted curves, b) Comparison of the wave induced forces with the 85%, 50%, 10%, 5%, 0.4% and 0.1% exceedance probabilities based on the GPD. The 25%, 50% and 100% error bands are included.

6.3.2 Hydraulic conditions: Extreme

For the extreme wave climate, the water depth is the same as in the operational conditions. In the extreme conditions, due to a higher value of H_{m0} and T_p, partially standing waves, slightly breaking waves, heavily breaking waves and already broken waves hit the structure. Figure 6.7 shows an example of a plunging wave that breaks just before reaching the structure. The air entrapment as a result of the wave overturning and the water mass splashing above the crown wall are captured by the numerical model.

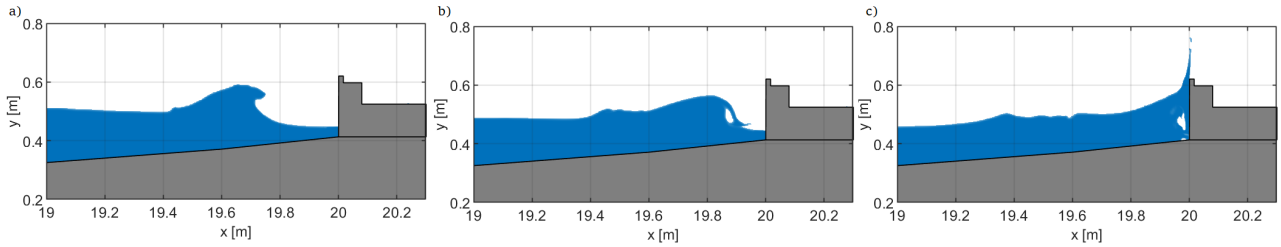

Figure 6.7: Wave breaking under extreme conditions
a) Plunging wave, b) wave bore and c) broken wave hitting the crown wall

Figure 6.8 shows the incident water surface elevation, recorded in the physical and numerical flume at wave gauge 10, in frequency and time domain. The spectrum analysis stipulates that the wave energy at gauge 10 for frequencies below 0.8 Hz is fairly captured by the numerical flume. Unlike the results shown for the operational conditions (Section 6.3.1), in this validation case there is an underestimation of the wave energy for waves with frequencies above 0.8 Hz. These higher frequencies with smaller wave heights are resolved at most by 12 cells/wave height, decreasing to almost 1 cell/wave height for the smaller waves. In the horizontal direction, there are more than 80 cells/wave length. The lower frequencies with small wave heights also experienced a resolution decrease in cells/wave height but not in cells/wave length. Thus, it appears that the number of cells/wave length is not sufficient to resolve the high frequency waves in the CoastalFOAM model for an extreme wave climate. This happened because the mesh optimization process focused on representing properly the highest waves.

Looking at the bulk wave statistics, differences of less than 3.0% and 1.5% were found for the significant wave height and peak period, respectively. In the time domain, Figure 6.8b and Figure 6.8c demonstrate that the CoastalFOAM model is able to reproduce the wave conditions generated during the physical modelling campaign for an extreme wave climate. A correlation coefficient of 0.92 proves that the overall shape of the time signal can be reproduced by the numerical flume.

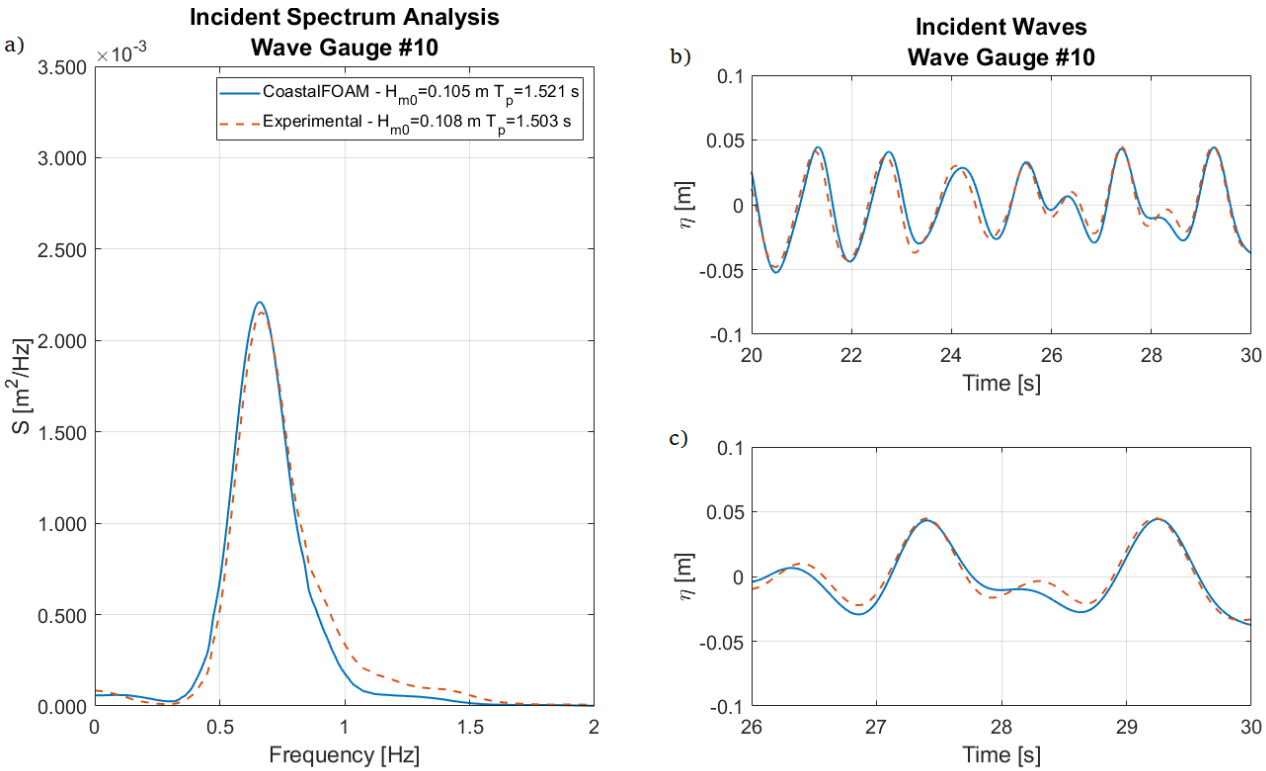

Figure 6.8: Incident water surface measured at wave gauge 10 located 2.4 m from the front face of the crest wall for the baseline layout under extreme conditions
a) Smooth energy spectrum including the significant wave height and peak period, b) time series of incident waves captured between 20-30 s and c) zoom in of time series of incident waves between 26-30 s.

The forces experienced by the front face of the crown wall subjected to extreme conditions are higher and more variable than during operational conditions. When the waves break on the slope, a lot of energy is already dissipated before reaching the wall; resulting in a lower dynamic force compared to the case when the waves break onto the wall. For non-breaking waves, a more gentle pressure increase is present, leading to less extreme forcing (as described in Section 6.3.1). Bullock et al. (2007) described that the higher pressure impacts are caused by wave conditions in the range between slightly breaking and broken waves. In this case, a rapid increase in the pressures is experienced by the vertical structure.

The capabilities of CoastalFOAM to simulate wave-structure interaction under extreme conditions are illustrated in Figures 6.9 and 6.10; where a comparison between the experimental and numerical pressures and dynamic forces is made. In the time domain, the shape of the pressures exerted on the wall at each location is well-captured by the numerical model. However, the high-peak impacts are in some cases underpredicted (as exemplified in Figure 6.9) or overpredicted by the model. This happens because the wave motion just in front of the wall has a large influence on the dynamic pressure experienced by the wall. The overprediction is better represented by the density scatter plot. The correlations exhibit the same behaviour as in the operational conditions; i.e., the pressure sensors 1-3 have higher correlations than the pressure sensors 4 and 5. Again, this is due to the location of the pressure transducers in the numerical and physical flume (see sensors placement in Chapter 5, Figure 5.12). The farthest the sensor is from the still water level, the harder is to predict the wave impact by the numerical flume. For extreme conditions, the numerical predictability of the dynamic forcing lowers to a correlation of 0.71.

As observed from the results, an accurate prediction of the pressures at the wall is difficult to achieve. An exact reproduction of the wave breaking pattern and of the breaking location must be delivered by the numerical model because these wave characteristics have a direct influence on the impact pressures.

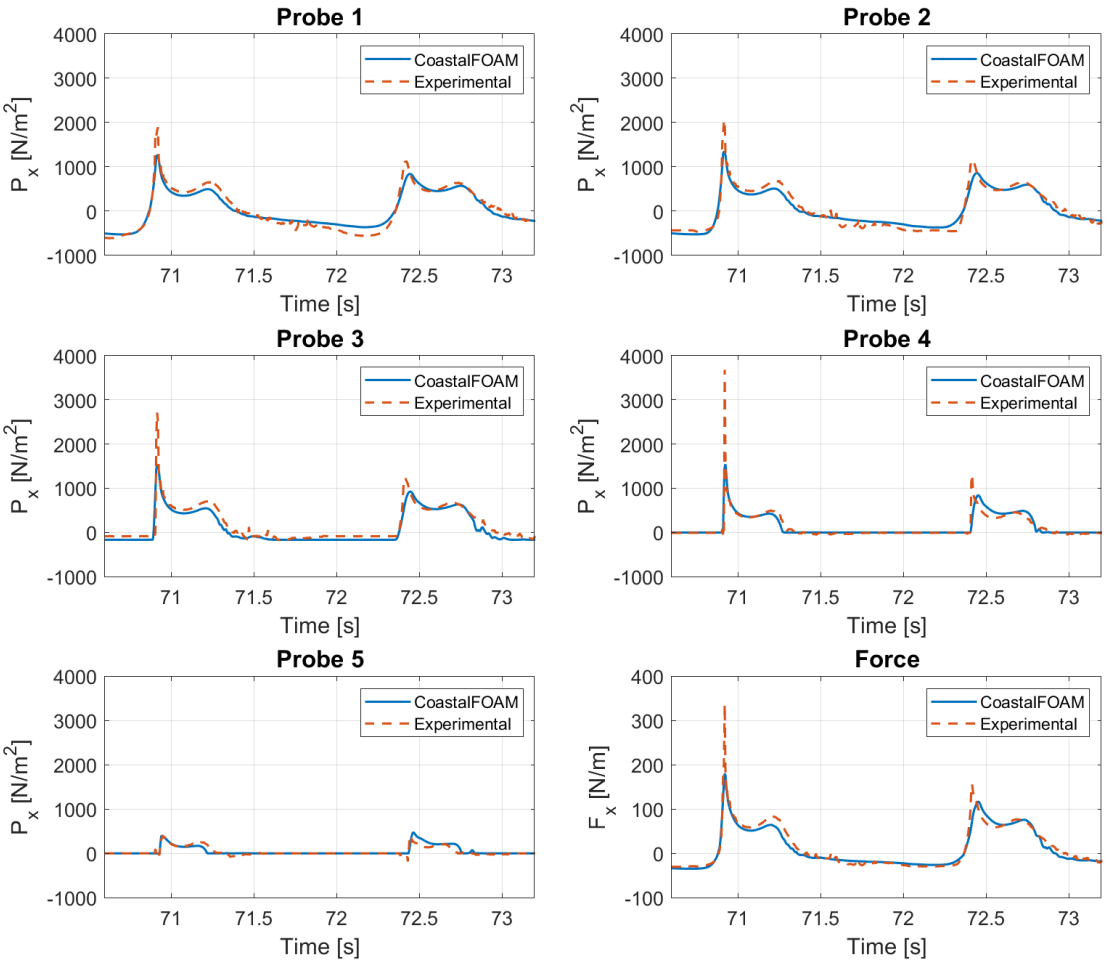

Figure 6.9: Comparison of the simulated and experimental pressure and force time series for the baseline layout under extreme conditions

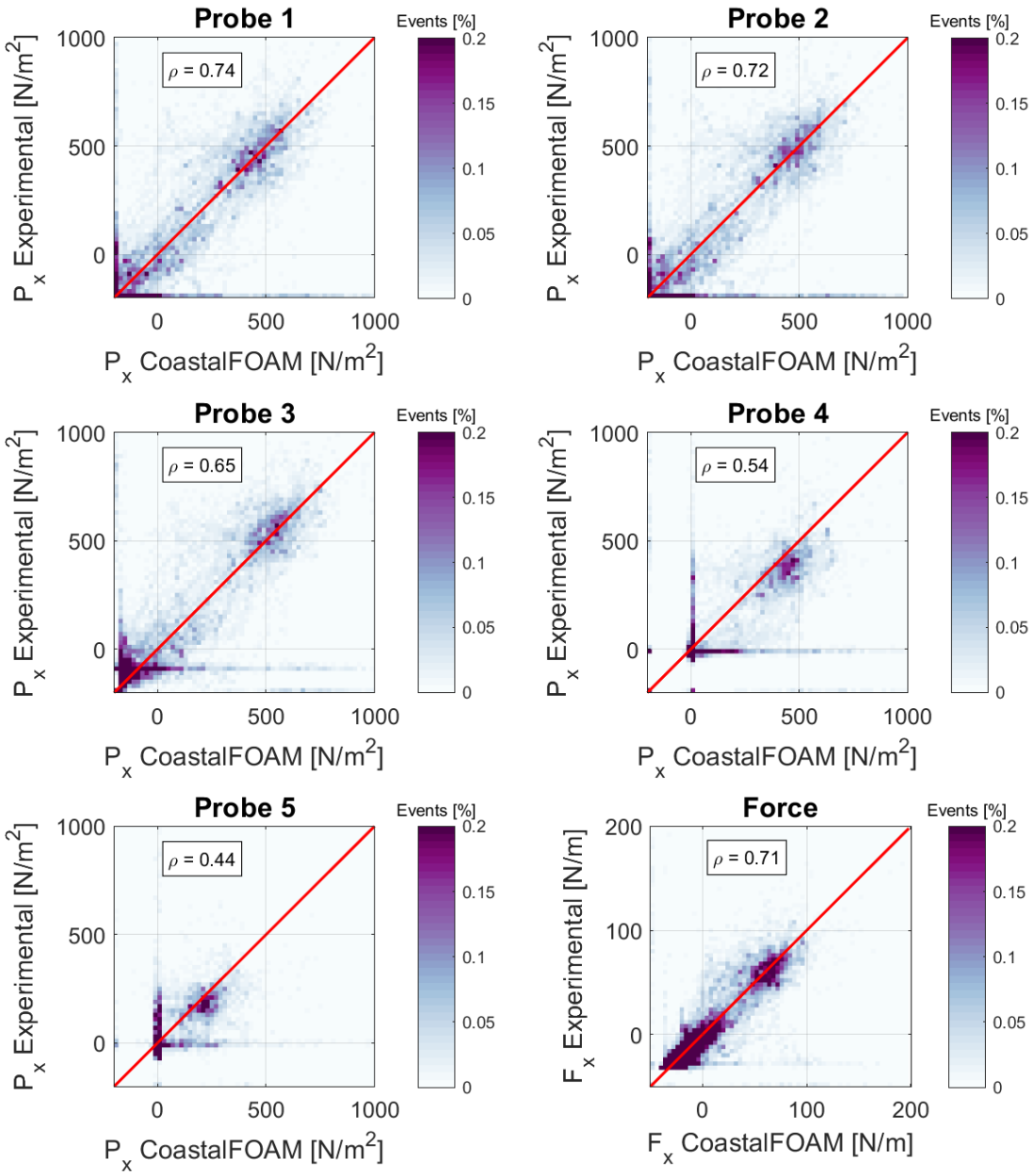

Figure 6.10: Density scatter plot comparing the simulated and experimental pressure and force exerted on the vertical face of the crown wall for the baseline layout under extreme conditions
The Pearson correlation coefficient is displayed for each pressure transducer and for the dynamic force integration. Negative and zeros values appeared because the hydrostatic pressure is removed from the signal. The color scale represents the percentage of events falling in each grid point

Figure 6.11 shows a force event where the classic church-roof shaped signal was captured by the physical and numerical models. This force event is associated to a very steep incoming wave. The duration of the impulse pressure caused by the abrupt change of direction of the water mass is less than 0.01 s. The reflecting pressure originated after the wave run-up and the water mass down rushing the wall displays a more quasi-static behaviour (see explanation in Chapter 2, section 2.2.2).

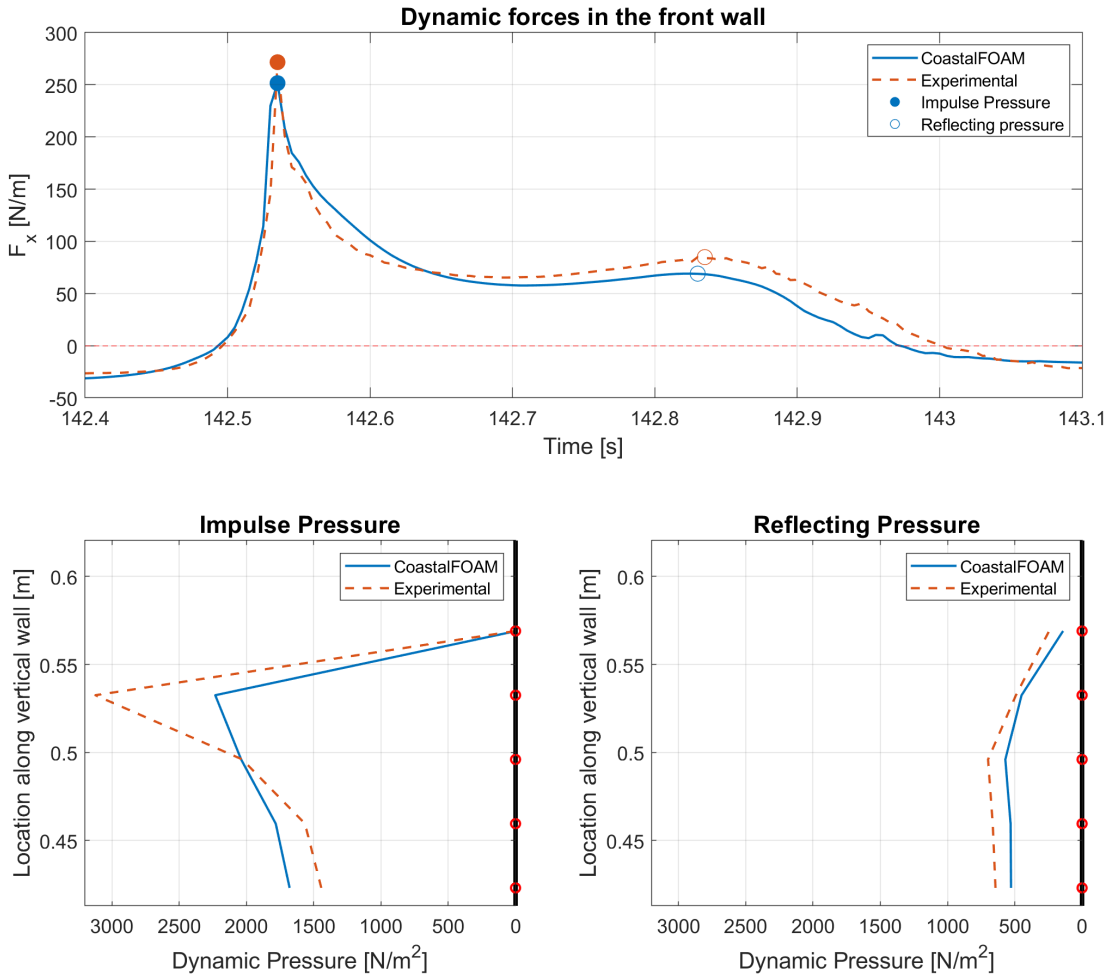

Figure 6.11: Force event and pressure distribution along the vertical wall caused by a highly steep wave under extreme conditions
a) Typical church-roof shaped signal. The filled circles represent the impulse forcing and the hallow circles, the reflecting forcing. b) Impulse pressure distribution. c) Reflecting pressure distribution. The red circles are the probes and the black line is the front face of the wall

The comparison between the experimental and numerical pressure distribution of the impulse and reflecting pressure associated to a force event indicate that the numerical spatial distribution is in good agreement with the experimental measurements. For the impulse and reflecting pressure, the point of application of the force is defined 0.49 m from the base of the wall, for the numerical and experimental measurements. For this specific force event, larger differences were found for the impulse pressure, where the numerical model overpredicts the pressures in the pressure sensors located below still water level. For the sensor 4, located just above still water level (see sensors placement in Chapter 5, Figure 5.12), there is an underprediction in the numerical model of approximately 30% for the impulse pressure. These differences in the spatial distribution of the impulse pressure may be caused by differences in the wave motion just in front of the wall and by the high spatial variability of the breaking wave induced pressures. Depending on the numerical settings, as it is addressed in Section 6.4, underpredictions or overpredictions of wave induced pressures are displayed along the entire simulation.

The modelled and measured force events are compared. For this validation case, a RMSE of 215.81 N/m and a Pearson correlation coefficient of 0.45 are obtained. There is a notable decrease in accuracy compared to the operational conditions simulation. For these specific settings, 6 force events were not included in the force event analysis because they were not captured by the numerical flume. The magnitude of 3 of those events is lower than 15 N/m. Two of the neglected force events have magnitudes below 25 N/m while one event has a magnitude of approximately 74 N/m. In line with the statement indicated in section 6.2.2, the more relevant information for the force event analysis is always considered.

Figure 6.12 compares statistically the force events captured by the physical and numerical model. For these specific settings, the numerical flume underpredicts all the wave induced forces. In general, the predictions lay in the 25% error band.

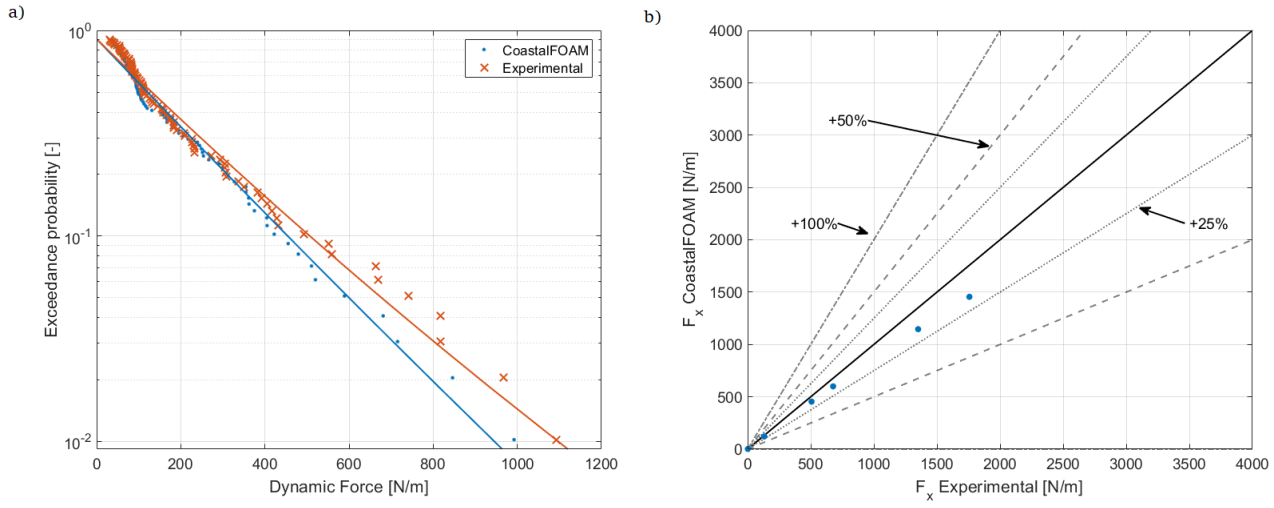

Figure 6.12: Experimental and numerical force events comparison for the baseline layout under extreme conditions
a) GPD fitted curves, b) Comparison of the wave induced forces with the 85%, 50%, 10%, 5%, 0.4% and 0.1% exceedance probabilities based on the GPD. The 25%, 50% and 100% error bands are included.

6.4 Sensitivity analysis: Ventilated boundary condition

An important setting of a CoastalFOAM model is the ventilated boundary condition. This setting influences the wave induced forces on the crown wall. In section 6.3, the degree of openness was set at 3.0%, as recommended by Jacobsen et al. (2018). To gain insight on the ventilated boundary condition, a detailed sensitivity analysis of the influence of varying the degree of openness (see definition in Chapter 4, Section 4.2.5) in the wave induced forces was included in this report. Furthermore, the effect of including or excluding the ventilated boundary condition based on the wave field is also addressed.

6.4.1 Hydraulic conditions: Operational

Under non-breaking waves, the influence of the ventilated boundary condition and different degrees of openness was studied. For the sensitivity analysis, a time frame of 100 s including 87 waves was simulated in CoastalFOAM. The degree of openness was changed between 0.5% and 6.0%. Besides, a simulation excluding the ventilated boundary condition was also executed.

Figure 6.13 exhibits the incident wave motion in the frequency and in the time domain at gauge 10, located 2.4 m from the front face of the crest wall, in the numerical and physical flume. The accuracy of the model is depicted in the time interval $t \in [70, 80]$. Table 6.2 summarizes the bulk wave statistics and the time signal correlation between the experimental and numerical incident water surface. For all the simulations, the correlations are above 0.90. For the different degrees of openness, the peak period and significant wave height were represented by the numerical flume with an error of less than 1.5% and 5%, respectively. For the reflection coefficient, the differences are larger. The results show that a higher degree of openness, associated with more aeration, results, as expected, in less wave reflection. For the case without the ventilated boundary condition, the reflection is highest since no aeration is present through the concrete wall. This was confirmed by the numerical flume, with a total reflection of the incident wave field.

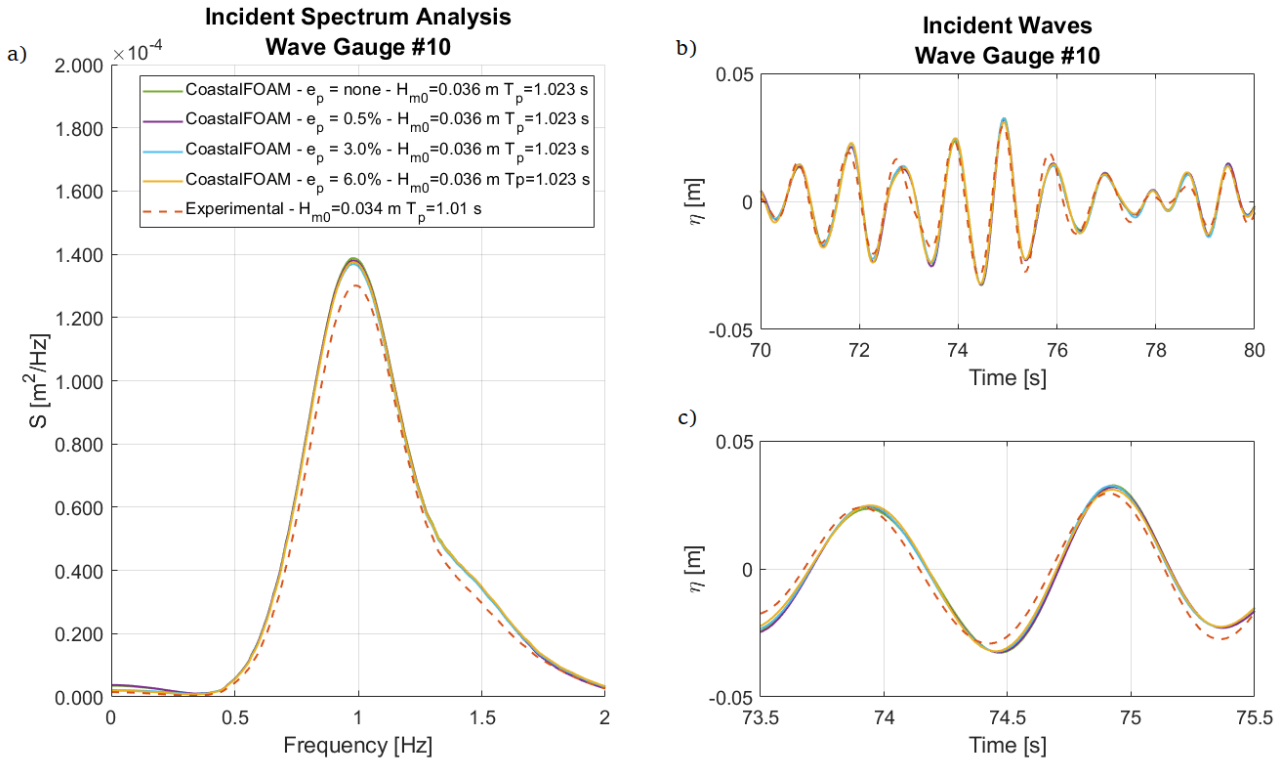

Figure 6.13: Incident water surface measured at wave gauge 10 located 2.4 m from the front face for different degrees of openness of the wall for the baseline layout under operational conditions
a) Smooth energy spectrum including the significant wave height and peak period, b) time series of incident waves captured between 70-80 s and c) zoom in of time series of incident waves between 73.5-75.5 s.

Table 6.2: Wave characteristics under operational conditions at Wave Gauge 10

Simulation	**Degree of openness**	**Kr [-]**	T_p **[s]** (1)	H_{m0} **[m]** (1)	$\rho\,\eta$ **[-]** (2)
BO01	None	1.00	1.02	0.036	0.92
BO02	0.50%	0.99	1.02	0.036	0.91
BO03	3%	0.86	1.02	0.036	0.91
BO04	6%	0.73	1.02	0.036	0.91
Experimental	[-]	0.91	1.01	0.034	[-]

(1) Incident Wave Conditions
(2) Pearson correlation coefficient considering all time series

The implementation of the ventilated boundary condition and the degree of openness of the wall affect the reflection caused by the impermeable breakwater and crest wall. Therefore, it also affects the wave motion near the wall and consequently the wave impact on the vertical structure. A comparison of the dynamic forces in the time domain is displayed in Figure 6.14, where two time frames are included. In the interval 73.5-78.5 s, a few steep waves reached the wall compared to the time frame between 28-33 s. This is noticed because in the second time interval, for the last two force events, the wave induced forces display a more asymmetric double peak behaviour. The results shown in Figure 6.14 confirm that the CoastalFOAM model is able to capture the timing and magnitude of the dynamic forces with more or less accuracy depending on the settings of the model (see wave induced forces time signal correlation coefficient in Table 6.3). For different degrees of openness and for the simulation without the ventilated boundary condition, there is not a significant difference in the outcome of CoastalFOAM when the full time series are analysed.

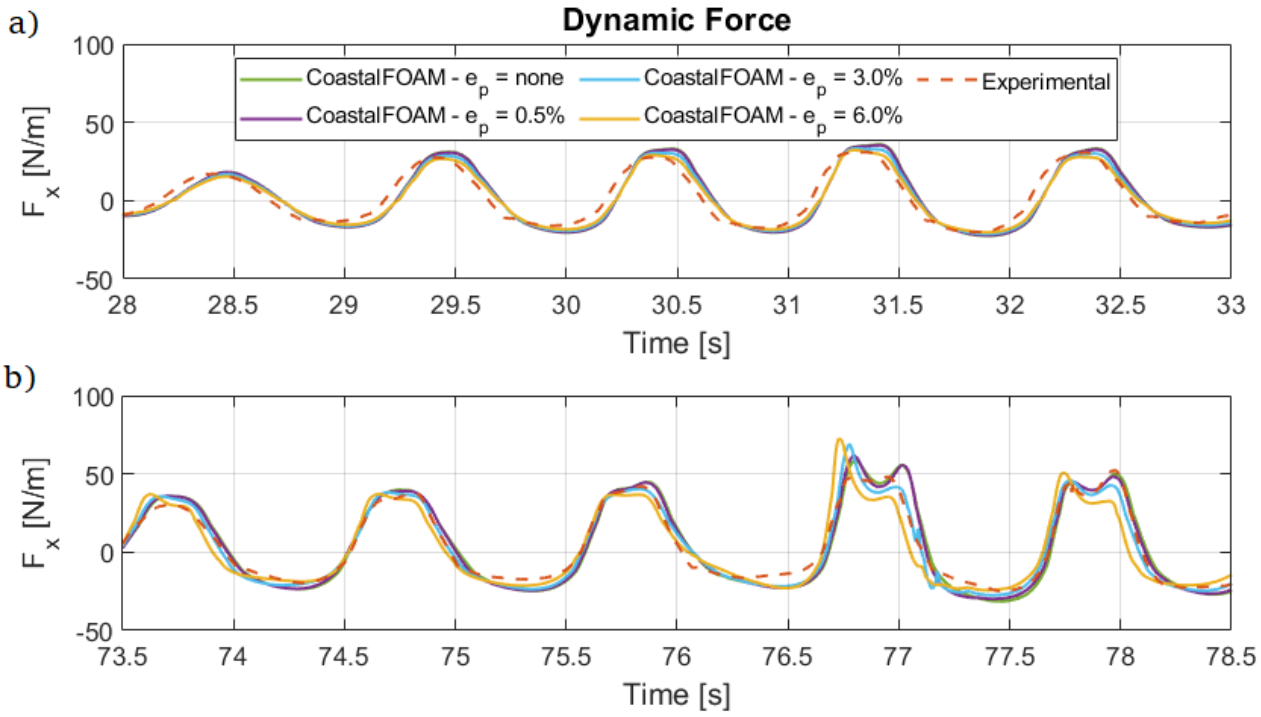

Figure 6.14: Time series of dynamic forces on the front face of the crown wall for different degrees of openness of the wall for the baseline layout under operational conditions
Comparison between experimental and numerical results. a) Time frame: 28-33 s, b) time frame: 73.5-78.5 s.

Table 6.3: Pearson correlation coefficient between experimental and numerical dynamic forces time series with different degrees of openness under operational conditions

Degree of openness	**None**	**0.50%**	**3.0%**	**6.0%**
ρ **Dynamic Forces**	0.91	0.93	0.91	0.90

The force event analysis is summarized in Table 6.4. When comparing event by event, the simulation with a degree of openness of 0.5% has the lower RMSE and the highest correlation, with a value of 0.93. Nonetheless, the results form the numerical flume are not that sensible to variations in the degree of openness of the wall. For all the simulations, correlations above 0.88 and RMSE below 6 N/m are obtained.

Table 6.4: Root Mean Square Error and Pearson correlation coefficient between experimental and numerical force events with different degrees of openness under operational conditions

Degree of openness	**RMSE (N/m)**	**Pearson Correlation**
None	4.90	0.93
0.5%	4.77	0.93
3.0%	4.93	0.91
6.0%	5.80	0.88

The exceedance curves for the force event analysis are presented in Figure 6.15. The left panel presents the maximum force events and the GPD fitted distribution while the right panel compares directly the numerical against the experimental maximum predicted forces. In all cases, the force events are predicted with an error lower than 50%.

A close look to the highest force event modelled in the numerical flume shows that for the numerical simulations with a degree of openness of 3.0% and 6.0%, there is just one force event that moves the fitted curves towards higher forces. As a result, these two simulations end up overpredicting the wave induced forces. Moreover, it affects the expected behaviour from the ventilated boundary condition. Now, when using these GPD fitted

curves, the wave induced forces for the lowest exceedance probabilities (0.4% and 0.1%) are larger than the case without ventilated boundary condition.

Focusing only on the other numerical simulations ($e_p = 0.5\%$ and $e_p = none$), a similar trend is identified. A lower ventilation through the wall exhibits the same behaviour as no ventilation through the wall.

Given these results, no recommendation can be drawn for the value of the degree of openness when the breakwater is subjected to normal conditions. By using any value for the degree of openness or even by excluding this boundary condition, a numerical model with enough accuracy is obtained.

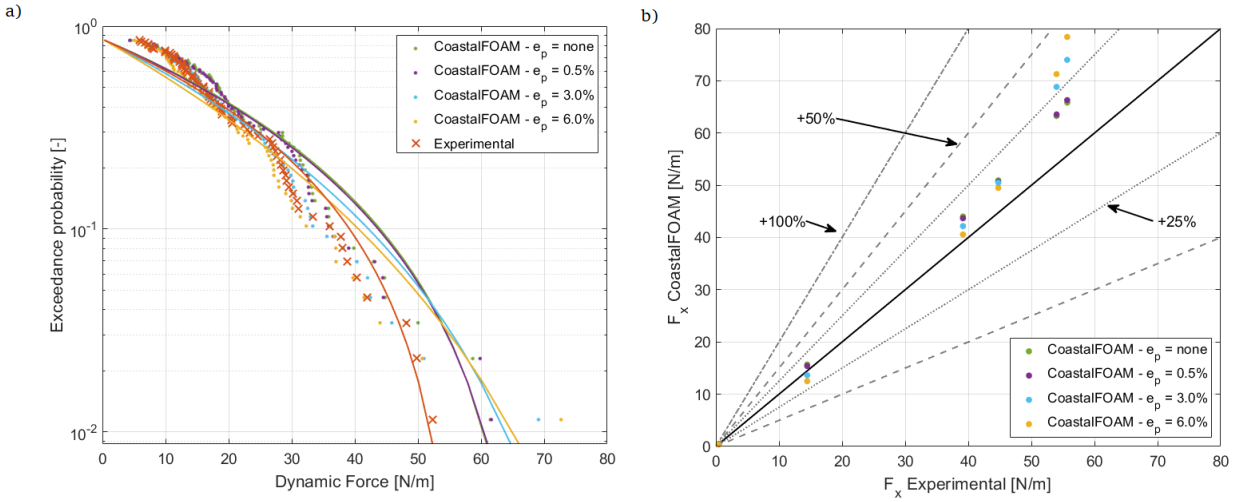

Figure 6.15: Experimental and numerical force events comparison for various degrees of openness for the baseline layout under operational conditions
a) GPD fitted curves, b) Comparison of the wave induced forces with the 85%, 50%, 10%, 5%, 0.4% and 0.1% exceedance probabilities based on the GPD. The 25%, 50% and 100% error bands are included.

6.4.2 Hydraulic conditions: Extreme

Under heavily breaking waves, the influence of the ventilated boundary condition and different degrees of openness was also studied. For the sensitivity analysis, a time frame of 150 s including 98 waves was simulated in CoastalFOAM. The degree of openness was changed between 0.001% and 6.0%. A simulation removing the ventilated boundary condition was also tested.

Figure 6.16 depicts the incident wave spectrum and the surface elevation measured in the time interval 20-30 s at gauge 10. The bulk hydrodynamics and the time signal correlation between the experimental and numerical incident water surface are summarized in Table 6.5. For different degrees of openness and for the simulation excluding the ventilated boundary condition, the time series correlations for the incident surface elevation registered 2.4 m away from the front face of the crest wall are above 0.90. The peak period and significant wave height were represented by the numerical flume with an error of less than 1.2% and 5%, respectively. In line with the results obtained for the normal conditions, the differences in the reflection coefficients are larger than 5%. As derived from Section 6.4.1, more aeration through the wall implies less wave reflection. The results show that there are no significant differences in the incident wave attack, at a location before the foreshore, for different degrees of openness.

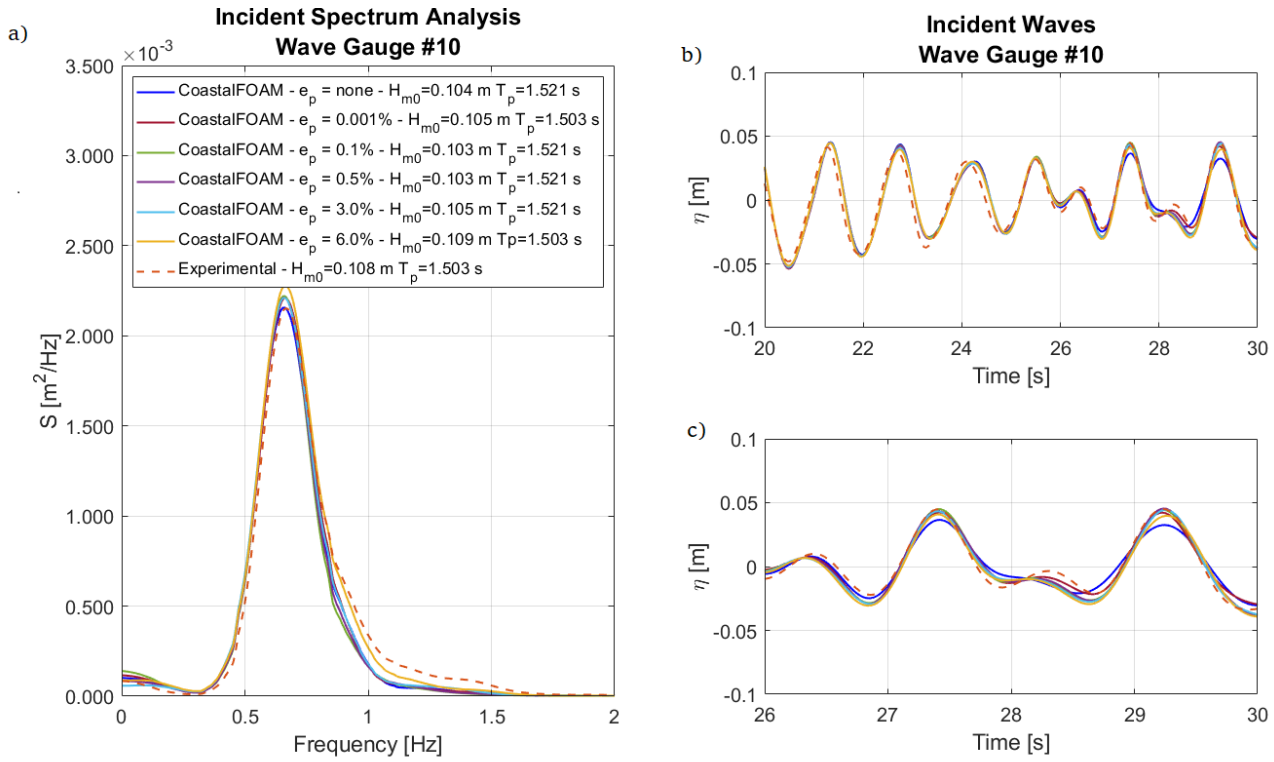

Figure 6.16: Incident water surface measured at wave gauge 10 located 2.4 m from the front face of the crest wall for different degrees of openness of the wall for the baseline layout under extreme conditions
a) Smooth energy spectrum including the significant wave height and peak period, b) time series of incident waves captured between 20-30 s and c) zoom in of time series of incident waves between 26-30 s.

Table 6.5: Wave characteristics under extreme conditions at Wave Gauge 10 for different degrees of openness

Siimulation	Degree of openness	Kr [-]	T_p [s] (1)	H_{m0} [m] (1)	$\rho\,\eta$ [-] (2)
BE01	None	0.71	1.52	0.104	0.93
BE02	0.001%	0.71	1.50	0.105	0.91
BE03	0.10%	0.71	1.52	0.103	0.92
BE04	0.50%	0.71	1.52	0.103	0.91
BE05	3.00%	0.63	1.52	0.105	0.92
BE06	6.00%	0.54	1.50	0.109	0.92
Experimental	[-]	0.66	1.50	0.108	[-]

(1) Incident Wave Conditions
(2) Pearson correlation coefficient considering all time series

The double peak and church-roof behaviour of the dynamic forces, caused by the extreme wave climate, is captured by the different numerical simulations. A slight time shift, an underestimation or overestimation for the dynamic pressure happens depending on the degree of openness and on the implementation of the ventilated boundary condition (see Figure 6.17). The dynamic forces time signal correlations, summarized in Table 6.6, are around 0.70. Based on the reproduction of the overall behaviour of the time signals for the extreme conditions, the numerical simulation excluding the ventilated boundary condition exhibits the best resemblance. These correlations also indicate that for extreme conditions, the numerical flume predicts the wave induced forces with less accuracy than for the operational conditions (see results in Section 6.4.1).

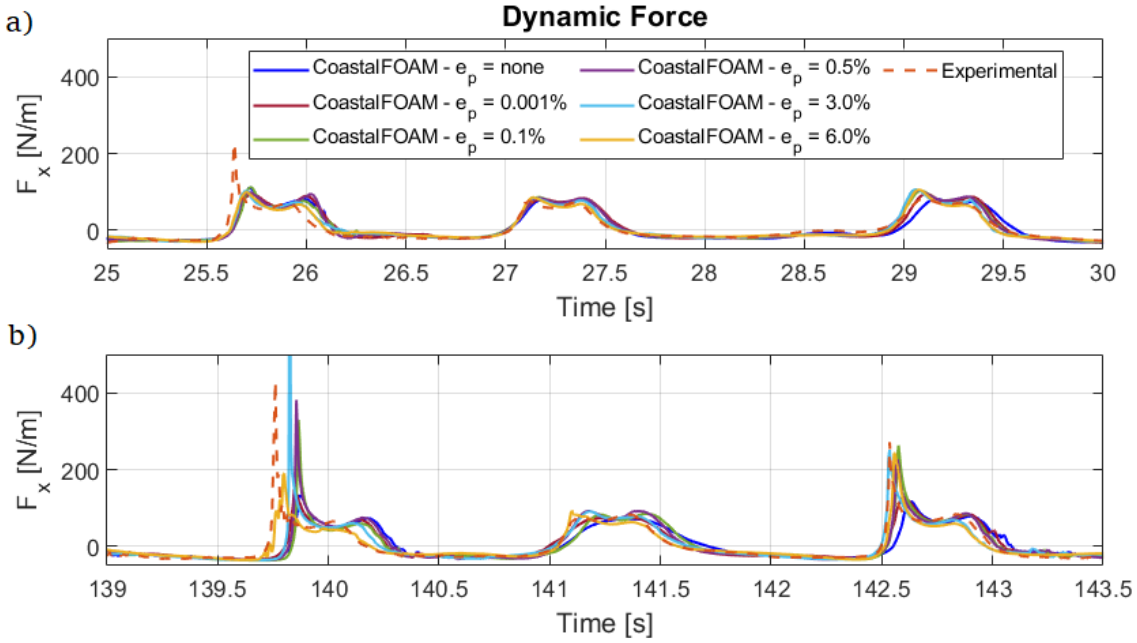

Figure 6.17: Time series of dynamic forces on the front face of the crown wall or different degrees of opennessof the wall for the baseline layout under extreme conditions
Comparison between experimental and numerical results, for different degree of openness. a) Time frame: 25-30 s, b) time frame: 139-143.5 s.

Table 6.6: Pearson correlation coefficient between experimental and numerical dynamic forces time series with different degrees of openness under extreme conditions

Degree of openness	**None**	**0.001%**	**0.10%**	**0.50%**	**3.00%**	**6.00%**	**Experimental**
ρ **Dynamic Forces**	0.73	0.69	0.66	0.71	0.71	0.68	[-]

A better comparison between the experimental and numerical results can be obtained by analysing the force events, as explained in section 6.2.2. The results of comparing event by event are summarized in Table 6.7. The simulation excluding the ventilated boundary condition has the lower RMSE and the highest correlation, with a value of 0.55. For the extreme conditions simulations, correlations between 0.35 and 0.55 were found, much lower than the correlations found for the operational conditions. There is a clear decrease in accuracy when modelling heavily breaking waves in the numerical flume.

Table 6.7: Root Mean Square Error and Pearson correlation coefficient between experimental and numerical force events with different degrees of openness under extreme conditions

Degree of openness	**RMSE (N/m)**	**Pearson Correlation [-]**
None	194.25	0.55
0.001%	310.61	0.44
0.10%	315.95	0.35
0.50%	213.96	0.43
3.00%	215.81	0.46
6.00%	201.54	0.50

Figure 6.18a presents the maximum force events and the GPD fitted distribution while Figure 6.18b compares directly the numerical against the experimental maximum forces. It is noted that a lower ventilation through the wall results in more entraped air, thus, higher forces exerted against the crest wall. The simulation performed with 0.5% of openness and the simulation without the ventilated boundary condition display an outlier behaviour. For the later, it was expected that the associated force events were higher, since no ventilation is

given in the numerical flume. However, its behaviour resembles more the numerical simulation with the 6.0% degree of openness.

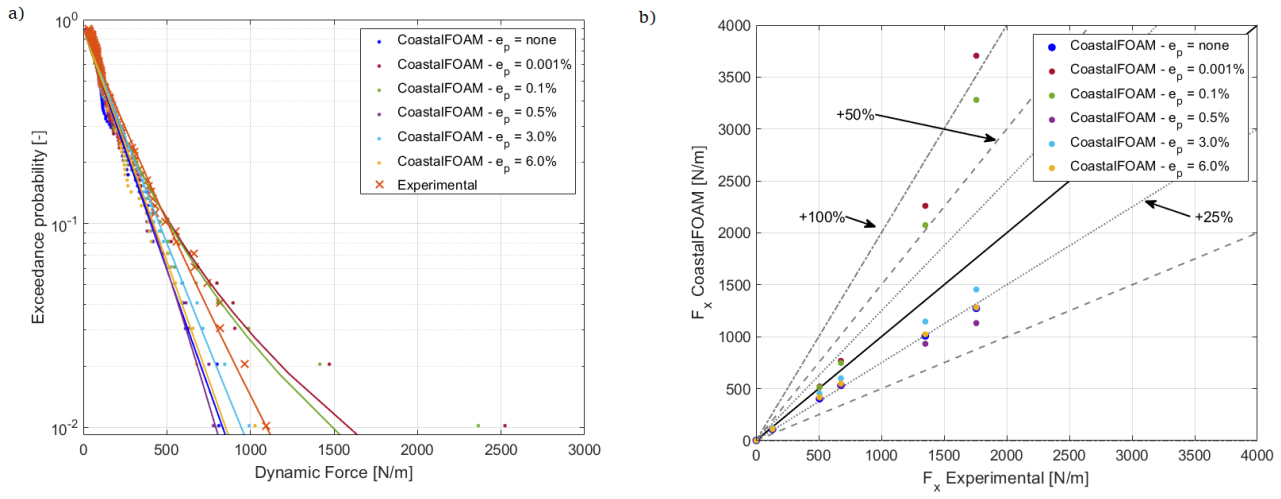

Figure 6.18: Experimental and numerical force events comparison for various degrees of openness for the baseline layout under extreme conditions
a) GPD fitted curves, b) Comparison of the wave induced forces with the 85%, 50%, 10%, 5%, 0.4% and 0.1% exceedance probabilities based on the GPD. The 25%, 50% and 100% error bands are included.

Under this wave climate, unlike under operational conditions, there is a notable influence of the degree of openness on the forces predictability. Based on the event by event comparison, not adding the ventilated boundary condition would be the recommendation. Nonetheless, based on the statistical analysis (GPD fit), including an openness of 3.0% achieves the best agreement against the experimental measurements. By using this degree of openness, the forces are predicted within the 20% error band (see Figure 6.18b).

6.5 Validation case: Tetrapods layout

The wave-structure interaction under operational and extreme conditions for a breakwater conformed of a Tetrapods layer is studied, testing if a CoastalFOAM model is able to model the interaction of irregular waves with permeable coastal structures conformed by artificial blocks under different wave climates. The wave damping caused by the porous layer and its effect in the reduction of the forces exerted on the wall are addressed.

This Section starts with the validation of the two cases associated to partly-permeable breakwaters: Tetrapods layout under operational and extreme conditions, following the methodology outlined in Section 6.2.1. Then, different settings for modelling the porous media layer are tested (see details of model set-up in Chapter 5, Section 5.2.6). To analyse the effect of the different settings, two properties are used: the wave reflection and the wave force.

6.5.1 Hydraulic conditions: Operational

Table 6.8 summarizes the settings for the Tetrapods case analysed in this section. Figure 6.19 exemplifies the wave behaviour for the Tetrapods layout under operational conditions.

Table 6.8: Case specific settings for Tetrapods layout under operational conditions

Simulation	Turbulence model	Degree of openness	Loss coefficient	n_p	KC	α	β
TT00	No	3.0%	1.5	0.5	2.187	200	1.1

More information about the numerical settings can be found in Appendix C.

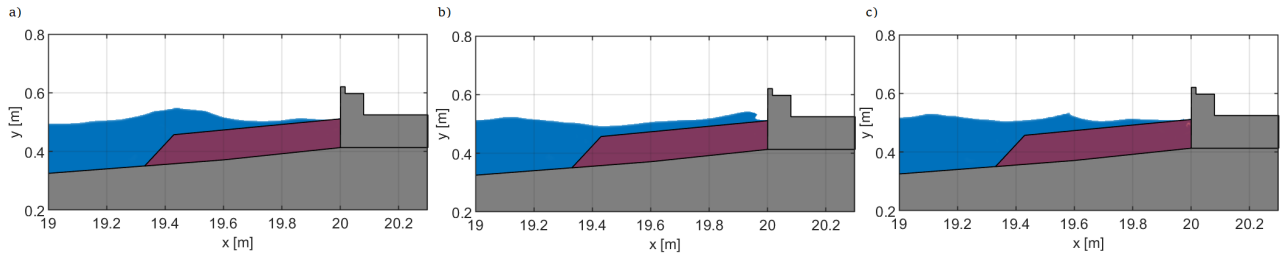

Figure 6.19: Wave attack under operational conditions for a breakwater with a Tetrapods layer
a) Incoming wave, b) plunging wave c) reflected wave interacting with incoming wave

Figure 6.20 shows the incident water surface elevation, recorded in the physical and numerical flume at wave gauge 10, in frequency and time domain. A close look to the spectrum analysis indicates that the wave energy, at gauge 10, for all frequencies is fairly captured by the numerical flume. There is a slight overestimation of wave energy, for frequencies above 0.8 Hz. However, the discrepancies are not very relevant since differences of less than 3.0% and 1.5% were found for the significant wave height and peak period, respectively. Overall, the time signals of incident surface elevation measured in both models are in good agreement. This is reflected in a Pearson correlation coefficient of 0.91.

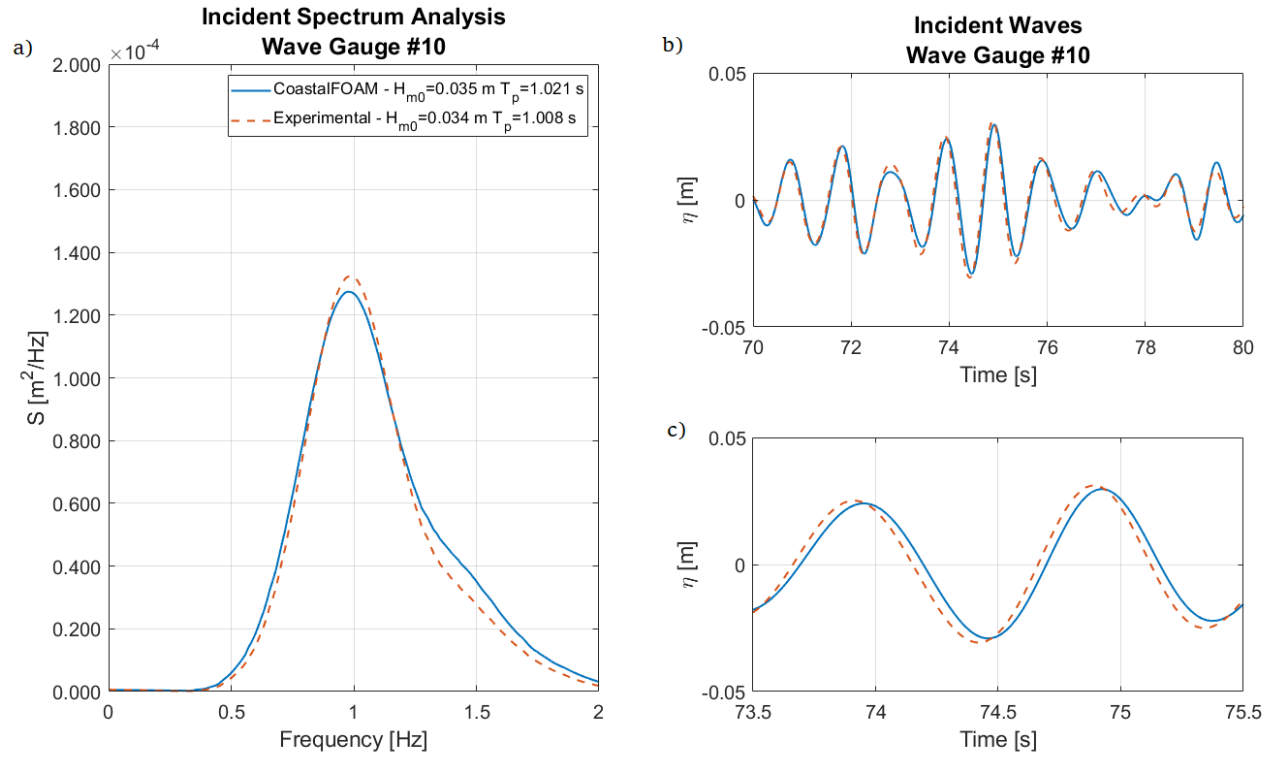

Figure 6.20: Incident water surface measured at wave gauge 10 located 2.4 m from the front face of the crest wall for the Tetrapods layout under operational conditions
a) Smooth energy spectrum including the significant wave height and peak period, b) time series of incident waves captured between 70-80 s and c) zoom in of time series of incident waves between 73.5-75.5 s.

Figures 6.21 and 6.22 present a comparison between the time signals of the wave induced pressures and forces measured in the the physical and numerical flume. The results from both models display the same pattern. Again, the first 4 pressure transducers have better correlations between the experimental and numerical measurements. The recordings from the pressure sensor 5 do not seem to contribute to the integrated force, under this mild wave climate. In general, CoastalFOAM is capable of predicting the behaviour of the dynamic forces subjected to normal conditions, when a porous media layer is included in the numerical flume. This is portrayed by a Pearson correlation coefficient of 0.87.

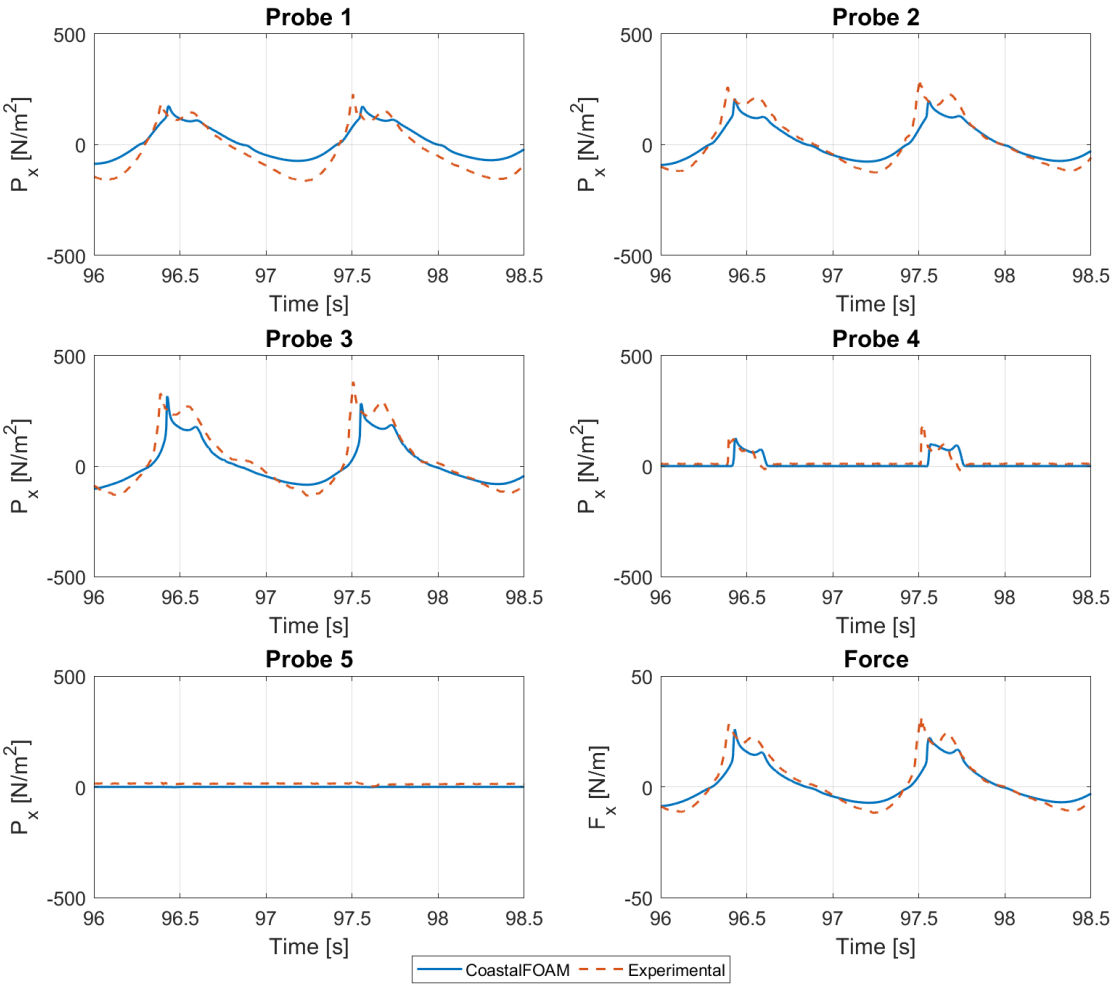

Figure 6.21: Comparison of the simulated and experimental pressure and force time series for Tetrapods layout under operational conditions
Negative values because the hydrostatic pressure is removed from the signal.

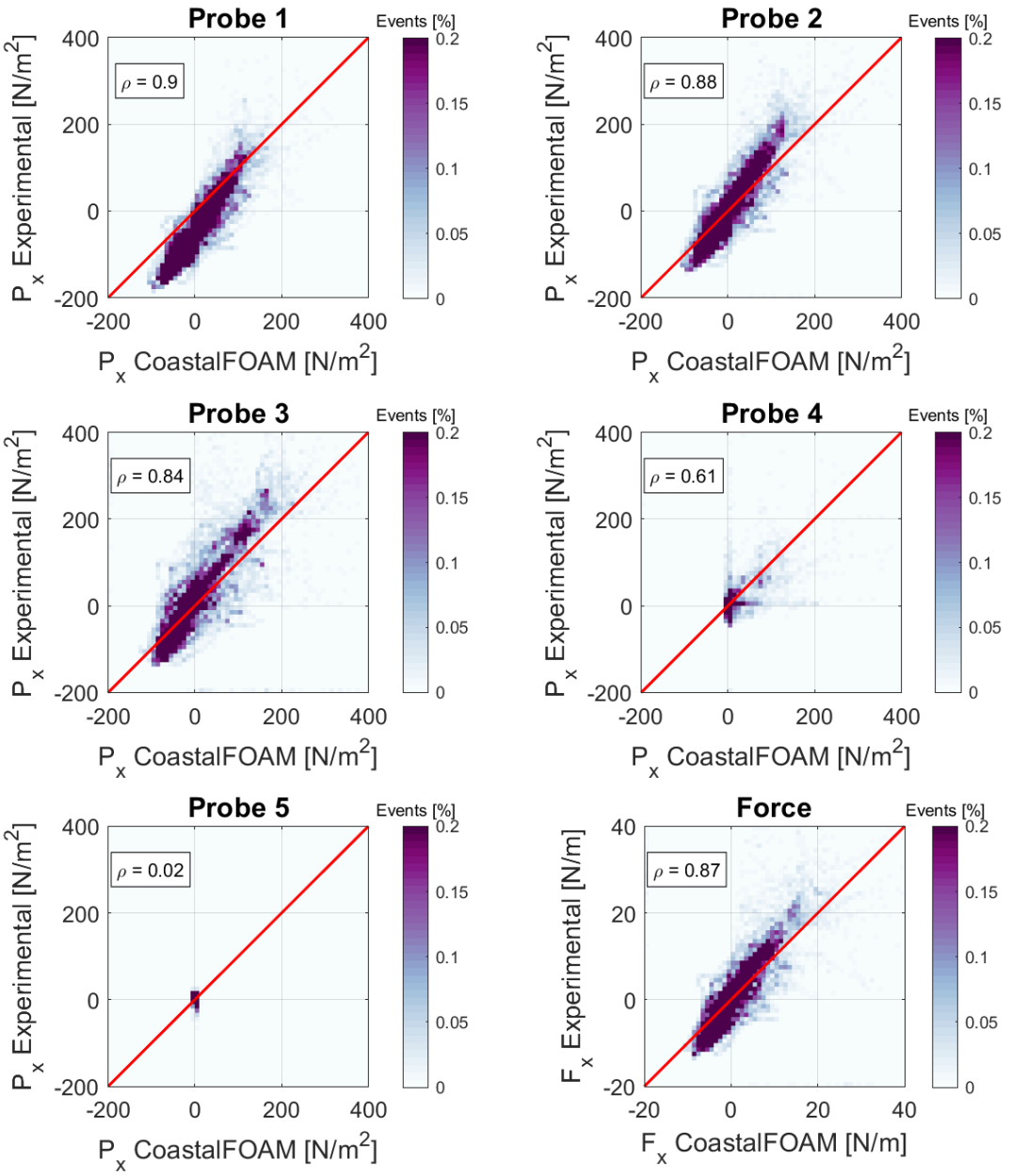

Figure 6.22: Density scatter plot comparing the simulated and experimental time series of pressure and force exerted on the vertical face of the crown wall for the Tetrapods layout under operational conditions The Pearson correlation coefficient is displayed for each pressure transducer and for the dynamic force integration. Negative and zeros values appeared because the hydrostatic pressure is removed from the signal. The color scale represents the percentage of events falling in each grid point

The spatial distribution of the pressure across the front face of the wall is illustrated for two different force events. Figure 6.23 compares the numerical and experimental pressures. The results show that the numerical model is in good agreement with the experimental measurements, displaying the same shape for the pressure distribution for different wave impacts. Depending on the event, the numerical model underpredicts or overpredicts the pressures in the pressure sensors. For the events showed in this report, the forces are applied 0.48 m from the base of the wall. This is the same application point obtained for the case Baseline layout under operational conditions.

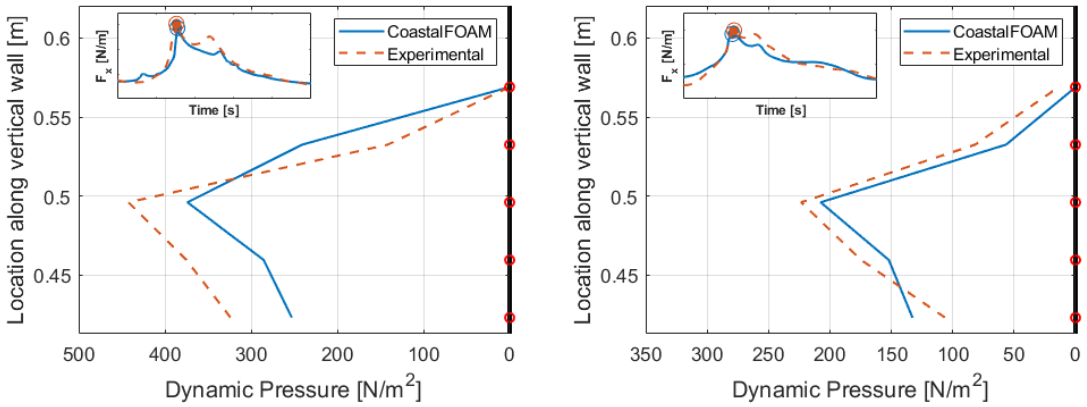

Figure 6.23: Distribution of pressure along the vertical wall for two different force events denoted as a) and b), for the Tetrapods layout under operational conditions
The red circles are the pressure sensors and the black line is the front face of the wall. In the graph located in the upper left corner, the force event in the time domain is illustrated. The orange and blue circles represent the moment in time where the pressure distribution is extracted

A comparison between the modelled and measured force events resulted in a RMSE of 6.0 N/m and a Pearson correlation coefficient of 0.86. For these specific settings, 2 force events were not included in the force event analysis because they were not captured by the numerical flume. The magnitude of these events is lower than 9 N/m. In line with the statement made in section 6.2.2, the more relevant information is always considered for the force event analysis.

The statistically force events comparison is presented in Figure 6.24. For these specific settings, the numerical flume predicts with high accuracy the maximum forces faced by the wall. In general, the wave induced forces predicted by the CoastalFOAM model lay in the 25% error band.

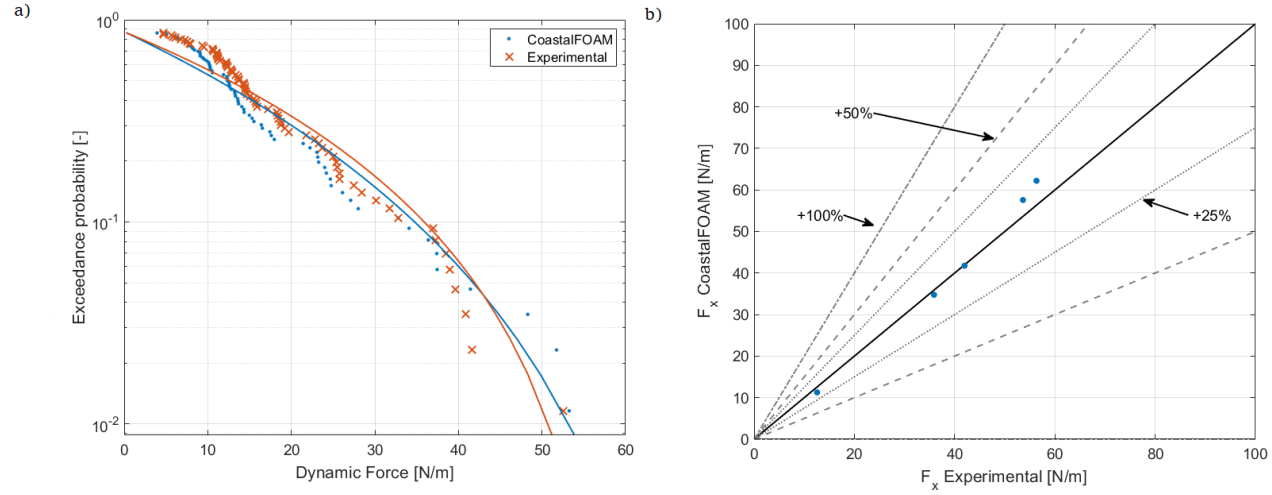

Figure 6.24: Experimental and numerical force events comparison for the Tetrapods layout under operational conditions
a) GPD fitted curves, b) Comparison of the wave induced forces with the 85%, 50%, 10%, 5%, 0.4% and 0.1% exceedance probabilities based on the GPD. The 25%, 50% and 100% error bands are included.

Comparison against Baseline layout

The presence of the Tetrapods layer changes the wave-structure interaction. Contrary to the partially standing wave pattern captured by the numerical and physical flume for the impermeable breakwater subjected to operational conditions, when a porous layer is added, the wave behaviour close to the wall changes towards a less reflective one. In some occasions, even a more plunging wave character is displayed (see example in Figure 6.19).

Another parameter affected by the inclusion of a porous layer is the reflection coefficient. The reason is that wave damping occurs inside the porous structure. Thus, the reflection coefficient changes from 0.91 to 0.22, according to the physical measures. In the numerical flume, the reduction stays in the same order of magnitude; from 0.86 to 0.18 (K_r estimated at gauge 10, based on the data from gauges 6-10).

The breaking pattern behaviour is also influenced by the addition of the Tetrapods layer. During wave attack, the waves experienced depth induced breaking due to a lower water depth close to the wall (see Figure 6.19).

A change of the wave climate near the crown wall has a direct influence in the type of force events experienced by the wall. Figure 6.25 displays average force events captured by both flumes when the breakwater is subjected to operational conditions. Figure 6.25a presents a force event associated with low steepness waves, the typical wave behaviour observed under operational conditions reaching the Holyhead breakwater. In contrast, Figure 6.25b shows a very different force event: the church-roof shape caused by steeper waves hitting the crown wall.

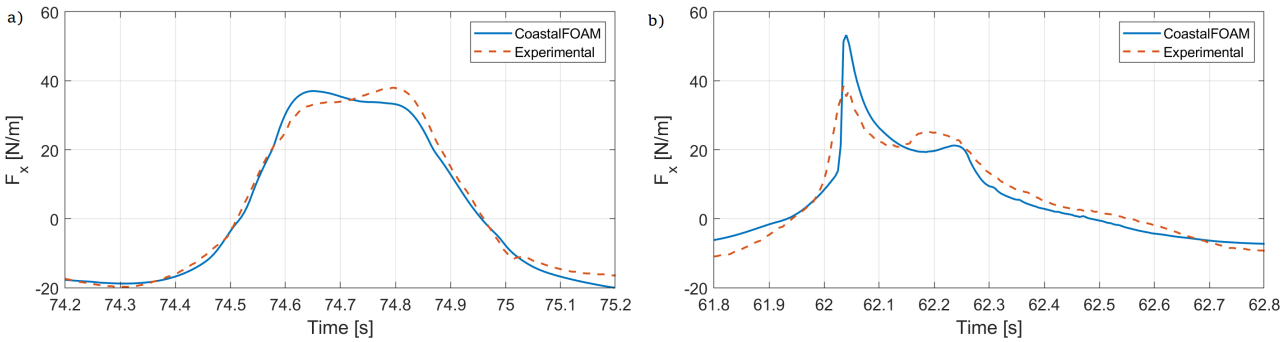

Figure 6.25: Average force event captured by the physical and numerical flumes when the breakwater is subjected to operational conditions
a) Impermeable breakwater. b) Breakwater with porous layer.

Notwithstanding the change in wave behaviour between the impermeable and partly-permeable breakwaters, the maximum forces associated to each force event exhibit practically the same magnitudes (see exceedance curves and GPD fits in Figure 6.26). A slight variation is appreciated in the numerical flume results, where the inclusion of the porous media damps the incoming waves, lowering slightly the forces at the wall. However, this effect can also be attributed to the combination of porous media drag coefficients used in this CoastalFOAM simulation (see settings in Table 6.8). A different combination of α, β and KC parameters could lead to a different outcome; thus, the sensitivity analysis of these parameters is presented in a following Section.

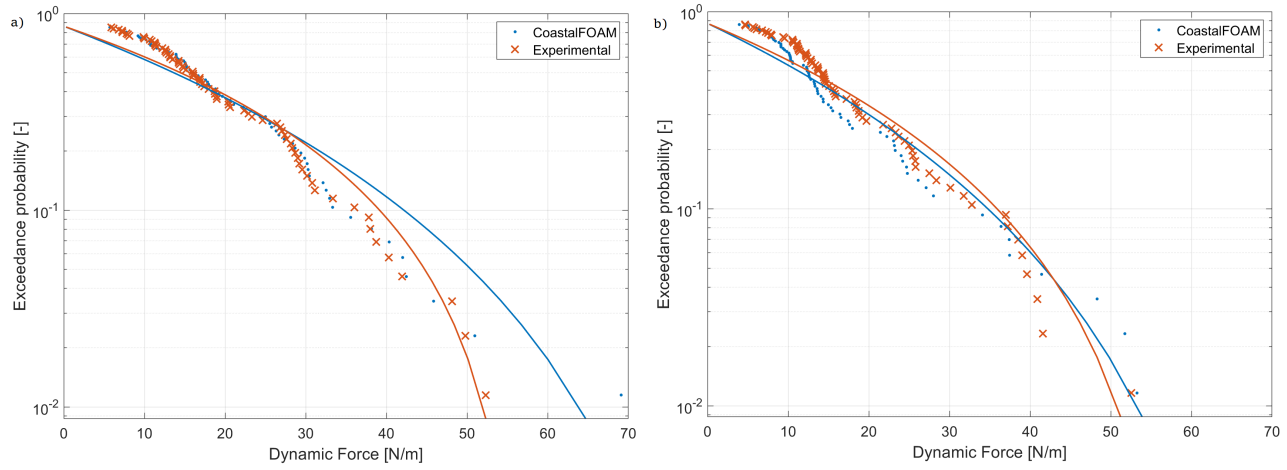

Figure 6.26: Comparison of force events under operational conditions for a) an impermeable breakwater and b) a breakwater including a Tetrapods layer
The maximum data is fitted by a GPD

6.5.2 Hydraulic conditions: Extreme

Heavily breaking waves reaching a partly-permeable breakwater were simulated in the physical and numerical flume. Table 6.9 summarizes the settings for the Tetrapods case under extreme conditions. Figure 6.27 illustrates the plunging wave attack near the crown wall when a porous layer is included at the front of the crest wall. The air inside the porous layer, as a result of the wave breaking process and wave-structure interaction, is captured by the numerical model.

Table 6.9: Case specific settings for Tetrapods layout under extreme conditions

Simulation	**Turbulence model**	**Degree of openness**	**Loss coefficient**	n_p	**KC**	α	β
TT02	No	3.0%	1.5	0.5	7.407	200	1.1

More information about the numerical settings can be found in Appendix C.

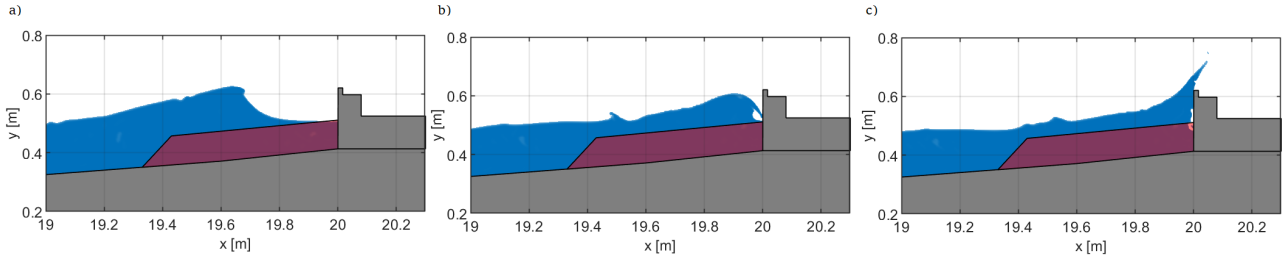

Figure 6.27: Wave attack under extreme conditions for a breakwater with a Tetrapods layer a) Plunging wave, b) overturning wave and c) wave impact and overtopping.

Figure 6.28 shows the incident spectrum analysis and a subset of the time series of the water surface elevation, recorded in the physical and numerical flume at wave gauge 10. For this validation case, there is a slight underestimation of wave energy for frequencies above 0.8 Hz. This does not appear to be significant because the bulk hydrodynamics indicate differences of less than 1.0% and 2.5% for the significant wave height and peak period, respectively. Thus, the energy distribution is well-captured by the numerical model.

In the time domain, Figure 6.28b and Figure 6.28c revealed that the numerical flume can reproduce the wave conditions generated during the physical modelling campaign for a extreme wave climate. Sometimes, larger or smaller incoming wave heights are predicted by CoastalFOAM. Nonetheless, a correlation coefficient of 0.91 between the experimental and numerical incident surface elevation time signal proves that overall, the shape of the time signal is fairly reproduced by the numerical flume.

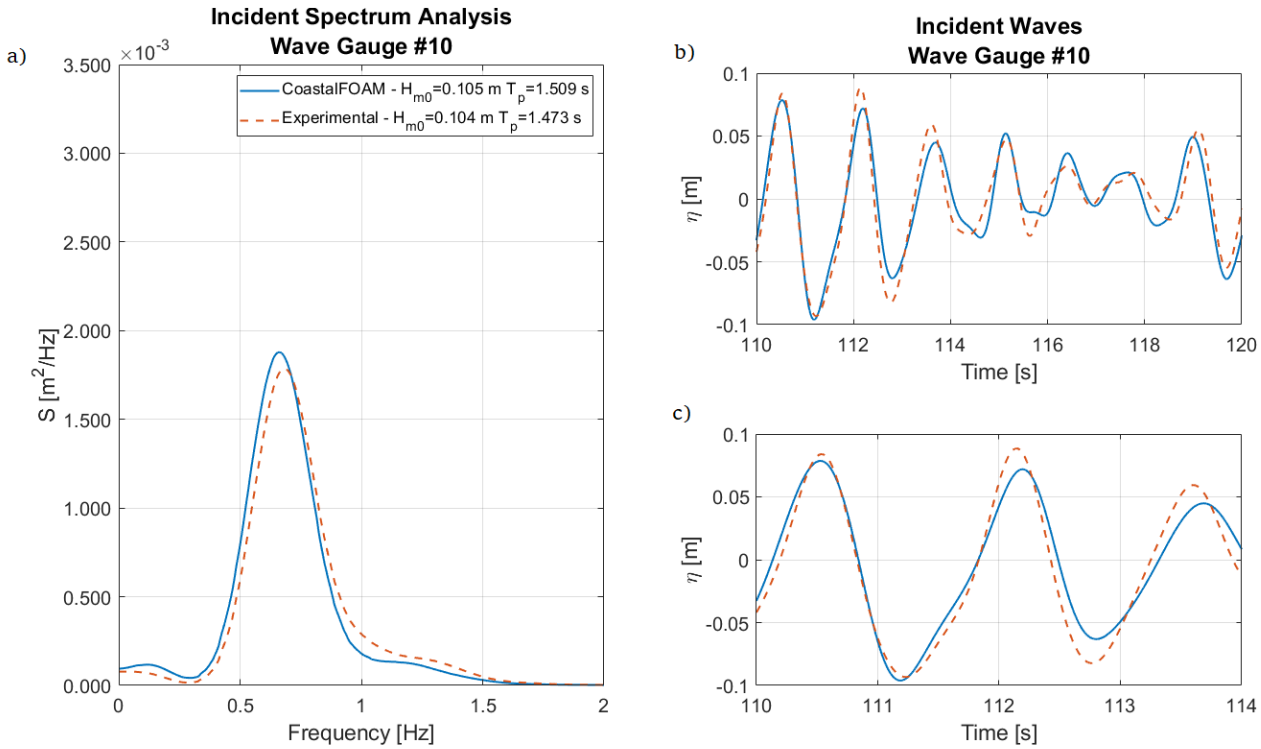

Figure 6.28: Incident water surface measured at wave gauge 10 located 2.4 m from the front face of the crest wall for the Tetrapods layout under extreme conditions
a) Smooth energy spectrum including the significant wave height and peak period, b) time series of incident waves captured between 70-80 s and c) zoom in of time series of incident waves between 73.5-75.5 s.

The capabilities of CoastalFOAM to simulate wave-structure interaction under extreme conditions, when a porous layer is included in the flume, are indicated in Figures 6.29 and 6.30; where a comparison between the experimental and numerical pressures and dynamic forces is undertaken. The time domain comparison shows that the timing, magnitude and shape of the pressures exerted on the wall at each location are well-captured by the numerical model. As seen in the other validation cases, the high-peak impacts are in some cases underpredicted (as exemplified in Figure 6.29) or overpredicted by the numerical model. The density scatter plot makes evident that under heavily breaking waves, the numerical predictability of the dynamic forcing lowers to correlations of about 0.70. For these settings, in the density scatter plot is not clear if the model is overall, overestimating or underestimating the wave induced pressures and forces.

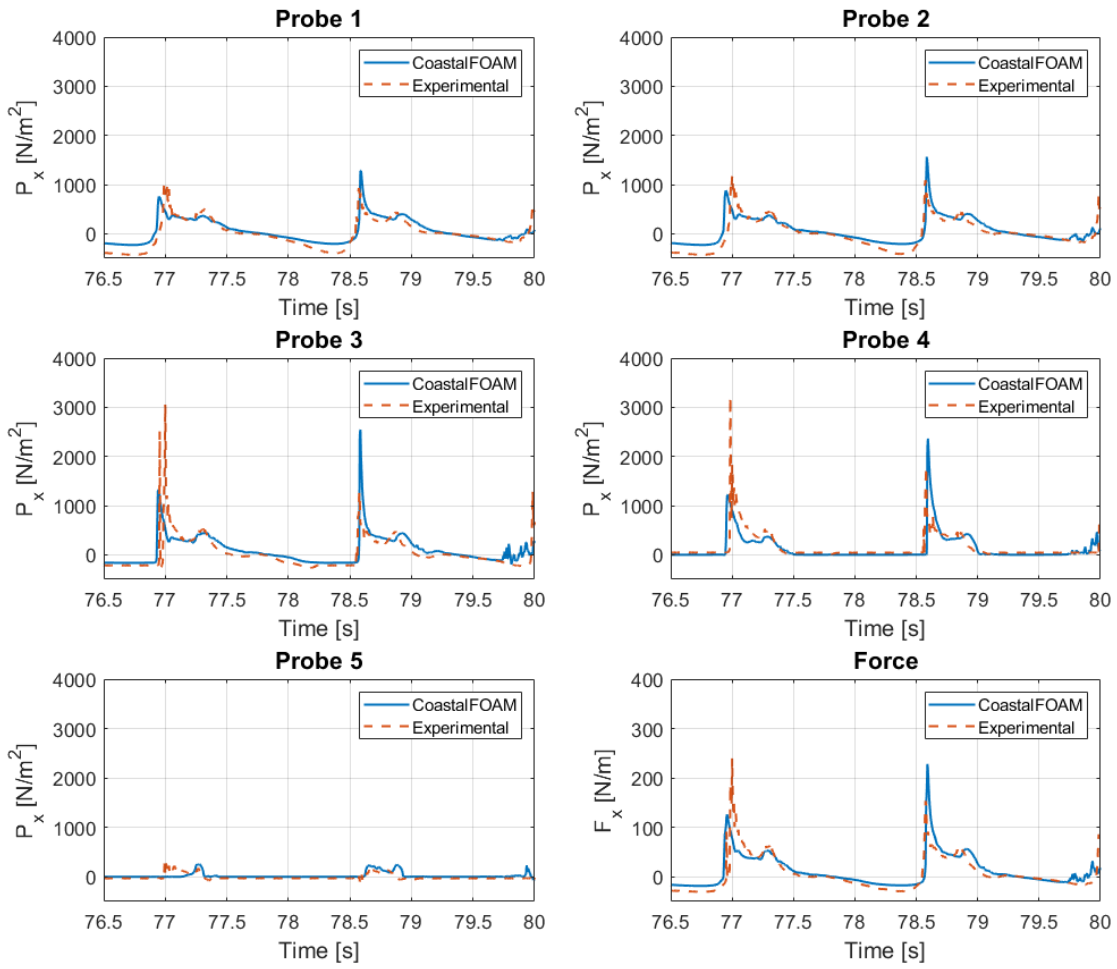

Figure 6.29: Comparison of the simulated and experimental pressure and force time series for Tetrapods layout under extreme conditions
Negative values because the hydrostatic pressure is removed from the signal.

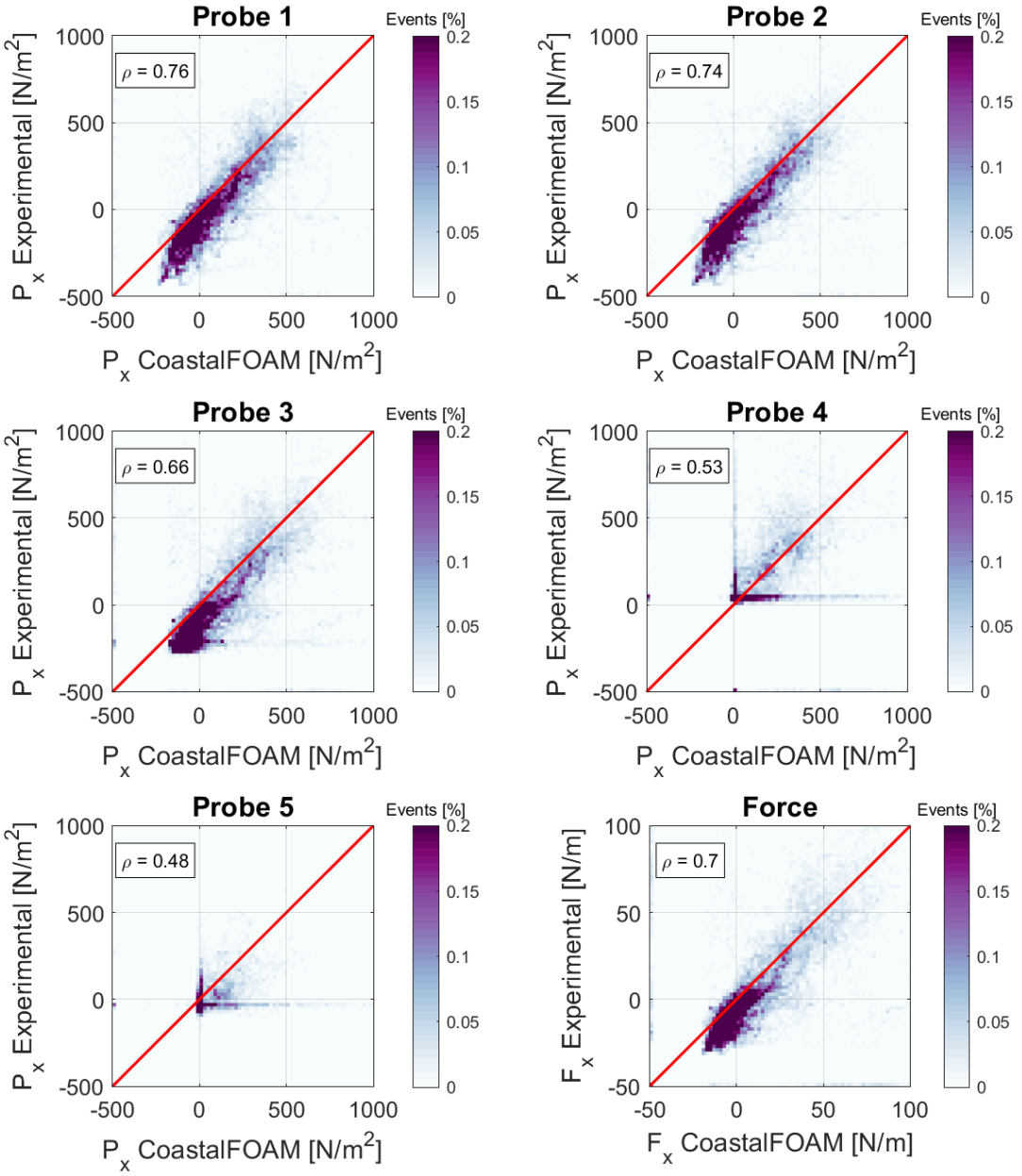

Figure 6.30: Density scatter plot comparing the simulated and experimental time series of pressure and force exerted on the vertical face of the crown wall for the Tetrapods layout under extreme conditions
The Pearson correlation coefficient is displayed for each pressure transducer and for the dynamic force integration. Negative and zeros values appeared because the hydrostatic pressure is removed from the signal. The color scale represents the percentage of events falling in each grid point

Figure 6.31 shows a force event where the classic church-roof shaped signal was captured by the physical and numerical flumes. A slight time shift between the numerical and experimental results is exhibit. For this force event, the impulse and reflecting pressures were analysed in more detail, by focusing on the pressure distribution across the wall. The shape is fairly captured by the numerical flume. The application point of the impulse and reflecting forces is located 0.49 m from the base of the wall, according to the experimental and numerical results.

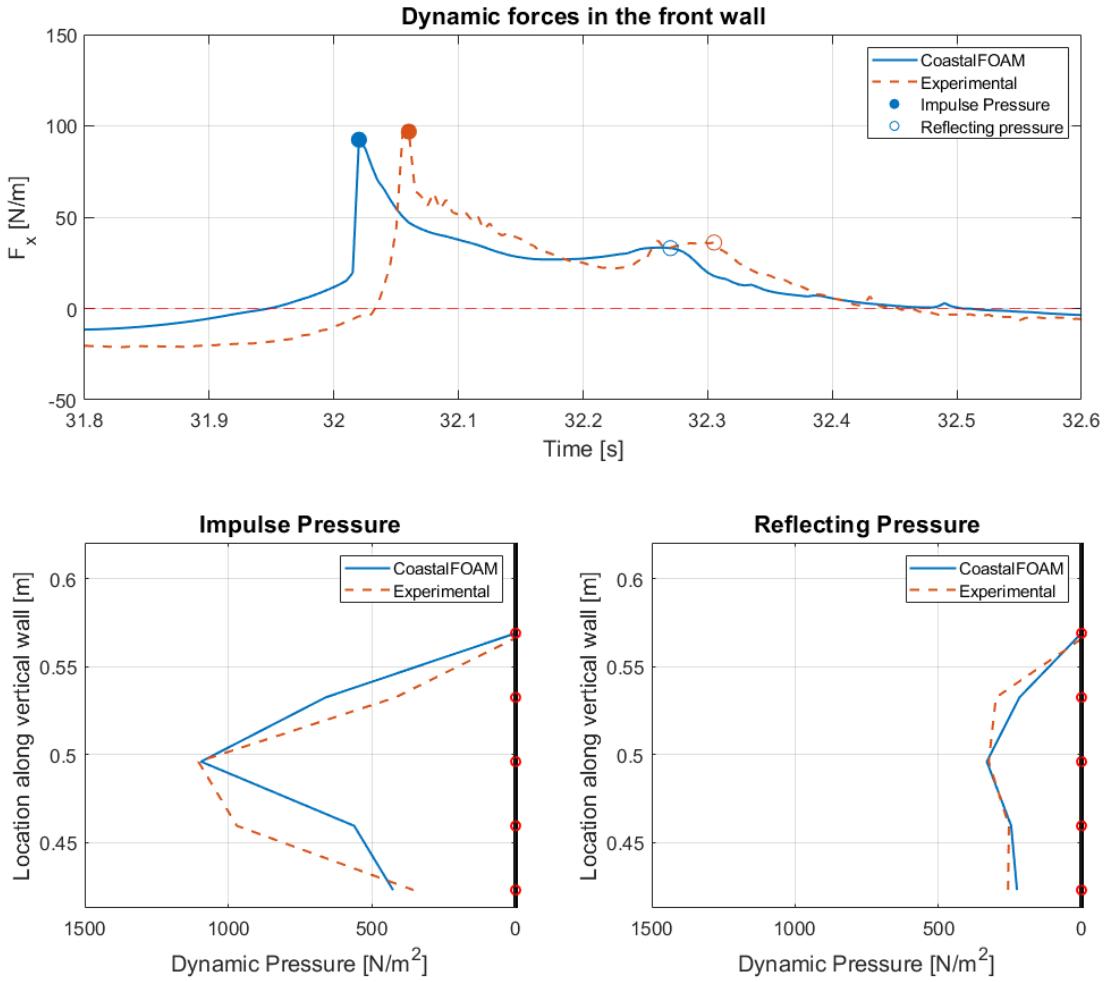

Figure 6.31: Force event and pressure distribution along the vertical wall caused by a steep wave under extreme conditions, for the Tetrapods layout
a) Typical church-roof shaped signal. The filled circles represent the impulse forcing and the hallow circles, the reflecting forcing. b) Impulse pressure distribution. c) Reflecting pressure distribution. The red circles are the probes and the black line is the front face of the wall

To gain more insight into the results from the numerical flume, the force event analysis was carried out. The event by event comparison between the modelled and measured force events returned a RMSE of 81.93 N/m and a Pearson correlation coefficient of 0.51. For these specific settings, 4 force events were removed in the force event analysis because they were not captured by the numerical flume. The magnitude of all those events lays below 40 N/m.

Figure 6.12 compares statistically the force events captured by the physical and numerical model. For these specific settings, the numerical flume underpredicts all the wave induced forces. In general, the predictions lay in the 25% error band.

Figure 6.32 compares statistically, the force events recorded in the physical modelling test and in the numerical flume. The numerical GPD fit is affected by the three highest force events, causing overpredictions of the maximum wave induced forces with errors below 55%.

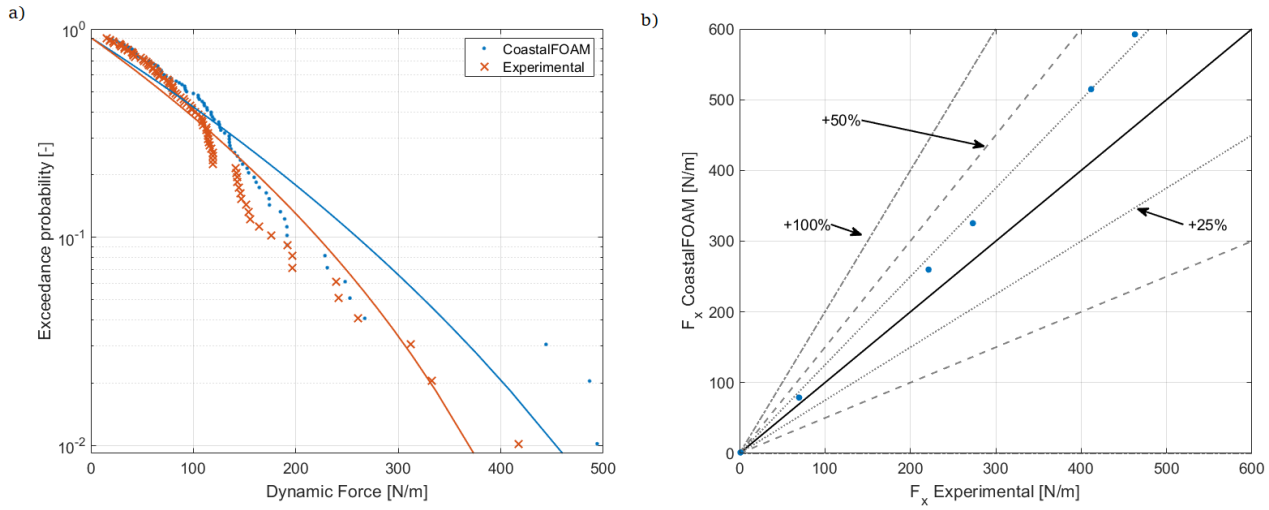

Figure 6.32: Experimental and numerical force events comparison for the Tetrapods layout under extreme conditions
a) GPD fitted curves, b) Comparison of the wave induced forces with the 85%, 50%, 10%, 5%, 0.4% and 0.1% exceedance probabilities based on the GPD. The 25%, 50% and 100% error bands are included.

Comparison against Baseline layout

Figure 6.33 presents typical results from the numerical wave flume, for an impermeable breakwater and a partly-permeable breakwater. In both simulations, a plunging wave is about to hit the crest wall. The wave shown for the impermeable breakwater has a smaller wave height than the wave shown for the Tetrapods layout; therefore, the resulting impact force is 309 N/m and 444 N/m, respectively. Despite the difference in wave heights, this Figure illustrates how the inclusion of a porous layer exerts a resistance force against the fluid motion, resulting in lower velocities inside the skeleton.

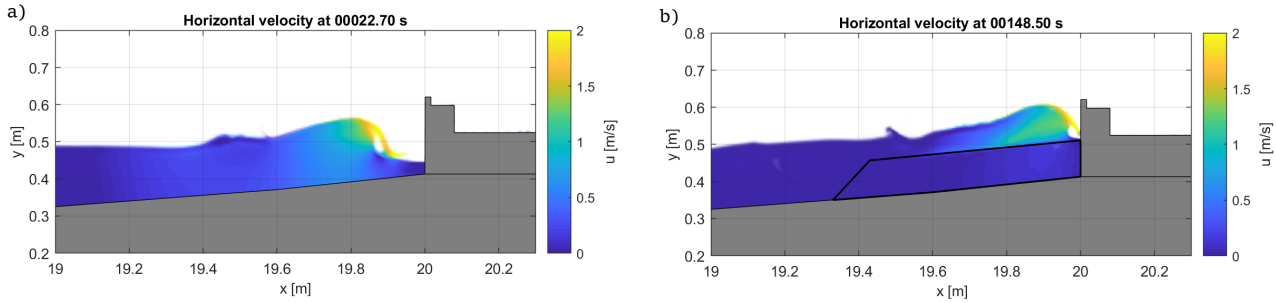

Figure 6.33: Horizontal velocity, total pressure and dynamic pressure for a plunging wave near the crest wall, for a) an impermeable breakwater and b) a breakwater with a Tetrapods layer
The maximum force associated to each wave impact is 308.6 N/m and 444.1 N/m, respectively

For the extreme wave climate, the wave character near the crown wall does not vary significantly, as it was the case for the milder wave climate (see comparison in Section 6.5.1). Nonetheless, similar to the operational conditions case, the reflecting pattern does changes due to the presence of the Tetrapods layer. The reflection coefficient decreases from 0.66 to 0.27, according to the physical modelling, and from 0.63 to 0.30, according to the numerical modelling.

Although the behaviour of the waves reaching the structure in the two breakwater layouts is similar, the wave energy that actually reaches and impacts the wall differs. This happens because the flow field penetration through the Tetrapods layer entails wave energy damping due to the turbulence levels inside the porous media. To graphically observed this behaviour, Figure 6.34 contrasts the maximum forces recorded for an impermeable breakwater and a partly-permeable breakwater. In the physical and numerical flume, the forces experienced by the wall decreased approximately by a factor of 2. Thus, the inclusion of a Tetrapods layer leads to significantly lower wave induced forces under extreme conditions.

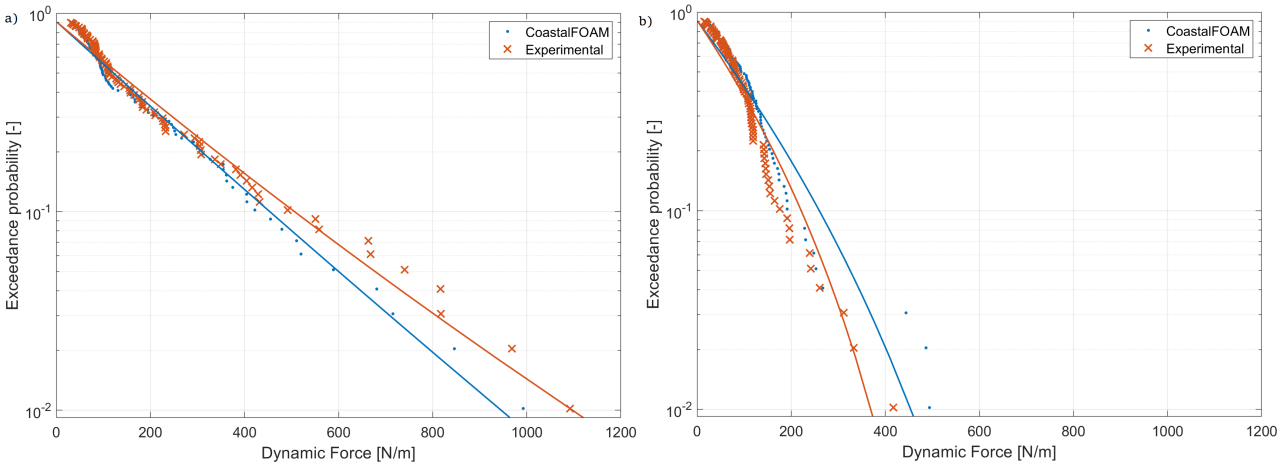

Figure 6.34: Comparison of force events under extreme conditions for a) an impermeable breakwater and b) a breakwater including a Tetrapods layer
In blue the numerical results and in dashed orange the experimental results. The maximum data is fitted by a GPD.

6.6 Sensitivity analysis: Porous media parameters

For the extreme wave climate, the influence of the combined porous media drag coefficients on the resulting forces exerted on the wall is studied. Only the extreme conditions were studied, since a correct reproduction of the physical results in CoastalFOAM is of higher importance for the design process.

For the sensitivity analysis, a time frame of 150 seconds with a total of 98 waves was used. Table 6.10 summarizes the different combination of porous media drag coefficients applied in the numerical flume to model the Tetrapods layer. A total of six simulations were run, where α, β and KC were varied. The parameter α, associated to laminar flow inside the skeleton, was changed between 200 and 1000, while the parameter β, associated to turbulent flow inside the skeleton, between 0.8 and 1.8. Therefore, simulations TT02, TT04 and TT05 focus on the importance of laminar flow inside the Tetrapods layer. On the other hand, simulations TT01, TT02 and TT03, on the importance of turbulent flow. The oscillatory flow, accounted in the KC number, was calculated as 7.41 for extreme conditions (see details in Chapter 5, Section 5.2.5). Simulation TT06 uses a KC of 10,000; removing the influence of the oscillatory movement in the porous media drag coefficients (see mathematical framework in Section 4.2.2).

Table 6.10: General settings for the sensitivity analysis of Tetrapods layer porous media coefficients

Simulation	Porosity	KC	alpha	beta
TT01	0.5	7.407	200	0.8
TT02	0.5	7.407	200	1.1
TT03	0.5	7.407	200	1.8
TT04	0.5	7.407	500	1.1
TT05	0.5	7.407	1,000	1.1
TT06	0.5	10,000	1,000	1.1

Figure 6.35 portrays the incident wave spectrum and the surface elevation measured in the time interval 110-120 s at Gauge 10. The bulk hydrodynamics are summarized in Table 6.11. For different combinations of porous media coefficients, the time series correlations for the incident surface elevation, registered 2.4 m away from the front face of the crest wall, are above 0.90. There are no significant differences in the incident wave attack for the different test cases. Moreover, giving the results presented in Table 6.11, no trend can be inferred between the linear and nonlinear drag coefficients and the reflection coefficient.

The bulk hydrodynamics show that the peak period and significant wave height are represented by the numerical flume with an error of less than 2.5% and 3%, respectively. Again, the larger differences are encountered for

the reflection coefficient. In this case, the errors are lower than 15%.

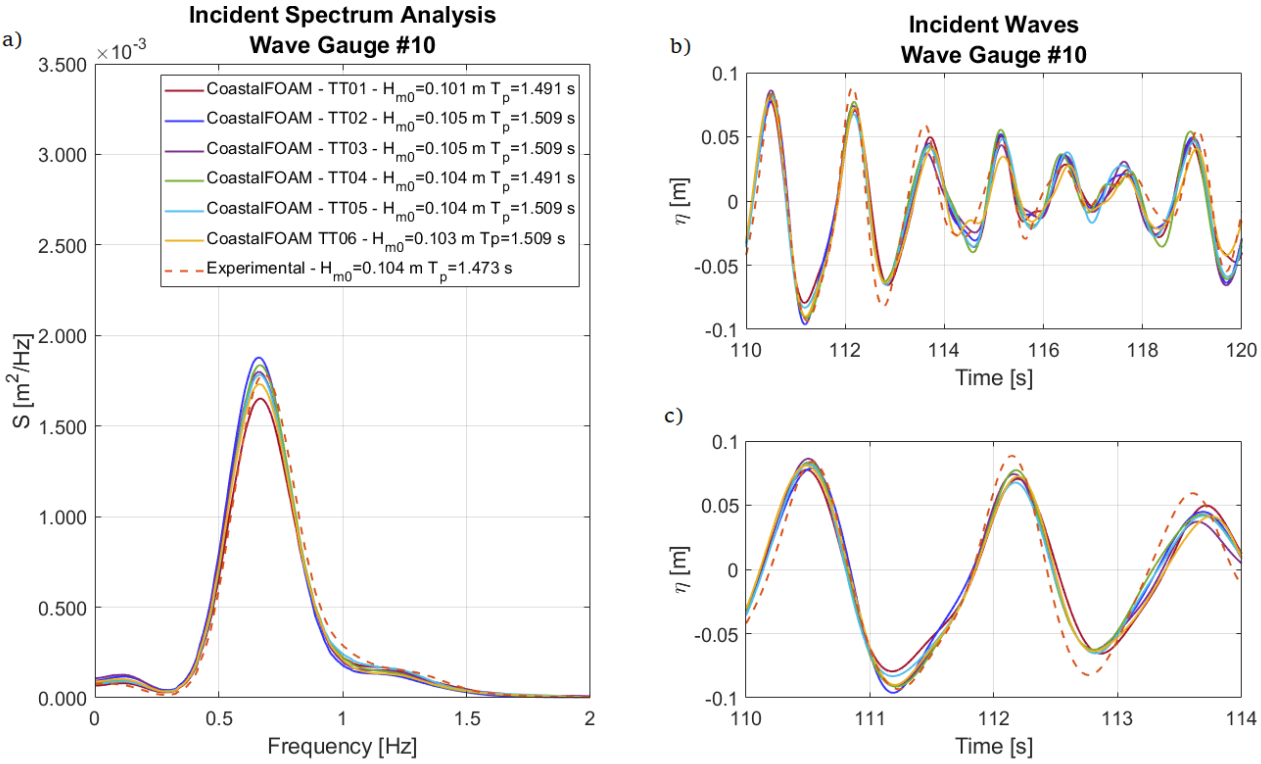

Figure 6.35: Incident water surface measured at wave gauge 10 located 2.4 m from the front face of the crest wall for different combination of porous media parameters for the Tetrapods layour under extreme conditions a) Smooth energy spectrum including the significant wave height and peak period, b) time series of incident waves captured between 110-120 s and c) zoom in of time series of incident waves between 110-114 s.

Table 6.11: Wave characteristics under extreme conditions at Wave Gauge 10 for different combinations of porous drag coefficients

Simulation	**Kr [-]**	T_p **[s]** (1)	H_{m0} **[m]** (1)	$\rho\,\eta$ **[-]** (2)
TT01	0.31	1.491	0.101	0.91
TT02	0.3	1.509	0.105	0.91
TT03	0.3	1.509	0.105	0.9
TT04	0.28	1.491	0.104	0.91
TT05	0.29	1.509	0.104	0.9
TT06	0.31	1.491	0.103	0.9
Experimental	0.27	1.473	0.104	[-]

(1) Incident Wave Conditions
(2) Pearson correlation coefficient considering all time series

In Figure 6.36, six force events with different magnitudes are presented. In all cases, the church-roof behaviour caused by steep waves is captured by the pressure transducers displayed in the numerical flume. Furthermore, for the different combination of porous media parameters, the numerical flume is able to reproduce the shape and the order of magnitude of the highest peak associated to each force event (reflected in time signal correlation coefficients of 0.70-0.74 summarized in Table 6.12). There are only small deviations in the exact time of the impulse force; which do not have a large influence in the design process.

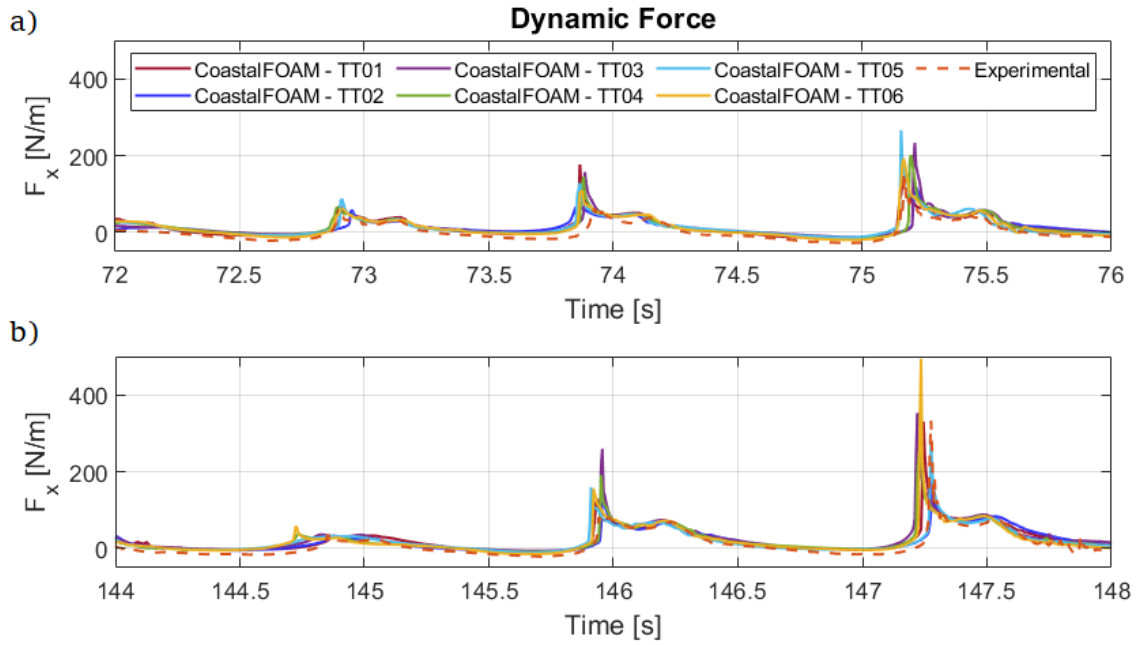

Figure 6.36: Time series of dynamic forces on the front face of the crown wall for different combination of porous media parameters for the Tetrapods layour under extreme conditions
Comparison between experimental and numerical results, for different porous drag coefficients (see details of each simulation in Table 6.10). a) Time frame: 72-76 s, b) time frame: 144-148 s.

Table 6.12: Pearson correlation coefficient between experimental and numerical dynamic forces time series with different combination of porous media parameters under extreme conditions

Simulation	**TT01**	**TT02**	**TT03**	**TT04**	**TT05**	**TT06**
ρ **Dynamic Forces**	0.74	0.70	0.70	0.72	0.72	0.71

Finally, the force events are studied. The results of comparing event by event are summarized in Table 6.13. Simulation TT06 ($\alpha = 1,000, \beta = 1.1$ and $KC = 10,000$) presents the lower RMSE while simulation TT03 ($\alpha = 200, \beta = 1.8$ and $KC = 7.407$), the highest correlation coefficient. Nonetheless, for all simulations, the RMSE have the same order of magnitude and the correlations vary at most, 0.13.

Table 6.13: Root Mean Square Error and Pearson correlation coefficient between experimental and numerical force events with different combination of porous media parameters under extreme conditions

Simulation	**RMSE (N/m)**	**Pearson Correlation [-]**
TT01	70.51	0.54
TT02	81.93	0.51
TT03	73.08	0.59
TT04	76.78	0.57
TT05	78.03	0.46
TT06	67.84	0.53

Figure 6.37a presents the force events and the GPD fitted distribution and Figure 6.37b compares directly the numerical against the experimental maximum forces. Despite the different parameters combination, all the numerical results are predicted within a 50% of error; being the error largest for the highest forces.

The exceedance curves indicate that simulations TT01 ($\alpha = 200, \beta = 0.8$ and $KC = 7.407$) and TT05 ($\alpha = 1,000, \beta = 1.1$ and $KC = 7.407$) are in better agreement with the experimental results, predicting the forces with errors below 15%. Nonetheless, the best fit is obtained from Simulation TT05. This set of coefficients have the same values recommended by van Gent (1995) for a rock layer.

Finally, the effect of including or excluding the effect of the oscillatory flow was studied in Simulations TT05 ($\alpha = 1,000, \beta = 1.1$ and $KC = 7.407$) and TT06 ($\alpha = 1,000, \beta = 1.1$ and $KC = 10,000$). By setting KC to 10,000, the contribution of the oscillatory flow is neglected. By excluding this contribution, the GPD force prediction error increased from 15% to 25%.

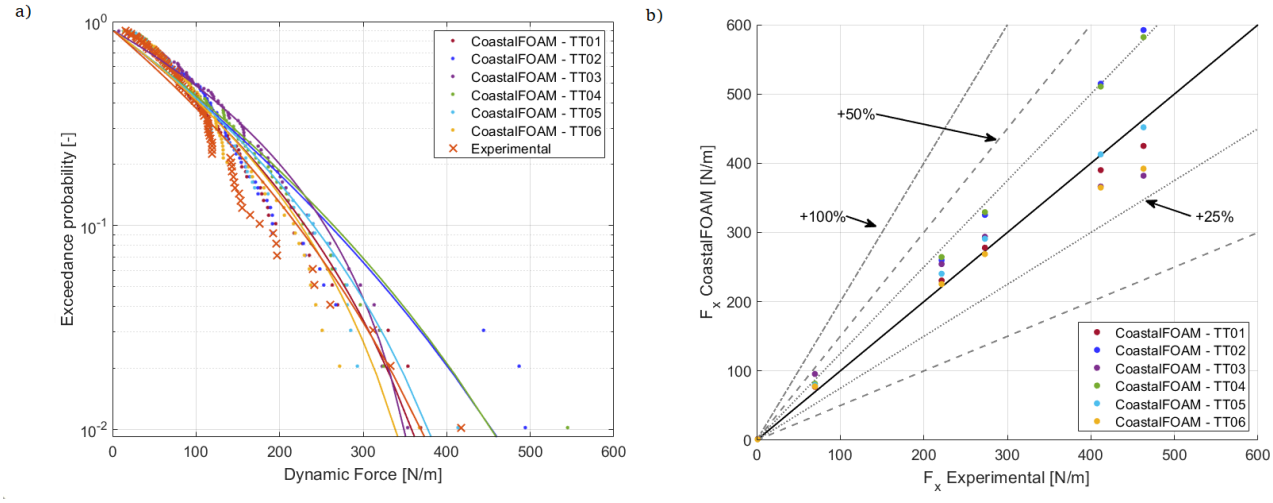

Figure 6.37: Experimental and numerical force events comparison for various combinations of porous media parameters for the Tetrapods layout under extreme conditions
a) GPD fitted curves, b) Comparison including 25 %, 50 % and 100 % boundary intervals.

6.7 Turbulence modelling

So far, the simulations did not include a turbulence model. In this section, the effect of adding a simple turbulence model is investigated. The requirement of a turbulence model becomes more relevant when heavily breaking waves are present in the numerical flume. Moreover, its implementation should have greater effect for the baseline layout than for the Tetrapods layout because in the Tetrapods layout, energy is being dissipated inside the porous media layer. Therefore, the numerical simulation was performed for the baseline layout under extreme wave climate. The results of this simulation are compared against the experimental results and against a simulation excluding a turbulence model.

For practical application, a simple constant eddy viscosity model was applied; thus, turbulence modelling is reduced to a one single scalar representing the entire flow domain. Typical values for the vertical eddy viscosity lie in the order of $\nu_{t,v} \sim 10^{-3} - 10^{-4}\, m^2/s$. Table 6.14 summarizes the settings applied in the simulations with and without the inclusion of a turbulence model. More information about the numerical settings can be found in Appendix C.

Table 6.14: Settings for turbulence modelling comparison

Simulation	Turbulence model	Eddy viscosity [m ^{2}/s]	Degree of openness	Loss coefficient
BE05	No	[-]	3.0%	1.5
BE07	Constant eddy viscosity	10^{-3}	3.0%	1.5

Figure 6.38 compares the numerical simulations against the experimental maximum dynamic forces. For the settings applied in CoastalFOAM (see Table 6.14), not including a turbulence model provides a better agreement with the physical test results. The simulation with the addition of the constant eddy viscosity underestimates almost by 50% the largest force events while the simulation without a turbulence model only underestimate the largest force events by 15%.

To understand why there is a high decrease in forces exerted on the walls by the turbulence model simulation, the wave motion near the wall was studied in detail and compared against the simulation without turbulence (see Figure 6.38). A close look at the wave spectrums exhibit a slight decrease of wave energy around the peak period and a small increase of wave energy at low and high frequencies at locations 18.5, 19.8 and 19.9 m.

Thus, extra energy damping is happening in the numerical flume, causing loss of energy that affects mainly the highest waves and therefore, the highest force events.

Although the numerical simulation of breaking waves involving large amounts of turbulence should become unstable when no closure model is included, the presence of numerical dissipation in OpenFOAM allowed to obtain a stable and accurate model. Tuning of the constant eddy viscosity or the inclusion of a more complex turbulence model may lead to better results; nonetheless, it is out of the scope of this research project.

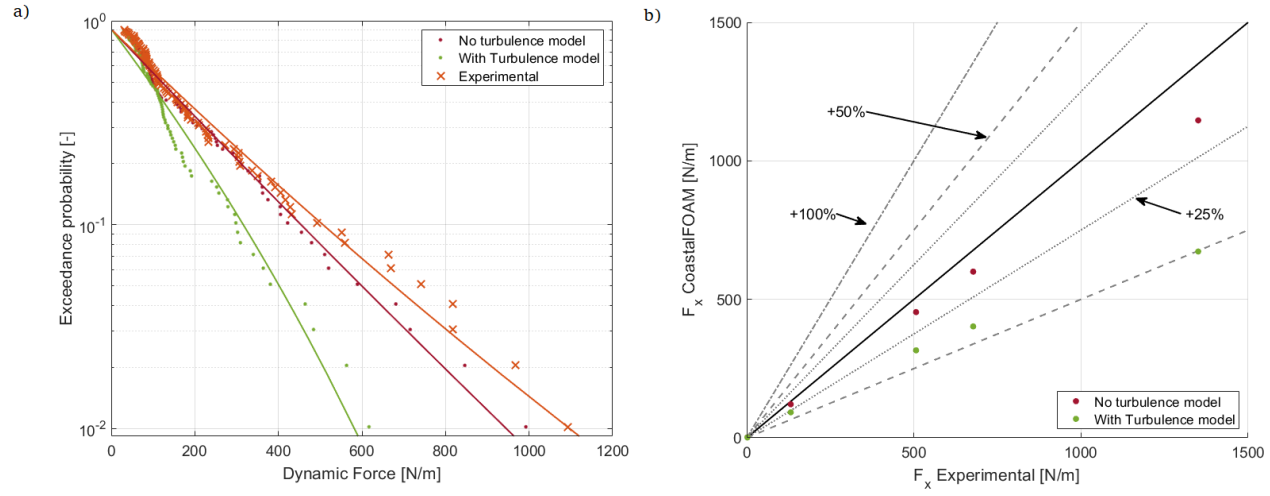

Figure 6.38: Experimental and numerical force events comparison for simulations including and excluding a turbulence model
a) GPD fitted curves, b) Comparison of the wave induced forces with the 85%, 50%, 10%, 5%, 0.4% and 0.1% exceedance probabilities based on the GPD. The 25%, 50% and 100% error bands are included.

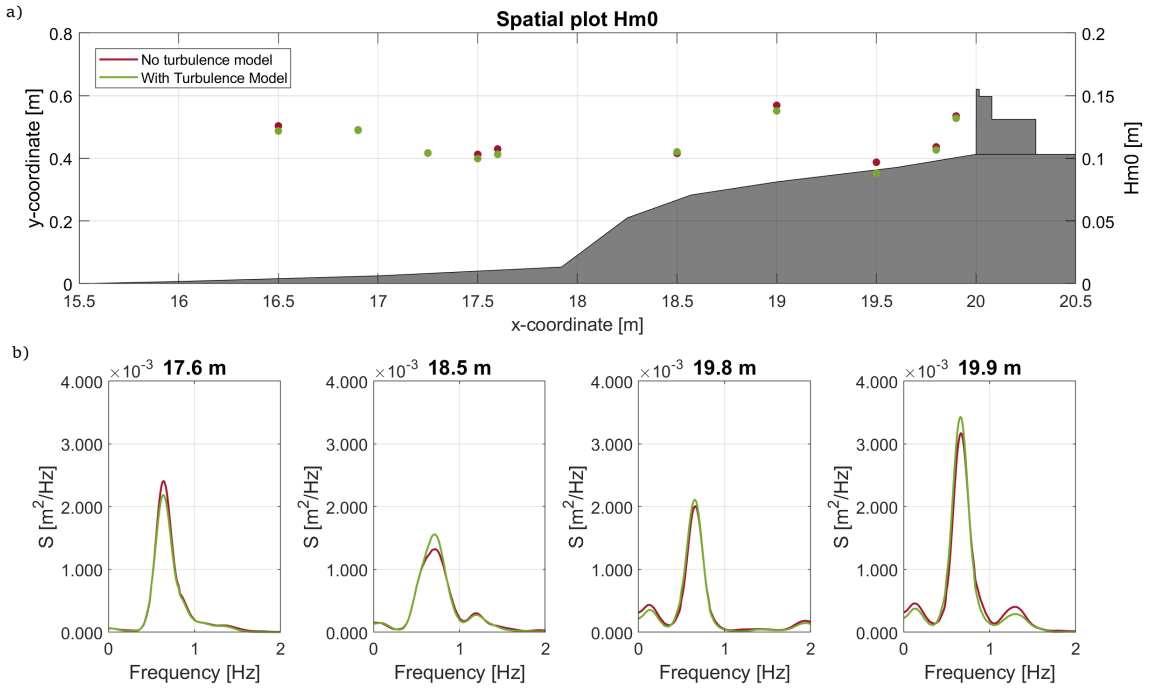

Figure 6.39: Wave propagation comparison between a simulation including a simple turbulence model and a simulation without a turbulence model
a) Spatial plot of significant wave heights recorded at 16.5, 16.9, 17.25, 17.5, 17.6, 18.5, 19, 19.5, 19.8 and 19.9 m from the wave paddle. b) Raw data spectrum analysis at locations: 17.6, 18.5, 19.8 and 19.9 m from wave paddle. In dark red, the results from the simulation without turbulence model and in green, results of a simulation including the constant eddy viscosity model.

Chapter 7

Discussion

7.1 Applicability and limitations of the model

The results obtained in this study reveal the capabilities of CoastalFOAM model to predict wave induced forces on crown walls under non-breaking and heavily breaking waves. The model validation shows that the numerical model is able to predict the dynamic forces in the front face of crown walls when impermeable and partly-permeable breakwaters armoured with Tetrapods units are included in the numerical flume. The validation confirmed that it is possible to accurately reproduce the wave conditions generated during the physical modelling campaign, but the accuracy in predicting the wave induced forces is less. In all the validation cases, correlations of above 90% were obtained when comparing the time series of the incident surface elevations. For the time series of the wave induced forces, the correlations rank above 65%.

Depending on the settings applied in CoastalFOAM, underestimations or overestimations of the maximum wave induced pressures were obtained. Several possible explanations for the discrepancies between the experimental and numerical pressures and integrated forces are provided. It is considered that the main reason for the differences is likely related to the prediction of the wave motion just in front of the crest wall because the wave characteristics have a direct influence on the impact pressures. An exact reproduction of the wave behaviour and of the breaking pattern in the numerical flume is required to predict as accurate as possible the wave induced forces. However, this is not an easy task due to the different physical processes that must be properly modelled by the numerical flume: wave reflection, wave breaking and flow through porous media.

Another possible explanation is that the placement of the pressure transducers and probes in both flumes is not exactly the same, leading to deviations in the recorded pressures. In the physical flume, the pressure transducers faces were located 1 cm behind the wall and to ensure that the pressure was flush with the wall, the cavity was filled with water and a membrane was added flush with the wall. In the numerical flume, the probes were placed 1 cm before the front face of the wall, close to the grid line defined at 19.9901 m from the wave maker. Furthermore, depending on the vertical location defined in CoastalFOAM, probes 1, 2, 3 and 5 were placed inside a grid cell while probe 4 was located in a grid line. Depending on where the pressures are estimated by the numerical model, either at the grid centres or grid lines, the placement of the probes in the numerical flume can become relevant. Also, on a similar topic, the pressure sensor in the physical model has a certain diameter. Thus, the recorded pressures are averaged over an area. In CoastalFOAM, the measurements are point pressures in the numerical domain, estimated from the grid cell or line. The differences in area may also lead to differences in the output pressure.

Other possible explanation is that the impact pressures caused by breaking waves have large spatial variability (Ramachandran et al., 2013). Therefore, differences arise when the highest pressures for each force event happened at different locations in the numerical and physical flume.

Additionally, impact pressures caused by breaking waves also have large temporal variability (Ramachandran et al. (2013) and Jacobsen et al. (2018)). On that account, Jacobsen et al. (2018) applied a low-pass filter of 50 Hz due to the large variability observed in the short-duration impacts. So far, in this report, no filtering was applied to either the experimental or the numerical wave induced force time signals. Therefore, to consider this temporal variability, a low-pass filter of 25 Hz is applied to the validation case: Tetrapods layout subjected to extreme conditions. The frequency of 25 Hz is much larger than the wave frequency and lower than that of the short-duration impacts. The filtering process was applied for the experimental and numerical raw time signals (see Figure 7.1). Simulation TT02 was used for this filtering process to compare against the results shown in section 6.5.2 (details of the numerical settings of simulation TT02 can be found in Appendix C). Once the data was filtered, the force event analysis was undertaken. The event by event comparison reveals that after filtering the force time signals, the RMSE reduces from 82 N/m to 52 N/m, while the correlation increases from 0.51 to 0.62 (see summary in Table 7.1). In terms of statistics, Figure 7.2 illustrates the exceedance curves, once

the force signals are filtered. By comparing against the exceedance curves where no filtering methodology was applied (see Chapter 6, Figure 6.32), it can be inferred that a better reproduction of the force events is obtained when the force time signals are filtered. For instance, before filtering the data, the numerical flume overpredicts the highest forces. However, after applying the low-pass filter, this overprediction cease to appear. Moreover, overall, the prediction errors decrease from 55% to 20%. Thus, applying a low-pass filter is recommended to reduce the high-variability of the short-duration impacts.

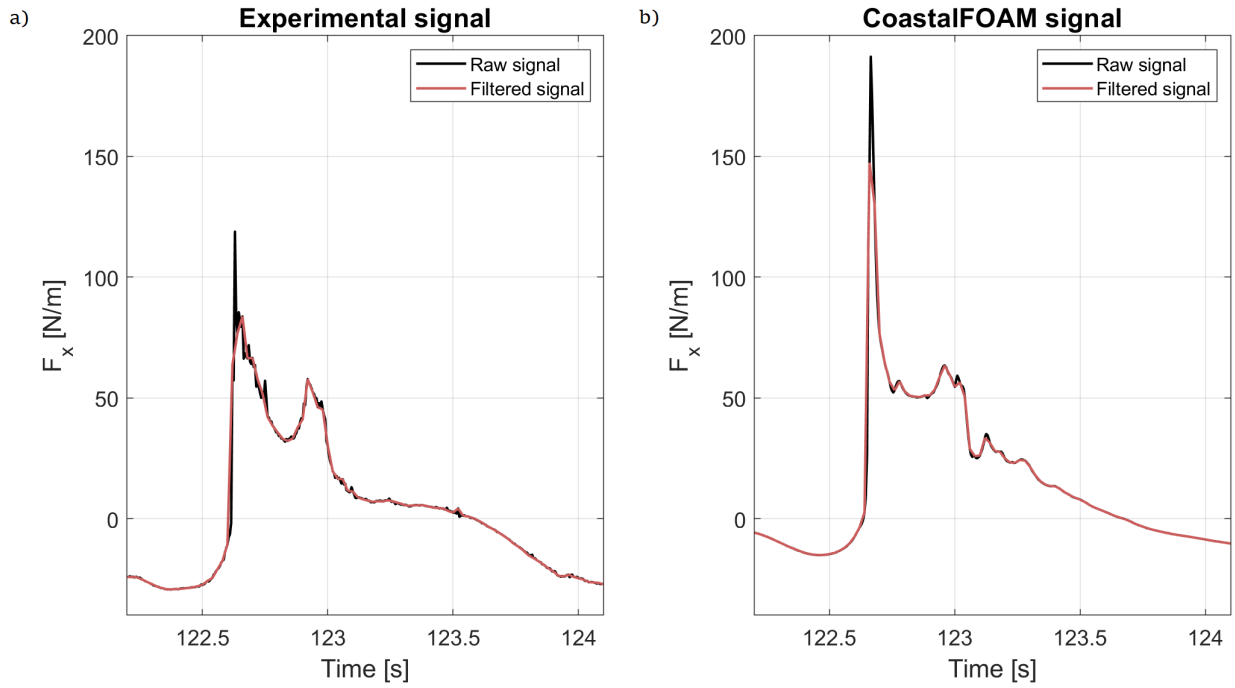

Figure 7.1: Horizontal forces on the crest walls for the validation case Tetrapods layout under extreme conditions, for an impact event captured between 122.2-124.1 s, for raw and filtered force time signals a) Experimental time signal, b) CoastalFOAM time signal

Table 7.1: Root Mean Square Error and Pearson correlation coefficient between experimental and numerical force events for the Tetrapods layout under extreme conditions, for raw and filtered time signals

Type of signal	**RMSE (N/m)**	**Pearson Correlation [-]**
Raw signal	81.93	0.51
Filtered signal	52.20	0.62

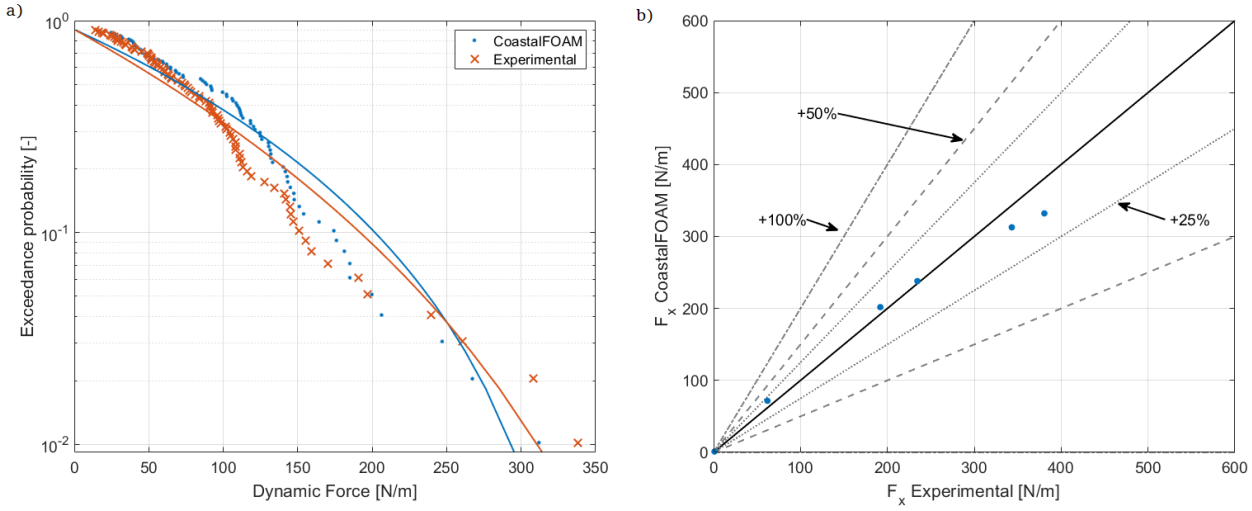

Figure 7.2: Experimental and numerical force events comparison for the Tetrapods layout under extreme conditions, once the force signals are filtered
a) GPD fitted curves, b) Comparison of the wave induced forces with the 85%, 50%, 10%, 5%, 0.4% and 0.1% exceedance probabilities based on the GPD. The 25%, 50% and 100% error bands are included.

Although there is still a 30% difference in accuracy between the physical and numerical flume when comparing the complete time series of pressure and dynamic force, overall, the OpenFOAM model is able to capture the shape and the order of magnitude of the force events. The differences are even less significant if the exceedance curves and the GPD fits of the wave induced forces are analysed. For the baseline layout under extreme conditions with a 3% degree of openness of the wall, the highest forces, associated to exceedance probabilities of 0.4% and 0.1%, are estimated with an error lower than 20%. For the Tetrapods layout under extreme conditions with a 3% degree of openness of the wall and with an $\alpha = 1,000, \beta = 1.1$ and $KC = 7.407$, the highest forces, associated to exceedance probabilities of 0.4% and 0.1%, are estimated within an error band of 10%. These final settings were obtained after the sensitivity analysis performed for the validation cases, based on varying the degree of openness of the ventilated boundary condition and the values of the porous media drag coefficients for the Tetrapods layer. Hereafter, the influence of these settings is explained more thoroughly.

According to this study, the ventilated boundary condition implemented in CoastalFOAM by Jacobsen et al. (2018) does not influence the estimation of the forces on crest walls subjected to non-breaking waves. For heavily breaking waves, a slight improvement in the wave induced forces based on the force event analysis is obtained, when an adequate degree of openness of the wall is applied. Despite this outcome, all the results show that this boundary condition affects the reflection caused by the impermeable breakwater and crest wall, thus affecting the wave motion near the wall and subsequently the wave impact on the vertical structure. One interesting finding is that the influence of adding the ventilated boundary condition and tuning the degree of openness depends on the wave climate. Under operational conditions, there is not a significant difference in the outcome of CoastalFOAM for different degrees of openness or even for the case without the ventilated boundary condition. Actually, excluding this boundary condition enables a better performance of the numerical flume in terms of force events. This happens because when non-breaking waves reach the wall, there is no air entrapment, thus, it is not necessary to add the ventilated boundary condition. When the breakwater is subjected to extreme wave loading, adding the ventilated boundary condition and defining the degree of openness of the wall has a larger influence on the wave induced forces and mainly on the force events analysis. In general, a higher degree of openness of the wall caused underestimation of the maximum dynamic pressures while lower degrees of openness resulted in overpredictions of the wave induced forces. The best comparison between the numerical and experimental forces for the extreme wave climate was obtained with a 3% degree of openness of the front face. For operational conditions, the same degree of openness can be applied, since the results are not that sensitive to the inclusion of the ventilated boundary condition. These findings allow to infer that when there is a lot of air-water mixture as a result of the breaking process, providing air ventilation between the water and the structural element is advisable to obtain more accuracy in the prediction of the wave induced forces.

On another topic, the wave-structure interaction with porous layers formed by artificial concrete units is validated based on the wave induced forces. The presence of the Tetrapods layer in the numerical flume was successfully accounted for by applying the volume averaging procedure followed by Jensen et al. (2014) and by applying the parametrisation derived by van Gent (1995) to solve for the resistance coefficients a and b. Due to

a lack of research in the field of porous media drag coefficients for artificial concrete units, different combinations of α, β and KC were applied in CoastalFOAM. Despite the different combinations of parameters, all the wave induced forces were predicted within an error band of 50%; being the error largest for the highest forces. The best comparison against experimental data was obtained for the combination: $\alpha = 1,000, \beta = 1.1$ and $KC = 7.407$, the same set of parameters recommended by van Gent (1995) for porous layers formed by rocks. These parameters differ from the optimal combination ($\alpha = 200, \beta = 0.7$ and $KC = 10,000$) found by Lee et al. (2019) for a Tetrapod covered caisson breakwater. Thus, further research in the estimation of porous media parameters for Tetrapods armour layers is recommended. The findings are also consistent with the investigation carried out by van Gent (1995), where the importance of incorporating the effect of non-stationary flow in the nonlinear resistance coefficient b was first established.

All the validation cases of this research project allowed to determine that for practical applications it is not essential to include a turbulence model in the numerical flume to obtain reliable forces on the front face of crest walls on top of impermeable and partly-permeable breakwaters subjected to non-breaking and heavily breaking waves. Other researchers (Jensen et al., 2014, Jacobsen et al., 2018) already reached to this conclusion when there is little energy dissipation caused by wave breaking and when there is large energy dissipation caused by high levels of turbulence inside a porous media. Now, the results from this investigation allow to extend the validity of not including a turbulence model in the numerical flume, for the cases when there is no energy dissipation inside a porous media but there is a lot of energy being dissipated by wave breaking (i.e. baseline layout validation cases). A possible explanation for this might be that the numerical dissipation in OpenFOAM is enough to mimic the physical dissipation caused by the wave motion in the surf zone. By adding a typical value for the constant eddy viscosity of $10^{-3}\, m^2/s$, an overestimation of the wave energy dissipation was experienced in the numerical flume, leading to a 50% underestimation of the wave induced forces (based on the exceedance curves).

The calibration process followed in this research project was based only on the degree of openness of the ventilated boundary condition for the impermeable breakwater. For the two validation cases based on the Tetrapods layout, the porous media empirical coefficients were also modified during the calibration process. If the values for the degree of openness and the porous media empirical coefficients for Tetrapods armour units were already known, the implementation of a numerical wave flume in absence of a physical model could have been applied.

The usage of a numerical flume has many advantages. First, more wave gauges along the flume or pressure transducers along the vertical wall can be included without compromising or affecting the wave propagation, breaking or reflection. Second, more information about the hydrodynamics can be recorded during the simulations with higher spatial and temporal resolution. For instance, velocities and pressures along the entire domain can be captured allowing for better understanding of the physical processes associated to different force events. In Figure 7.3, the dynamic pressure during an impact event is illustrated, for the Tetrapods layout under extreme conditions. Different stages of the wave are included in Figure 7.3: the wave approaching the wall, the wave impacting the wall and the run-down stage of the wave. Appendix D includes more hydrodynamic information obtained from the numerical flume for the baseline layout and Tetrapods layout subjected to extreme wave climate.

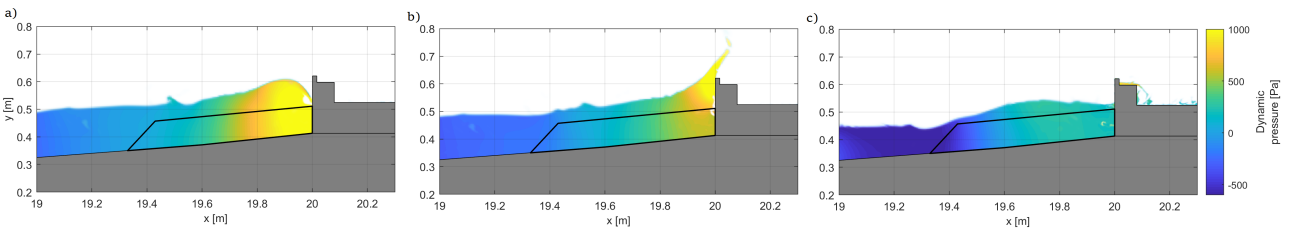

Figure 7.3: Visualization of dynamic pressures for an impact event on the crown wall, for the validation case: Tetrapods layout subjected to extreme wave
The impact event is represented by a) the wave approaching the wall, b) the wave impacting the wall and c) the run down stage of the wave

Third, the wave induced forces can be calculated based on pressure recordings along the whole wall and not just based on spatially integrating the few point measurements of pressures. This is exemplified in Figure 7.4 for two different wave impacts. When using the patch integration method, larger horizontal forces are captured by the numerical flume. The differences lay around 10-15 % between the two force integration methodologies. In the physical model, when an array of pressure sensors is deployed, the forces can only be estimated based

on a few point measurement. Thus, the experimental results generally underestimate to some extent the actual forces experienced by the wall. This limitation in the physical flume was already mentioned by Ramachandran et al. (2013). Fourth, once a numerical flume is already calibrated, different wave conditions or configurations could be tested. Given these advantages, it is considered beneficial to have a numerical model, like the one developed in this study, as an aid in the design process.

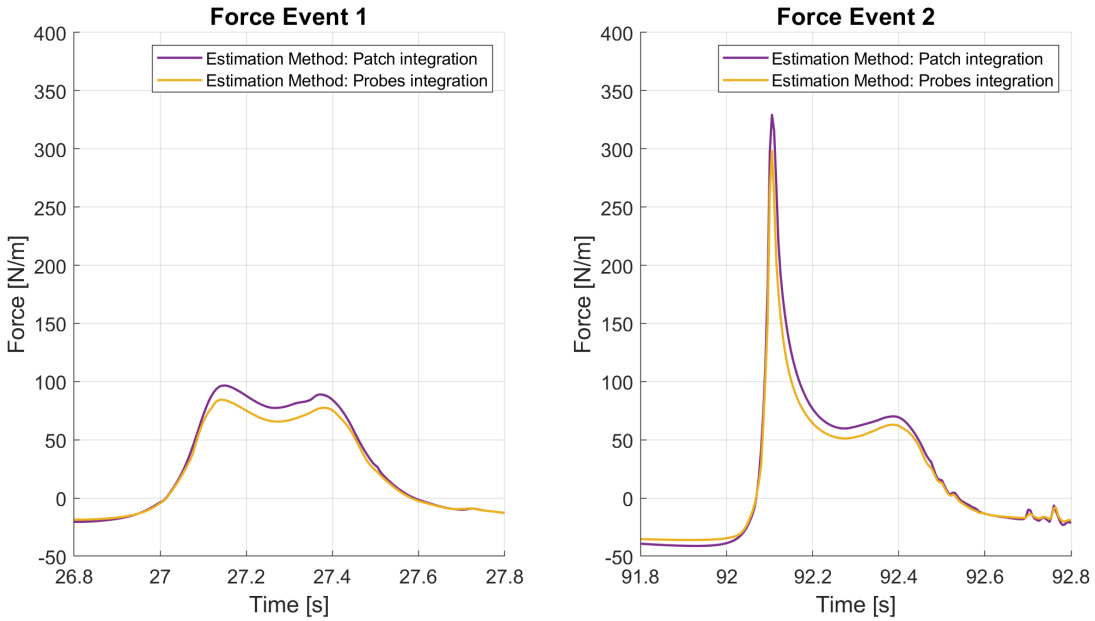

Figure 7.4: Comparison of force estimation methods in the numerical flume for two different force events recorded for the baseline layout subjected to extreme wave climate

Even though CoastalFOAM is capable of predicting with some degree of accuracy the dynamic forces exerted in the front face of crown walls, there are still some limitations. After a thorough analysis of the results obtained from all the numerical simulations, it was noticed that the smaller force events are sometimes not captured by the numerical flume. This depends on the degree of openness and on the combination of porous media drag coefficients used in CoastalFOAM. Nevertheless, the larger force events are always encountered no matter the settings applied in the numerical flume. At the end, the larger events are the important forces to be modelled for the proper design of the crest wall; therefore, this problem (i.e. missing the smaller forces) is not considered very relevant. Other limitation was found when the event by event comparison between the experimental and numerical forces was undertaken. When modelling heavily breaking waves, a noticeable decrease in accuracy is obtained compared to the operational conditions simulations (correlation decreases from 0.91 (0.86) to 0.46 (0.51) for baseline and Tetrapods layout, respectively). When the force events are analysed statistically (i.e. based on the exceedance curves), better comparisons are obtained between the experimental and numerical results. At the end, in the design phase, only the highest forces or the forces with small exceedance probabilities are used. Thus, based on this design approach, the CoastalFOAM model returns reliable forces for the design of the crest walls. Another limitation is the large computational time required by the coupled model when large wave trains must be simulated. Since it is still hard to know which waves are required to obtain the higher force events in the flume, this continue to be an issue that must be addressed in future investigations to motivate even further the application of numerical flumes in design stages.

7.2 Computational efficiency of the model

The model developed in this study consists of approximately 97,000 cells to simulate operational conditions, and approximately 114,000 cells to simulate extreme conditions. The differences are solely due to the length of the relaxation zones in OpenFOAM (see details in Chapter 5). For a simulation of 100 s of an impermeable and partly-permeable breakwater subjected to non-breaking waves, approximately 87 waves were propagated in CoastalFOAM. For the simulation of 150 s of an extreme wave climate with heavily breaking waves, on average, 98 waves were propagated in CoastalFOAM.

A comparison of the computational time required for modelling operational and extreme conditions is presented in table 7.2. The computational time required for operational conditions is used as reference (denoted as 1). For both layouts, it takes practically 7 times longer to solve the extreme wave field in CoastalFOAM, when the same grid resolution is applied.

Table 7.2: Computational time required in each validation case

Validation case	**Number of cells [-]**	**Simulation time [s]**	**Computational time [-]** (1)
Baseline layout under operational conditions	96,652	100	1
Baseline layout under extreme conditions	113,717	150	7.3
Tetrapods layout under operational conditions	96,652	100	1
Tetrapods layout under extreme conditions	113,717	150	7.2

(1) Reference time: Operational conditions

Although OpenFOAM is not the most computationally efficient model, the results obtained by applying this solver are very accurate. Moreover, this model provides relatively sufficient resolution in the hydrodynamics, while other simpler models can only be used to predict the mean hydrodynamics. The computational time required in the numerical flume during this research is considered acceptable given its high level of accuracy, as detailed in this report.

Chapter 8

Conclusions and recommendations

8.1 Conclusions

The purpose of the current study was to determine the capability of the OpenFOAM model to accurately estimate the forces on the front face of crest walls on top of impermeable and partly-permeable breakwaters subjected to non-breaking and heavily breaking waves. The assessment was based on a real life case study, the Holyhead breakwater located in Wales. Four physical tests have been used to validate a 2DV OpenFOAM model. The results obtained from the numerical flume made it possible to answer the research question posed in Chapter 1:

> **How accurate is OpenFOAM to predict the wave loads against the front face of crest walls on top of impermeable and partly-permeable breakwaters under heavily breaking waves?**.

In this section each sub-question is addressed individually.

> 1. How accurate is OpenFOAM in predicting forces on the front face of crest walls subjected to non-breaking and heavily breaking waves in case of an impermeable structure/foreshore?

The two validation cases where the baseline layout was subjected to operational and extreme conditions prove the capabilities of OpenFOAM to predict with some degree of accuracy the wave induced forces on the front face of crest walls subjected to non-breaking and heavily breaking waves in case of an impermeable structure/foreshore. This is exemplified by correlations higher than 65% when comparing the experimental and numerical time series of wave induced forces. Furthermore, once the calibration process was undertaken, based solely on modifying the degree of openness of the ventilated boundary condition, the maximum forces were underestimated with an error lower than 20% (based on the exceedance curves). The larger deviations were found for the highest forces,- associated to exceedance probabilities of 0.4% and 0.1%, experienced by the wall during the whole simulation period.

Although the model is able to predict the dynamic forces exerted in the front face of crown walls, there are still some limitations. In the numerical flume, sometimes the smallest force events are not captured depending on the settings used. This issue does not pose a drawback in the implementation of the numerical flume during design stages since the largest forces are the ones used to assess the stability of the crest wall. Other limitation was found when the event by event comparison between the experimental and numerical forces was undertaken. Event though the correlations decrease to values around 0.50 for extreme wave climate, the results from the numerical flume are considered useful during design stages since the exceedance curves display errors lower than 20% for the highest forces. These highest forces are the ones used for the crest wall design. Another limitation is the required computational time to model large wave trains since it is still hard to know which waves are required to obtain the higher force events in the flume. Despite the limitations, the findings from this research project provide a step forward in the direction of wider applicability of the numerical flume by showing that a calibrated model can predict with high accuracy the largest wave induced forces.

> 2. How accurate is OpenFOAM in predicting forces on the front face of crest walls subjected to non-breaking and heavily breaking waves in case of a permeable structure/foreshore including Tetrapods?

The two validation cases where the Tetrapods layout was subjected to operational and extreme conditions demonstrate that OpenFOAM is capable of modelling the wave-structure interaction with porous layers formed by artificial concrete units. Once the model is calibrated, the numerical flume can solved the maximum wave induced forces with errors lower than 10%, based on the results from the exceedance curves. For the same numerical simulation, sometimes the numerical flume overestimates or underestimates the different forces events.

Different combinations of the porous media parameters were evaluated in the OpenFOAM model during the calibration process. In all cases, the maximum forces were predicted within an error band of 50% (based on the exceedance curves). The best comparison between experimental and numerical wave induced forces was achieved for the set: $\alpha = 1,000, \beta = 1.1$ and $KC = 7.407$. These are the exact same values recommended by van Gent (1995) for porous layers formed by rocks. These parameters differ from the optimal combination ($\alpha = 200, \beta = 0.7$ and $KC = 10,000$) found by Lee et al. (2019) for a Tetrapod covered caisson breakwater. Thus, further research in the estimation of porous media parameters for Tetrapods armour layers is recommended. Moreover, the findings support the idea that the unsteady behaviour of the flow caused by the waves must be included in the estimation of the nonlinear resistance coefficient of the Darcy-Forchheimer equation. The exclusion of the flow oscillation in the numerical modelling of turbulence inside the porous media leads to less accurate predictions of the wave motion close to the wall and of the pressures exerted on the front face of the crown wall.

> 3. What is the effect of applying the ventilated boundary condition and varying the degree of openness of the ventilated boundary condition in the estimation of forces in the front face of crest walls on top of impermeable breakwaters subjected to non-breaking and heavily breaking waves?

This thesis has provided a deeper insight into the application of the ventilated boundary condition developed by Jacobsen et al. (2018) to solve for the spurious entrapment of air between the water surface and the structural elements. For operational conditions, the inclusion of the ventilated boundary condition does not influence the performance of the numerical model. On the contrary, for extreme conditions, the estimation of wave induced forces improves by adding the ventilated boundary condition. There is a notable influence of the degree of openness on the predicted forces. A higher degree of openness of the wall resulted in underestimation of the maximum dynamic pressures while lower degrees of openness relate to overestimation of the wave induced forces.

In conclusion, the best comparison between the numerical and experimental forces for the extreme wave climate was obtained with a 3% degree of openness of the front face. For operational conditions, the same degree of openness can be applied, since the results are not that sensitive to the inclusion of the ventilated boundary condition. These findings reveal that under breaking waves, it is advisable to add the ventilated boundary condition to obtain more accuracy in the prediction of the dominant wave induced forces. The reason behind it is that some air ventilation is required in the interface between water surface and structural elements to mimic accordingly the air-water mixture when the structure is subjected to breaking waves. Therefore, this work provides additional validation cases to the work developed by Jacobsen et al. (2018), by modelling different wave climates and coastal structures. Nonetheless, there is still room for improvement in this area, where a better understanding of this boundary condition and of the air entrapment during wave-structure interaction must be further research.

> 4. How essential is the usage of a turbulence model in OpenFOAM to get reliable forces on the front face of crest walls on top of impermeable and partly-permeable breakwaters subjected to non-breaking and heavily breaking waves?

The results from the four validation cases included in this research project revealed that for practical applications it is not essential to include a turbulence model in the numerical flume to obtain reliable forces on the front face of crest walls on top of impermeable and partly-permeable breakwaters subjected to non-breaking and heavily breaking waves. This conclusion was already drawn by other researchers (Jensen et al., 2014, Jacobsen et al., 2018) when the main source of energy dissipation happened inside a porous media layer. By including an impermeable breakwater and heavily breaking waves in the numerical flume, where the main source of energy dissipation is now related to the breaking process, the exclusion of a turbulence model can be generalized.

The validity of not including a turbulence model in the numerical flume may be explained by the fact that the numerical dissipation in OpenFOAM is enough to mimic the physical dissipation caused by the wave breaking in the surf zone. Nevertheless, further research should be undertaken to validate this assumption.

8.2 Recommendations

In this section, some practical recommendations are detailed. First, from the experienced gained by developing a numerical model in CoastalFOAM, recommendations about the model set-up and data analysis are given. Finally, the findings showed that there is still room for improvement for the application of OpenFOAM as a tool in the analysis and design process of coastal structures. Thus, this section ends with recommendations for

future research.

8.2.1 Model set-up

This study used a coupled model for the estimation of wave induced forces exerted on the front face of crest walls placed on top of impermeable and partly-permeable breakwaters subjected to non-breaking and heavily breaking waves. The coupled model consisted of two numerical solvers: OCW3D and OpenFOAM (see details in Chapter 4, Section 4.3). Thus, for the model set-up, it is recommended to follow the procedure outlined in Figure 8.1.

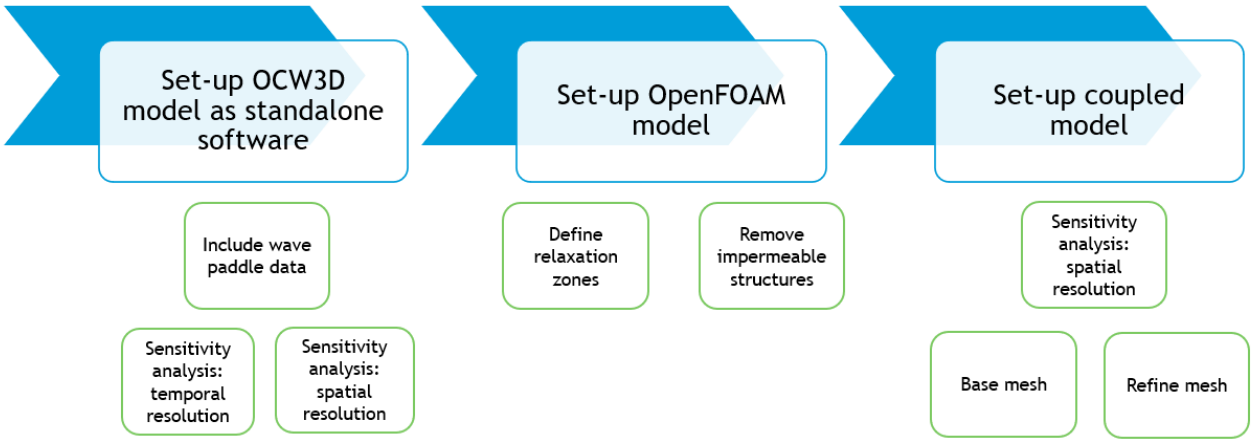

Figure 8.1: Recommended model set-up procedure when applying a coupled model

First, use the OCW3D model as a standalone software. After including the wave paddle time signal as boundary condition, the water surface elevation estimated by the numerical solver must be compared against the experimental measurements. If differences arise between the two modelling methods (i.e. physical and numerical) modifications on the wave paddle signal must be performed. In this research project, the FFT signal reconstruction method proved to be sufficient for the reproduction of the water surface elevation. Results from other research projects evidence the need to calibrate the wave paddle signal (Moretto, 2020 and Patil, 2019). Once the OCW3D is capable of reproducing the surface elevation with certain degree of accuracy, a sensitivity analysis to define the number of grid points, number of vertical layers and time step should be performed.

After defining the settings of the OCW3D model, the following step is to set-up the OpenFOAM model. Again, is recommended to use the OpenFOAM model first as a standalone software to define the first settings: length of the model, relaxation zones and placement of the coastal structure. When impermeable structures are included in the numerical flume, it is advisable to remove them from the domain to reduce the computational time required during the simulations.

Finally, the numerical model is coupled. Now, the mesh resolution in OpenFOAM must be defined. It is recommended to conduct a sensitivity analysis where different grid sizes and refinement regions are tested. A compromise between accuracy and computational time based on the purpose of the model allows to select the final mesh resolution.

8.2.2 Data analysis

This section gives a recommended procedure for post-processing and comparing the wave induced forces between the experimental and numerical flume.

Step 1: Alignment of the modelled and measured dynamic pressure time signals. This step is usually required because of the warm up period used in the physical flume for the measuring devices.

Step 2: Force estimation by the probe integration method, for both the numerical and experimental recordings.

This method is preferred for the sake of comparison against the experimental results, when an array of pressure sensors is deployed in the physical flume.

Step 3: Application of a low-pass filter to remove the large variability captured during the short-duration impacts. The cut-off frequencies have to be larger than the wave frequencies and lower than the short duration impacts.

Step 4: Time domain comparison of pressures and forces exerted on the wall (excluding the hydrostatic pressure), once the time signals are filtered.

Step 5: Comparison of the pressure distribution (excluding the hydrostatic pressure) across the front face of the crest wall for different wave steepness. In this step, the application point of the forces can be extracted from the experimental and numerical data, allowing the evaluation of overturning stability during design stages.

Step 6: Comparison of the force events. This comparison must be done event by event and in terms of exceedance probability curves.

Step 7: Numerical wave induced force estimation by applying the patch integration method. As indicated in Chapter 5, section 5.3, the patch integration provides a better picture of the actual forces experienced by the wall under wave attack. For design or analysis purposes, it is advisable to estimate the forces using this approach.

8.2.3 Future research

Even though CoastalFOAM is capable of predicting the dynamic forces exerted in the front face of crown walls, there are still some limitations. The main issue with the implementation of CoastalFOAM against physical modelling or even against other numerical solvers is the large computational time required when large wave trains must be simulated. Thus, more efforts are needed to make the CoastalFOAM model more computationally efficient. Some ideas for improvements and for further research are presented below:

- Apply a coarser mesh resolution in OpenFOAM. In this research project, the grid size and refinement level was defined for the operational conditions. Previous investigations stated a recommended number of grid cells per wave height and per wave length. Since the smaller significant wave height was the one associated to the operational conditions, the sensitivity analysis to define the mesh resolution was based on this wave climate.
- Develop a decoupled numerical model. The coupling between OCW3D and OpenFOAM usually increases the computational time. This finding was already mentioned by Moretto (2020). Besides, during the calibration process, the same boundary conditions are run several times. Thus, an attractive solution would be to developed a decoupled model; i.e., to run both models separately. The idea would be to first run the OCW3D model and store the hydrodynamics at the coupling point. This information will then be used as target solution in the inlet relaxation zone of the OpenFOAM domain. In this way, the OCW3D model only needs to be run one time for each wave condition.
- More validation cases including more wave conditions and coastal structures must be simulated in the numerical flume to extend the validity of settings such as the degree of openness of the wall, the usage of a turbulence model and the values for the porous media drag coefficients for permeable layers. Hence, the number of simulations required to calibrate a numerical flume for coastal applications would be reduced.
- Greater efforts are needed to understand which waves are responsible for the highest force events. By knowing in advance which waves should be modelled, the simulation time and thus, the computational time needed to obtain the design loads faced by the crest walls would be reduced significantly. This would be a proper approach if high correlations between the experimental and numerical force events were obtained when heavily breaking waves are being studied.

References

Battjes, J. A., & Groenendijk, H. W. (2000, June). Wave height distributions on shallow foreshores. *Coastal Engineering*, *40*(3), 161–182. doi: 10.1016/S0378-3839(00)00007-7

Bekker, J. (2017). *Experimental research into the effect of freeboard on the stability of a crown wall on a rubble mound breakwater* (Msc Thesis). TU Delft.

Berberović, E., van Hinsberg, N., Jakirlić, S., Roisman, I., & Tropea, C. (2009). Drop impact onto a liquid layer of finite thickness: Dynamics of the cavity evolution. *American Physical Society*, *79*(3), 15. doi: 10.1103/PhysRevE.79.036306

Boersen, S., Scholl, O., Jacobsen, N., & van der Lem, C. (2019). Applying a numerical wave flume to predict wave overtopping. In *Proceedings of the 38th IAHR World Congress.* Panama City, Panama. doi: 10.3850/38WC092019-1337

Bradbury, A., Allsop, W., & Stephens, R. (1988). *Hydraulic performance of breakwater crown walls* (Report No SR 146 ed.). HR Wallingford.

Brown, S., Greaves, D., Magar, V., & Conley, D. (2016). Evaluation of turbulence closure models under spilling and plunging breakers in the surf zone. *Coastal Engineering*, *114*, 177–193. doi: 10.1016/j.coastaleng.2016.04.002

Bullock, G., Obhrai, C., Peregrine, D., & Bredmose, H. (2007, August). Violent breaking wave impacts. Part 1: Results from large-scale regular wave tests on vertical and sloping walls. *Coastal Engineering*, *54*(8), 602–617. doi: 10.1016/j.coastaleng.2006.12.002

Chen, W., Warmink, J., van Gent, M., & Hulscher, S. (2021). Numerical modelling of wave overtopping at dikes using OpenFOAM®. *Coastal Engineering*, *166*, 103890. doi: 10.1016/j.coastaleng.2021.103890

CUR, CIRIA, & CETMEF. (2007). *Rock Manual, The use of rock in hydraulic engineering* (Second ed.). London.

Devolder, B. (2018). *Hydrodynamic Modelling of Wave Energy Converter Arrays* (PhD Thesis). Ghent University and KU Leuven.

DHI. (2019). *11824034 Holyhead Breakwater 2D Physical Model Test Report* (Tech. Rep.).

Engsig-Karup, A. P., Bingham, H., & Lindberg, O. (2009, April). An efficient flexible-order model for 3D nonlinear water waves. *Journal of Computational Physics*, *228*(6), 2100–2118. doi: 10.1016/j.jcp.2008.11.028

Goda, Y. (2010, March). Reanalysis of Regular and Random Breaking Wave Statistics. *Coastal Engineering Journal*, *52*(1), 71–106. doi: 10.1142/S0578563410002129

HASKONING DHV UK LTD. (2020, September). *PB9014-RHD-ZZ-XX-RP-Z-9999 Design Report Holyhead Breakwater Refurbishment* (Design Report).

Hsu, T.-J., Sakakiyama, T., & Liu, P. L.-F. (2002, June). A numerical model for wave motions and turbulence flows in front of a composite breakwater. *Coastal Engineering*, *46*(1), 25–50. doi: 10.1016/S0378-3839(02)00045-5

Hu, K. (2000). *High-resolution finite volume methods for hydraulic flow modelling* (PhD Thesis). Manchester Metropolitan University.

Irribaren, M. R., & Nogales, M. C. (1964). *Obras marítimas: Oleaje y Diques*. Madrid: Editorial Dossat Madrid S.A.

Jacobsen, N., Fuhrman, D., & Fredsøe, J. (2012, November). A wave generation toolbox for the open-source CFD library: OpenFoam®: WAVE GENERATION TOOLBOX. *International Journal for Numerical Methods in Fluids*, *70*(9), 1073–1088. doi: 10.1002/fld.2726

Jacobsen, N., van Gent, M., Capel, A., & Borsboom, M. (2018). Numerical prediction of wave loads on crest walls on top of rubble mound structures. *Coastal Engineering*, *142*, 110–124. doi: 10.1016/j.coastaleng.2018.10.004

Jacobsen, N., van Gent, M., & Fredsøe, J. (2017, February). Numerical modelling of the erosion and deposition of sand inside a filter layer. *Coastal Engineering*, *120*, 47–63. doi: 10.1016/j.coastaleng.2016.09.003

Jacobsen, N., van Gent, M., & Wolters, G. (2015, August). Numerical analysis of the interaction of irregular waves with two dimensional permeable coastal structures. *Coastal Engineering*, *102*, 13–29. doi: 10.1016/j.coastaleng.2015.05.004

Jensen, B., Jacobsen, N., & Christensen, E. D. (2014, February). Investigations on the porous media equations and resistance coefficients for coastal structures. *Coastal Engineering*, *84*, 56–72. doi: 10.1016/j.coastaleng.2013.11.004

Jonker, R. G. (2020). *Homogeneous detached composite breakwater. CFD study of the design sensitivities in the 2D geometrical layout using a detached homogeneous low-crested structure to reduce sea wall overtopping* (Msc Thesis). TU Delft.

Karagiannis, N., Karambas, T., & Koutitas, C. (2015). Wave overtopping numerical simulation using OpenFoam. In *E-Proceeding of the 36th IAHR world congress.* The Hague, the Netherlands.

Larsen, B. E., & Fuhrman, D. R. (2018). On the over-production of turbulence beneath surface waves in Reynolds-Averaged Navier–Stokes models. *Journal of Fluid Mechanics*, *853*, 419–460. doi: 10.1017/jfm.2018.577

Lee, G. S., Oh, S.-H., & Yoon, S. B. (2019, December). Evaluation of Empirical Porous-Media Parameters for Numerical Simulation of Wave Pressure on Caisson Breakwater Armored with Tetrapods. *Journal of Korean Society of Coastal and Ocean Engineers*, *31*(6), 344–350. doi: 10.9765/KSCOE.2019.31.6.344

Lin, P., & Liu, P. L.-F. (1998a, March). A numerical study of breaking waves in the surf zone. *Journal of Fluid Mechanics*, *359*, 239–264. doi: 10.1017/S002211209700846X

Lin, P., & Liu, P. L.-F. (1998b, July). Turbulence transport, vorticity dynamics, and solute mixing under plunging breaking waves in surf zone. *Journal of Geophysical Research: Oceans*, *103*(C8), 15677–15694. doi: 10.1029/98JC01360

Losada, Martin, F. L., & Medina, R. (1995). *Wave kinematics and dynamics in front of reflective structures. Wave forces on inclined and vertical wall structures.* New York : American Society of Civil Engineers.

Losada, I., Lara, J., & del Jesus, M. (2016). Modeling the Interaction of Water Waves with Porous Coastal Structures. *Journal of Waterway, Port, Coastal, and Ocean Engineering*, *142*(6), 03116003. doi: 10.1061/(ASCE)WW.1943-5460.0000361

Losada, I., Lara, J., Guanche, R., & Gonzalez-Ondina, J. (2008). Numerical analysis of wave overtopping of rubble mound breakwaters. *Coastal Engineering*, *55*(1), 47–62. doi: 10.1016/j.coastaleng.2007.06.003

Martin, F. L. (1995). Estudio hidrodinámico de la interacción de ondas de gravedad con estructuras reflejantes..

Martin, F. L., Losada, M. A., & Medina, R. (1999). Wave loads on rubble mound breakwater crown walls. *Coastal Engineering*, *37*(2), 149–174. doi: 10.1016/S0378-3839(99)00019-8

Moretto, M. L. A. (2020). *An efficient numerical approach to model wave overtopping of rubble mound breakwaters* (Msc Thesis). TU Delft.

Neves, M. G., Reis, M. T., Gadelho, J. F., Lara, J. L., Pinto, F. T., Lopes, H. G., & Cabral, J. P. (2011). Numerical modelling of waves interacting with the breakwaters of Leixões harbour, Portugal. , 12.

Nørgaard, J. Q. H., Andersen, T. L., & Burcharth, H. F. (2013, October). Wave loads on rubble mound breakwater crown walls in deep and shallow water wave conditions. *Coastal Engineering*, *80*, 137–147. doi: 10.1016/j.coastaleng.2013.06.003

Patil, A. (2019). *Numerical investigation of nearshore wave transformation and surf zone hydrodynamics* (Msc Thesis). TU Delft.

Paulsen, B. T., Bingham, H. B., & Bredmose, H. (2013). *Efficient computations of wave loads on offshore structures.* Tecnical University of Denmark.

Pedersen, J. (1996). *Wave Forces and Overtopping on Crown Walls of Rubble Mound Breakwaters* (PhD Thesis). Aalborg University.

Ramachandran, K., Schimmels, S., Stagonas, D., & Müller, G. (2013). Measuring Wave Impact on Coastal Structures with High Spatial and Temporal Resolution – Tactile Pressure Sensors a Novel Approach. , 16.

Sakakiyama, T., & Liu, P. L.-F. (2001, December). Laboratory experiments for wave motions and turbulence flows in front of a breakwater. *Coastal Engineering*, *44*(2), 117–139. doi: 10.1016/S0378-3839(01)00027-8

Sigalas, N. (2019). *Investigation of crown wall stability on top of rubble mound structures with OpenFOAM®* (Msc Thesis). TU Delft.

Suzuki, T., Altomare, C., Veale, W., Verwaest, T., Trouw, K., Troch, P., & Zijlema, M. (2017, April). Efficient and robust wave overtopping estimation for impermeable coastal structures in shallow foreshores using SWASH. *Coastal Engineering*, *122*, 108–123. doi: 10.1016/j.coastaleng.2017.01.009

United Nations. (2017). Factsheet: People and Oceans.

van den Bos, J., & Verhagen, H. (2018). *Breakwater design. Lecture notes CIE5308.* Delft University of Technology.

van den Bos, J., Verhagen, H. J., & Kuiper, C. (2015). Numerical Modelling of Wave Reflection and Transmission

in Vertical Porous Structures. In *Coastal Structures and Solutions to Coastal Disasters 2015* (pp. 876–890). Boston, Massachusetts: American Society of Civil Engineers. doi: 10.1061/9780784480304.090

van Gent, M. (1995). *Wave interaction with permeable coastal structures* (PhD Thesis). TU Delft.

van Gent, M., Jacobsen, N., & Wolters, G. (2018, January). Modelling of open filters under wave loading. In *Coasts, Marine Structures and Breakwaters 2017* (pp. 1081–1090). Liverpool, UK: ICE Publishing. doi: 10.1680/cmsb.63174.1081

van Heemst, C. C. (2014). *Stability of a Crown Wall on a Breakwater: A refinement of existing design formulae* (Ms). TU Delft.

Van Melis, T. J. (2019). *Tolerable wave overtopping during construction of a breakwater* (Msc Thesis). TU Delft.

Weller, H. G., Tabor, G., Jasak, H., & Fureby, C. (1998). A tensorial approach to computational continuum mechanics using object-oriented techniques. *Computers in Physics*, *12*(6), 620. doi: 10.1063/1.168744

Wilcox, D. (2006). *Turbulence modeling for CFD* (3rd ed.). DCW Industries.

Zelt, J., & Skjelbreia, J. E. (1993, June). Estimating Incident and Reflected Wave Fields Using an Arbitrary Number of Wave Gauges. In *Coastal Engineering 1992* (pp. 777–789). Venice, Italy: American Society of Civil Engineers. doi: 10.1061/9780872629332.058

Zijlema, M., Stelling, G., & Smit, P. (2011, October). SWASH: An operational public domain code for simulating wave fields and rapidly varied flows in coastal waters. *Coastal Engineering*, *58*(10), 992–1012. doi: 10.1016/j.coastaleng.2011.05.015

Appendices

Appendix A

OCW3D Sensitivity Analysis

A.1 Introduction

In this appendix, a grid and a temporal resolution sensitivity study is conducted for the OCW3D numerical model, for the extreme and experimental wave climate. Based on the recommendations stated by other researchers in Section 5.2.3 and the results of this sensitivity analysis, a final mesh and time step are selected to implement in the coupled model.

A.2 Vertical grid resolution

Figure A.1 illustrates the effect of the number of vertical layers in the convergence of the numerical model. For operational conditions, 11 layers is enough to reproduce the surface elevation accurately. In case of the extreme conditions, as waves are steeper, a total of 16 vertical layers are required.

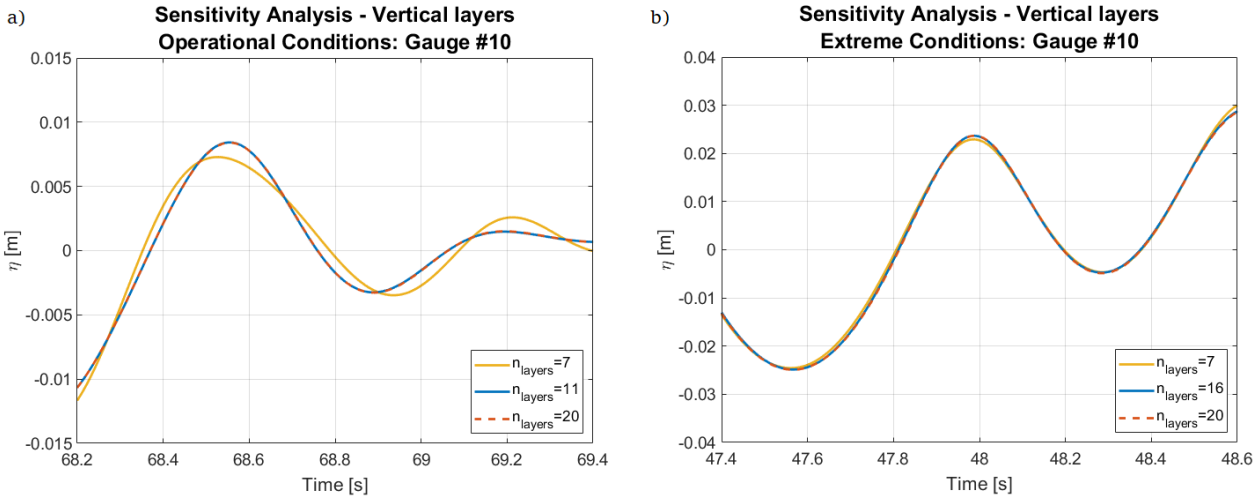

Figure A.1: OCW3D vertical grid sensitivity analysis: a) Operational Conditions, b) Extreme conditions

A.3 Horizontal grid resolution

According to the sensitivity analysis, the horizontal discretization has more influence in the model outcome than the number of vertical layers. Figure shows the variation of the water surface for three different grid sizes. The conclusion is to use 1600 grid points for operational conditions and 1800 grid points for extreme conditions.

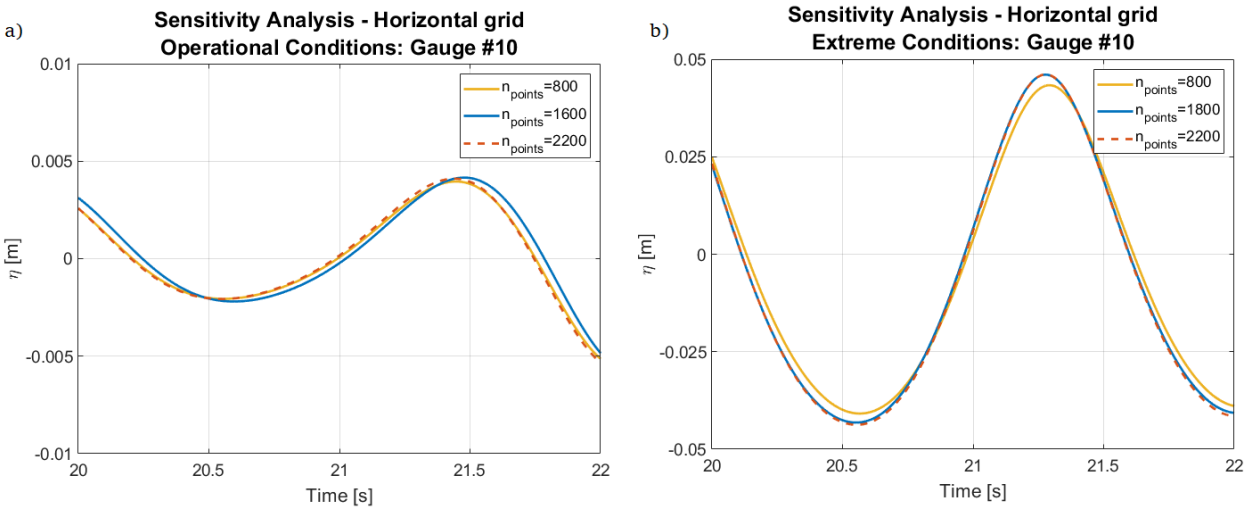

Figure A.2: OCW3D Horizontal grid sensitivity analysis: a) Operational Conditions, b) Extreme conditions

A.4 Temporal resolution

As explained in Chapter 5, section 5.2.2, the wave paddle interpolation procedure has a high impact on the numerical model. For this reason, small time steps were used to produce a smooth wave paddle velocity signal. Table A.1 and Table A.2 compare the water surface elevation between the numerical results and the experimental results measured at gauges 3, 5 and 9. The time step selected for each wave climate is the one who returned a higher correlation with the experimental surface elevation. The final settings are summarized in Table A.3.

Table A.1: Pearson Correlation Coefficient: Experimental vs OCW3D Surface Elevation for Operational Conditions

$\Delta t\,[s]$	**Gauge 3**	**Gauge 5**	**Gauge 9**
0.025	0.7606	0.8117	0.7058
0.01	0.7619	0.8142	0.7284

Table A.2: Pearson Correlation Coefficient: Experimental vs OCW3D Surface Elevation for Extreme Conditions

dt [s]	**Gauge 3**	**Gauge 5**	**Gauge 9**
0.01	0.8929	0.8073	0.7163
0.002	0.9023	0.8214	0.7383

A.5 Final OCW3D settings

Table A.3: Final settings for the OCW3D model

Hydraulic Conditions	Number of vertical layers	Number of horizontal grid points	$\Delta t\,[s]$
Operational conditions - high water	11	1600	0.01
Extreme conditions - high water	16	1800	0.002

Appendix B

OpenFOAM Sensitivity Analysis

B.1 Introduction

This appendix shows the results of using two different grid resolutions in OpenFOAM for the case: Baseline layout subject to operational conditions. The comparison is based on the surface elevation and forces exerted on the front wall and includes the computational time required for each simulation. According to these results, the final mesh in OpenFOAM was selected.

B.2 Grid resolution

A sensitivity analysis was undertaken to define a proper mesh resolution which provided accurate results but at the same time, was computationally efficient. The analysis was carried out under operational conditions because when the fine mesh was applied for the extreme conditions, very large computational times arose, delaying this study.

Figure B.1 and Table B.1 illustrate the base mesh used in each simulation, along with the refinement regions and the level of refinement per region. The Fine grid consists of square cells of 0.002 m near the water surface corresponding to nearly 22 cells/wave height. The Coarse grid, on the other hand, consists of cell sizes of 0.005 m near the water surface, resulting in nearly 9 cells/wave height. For the first grid type, simulating 100 s takes about 25 h, while for the coarse grid, the computational time reduces to 3 h.

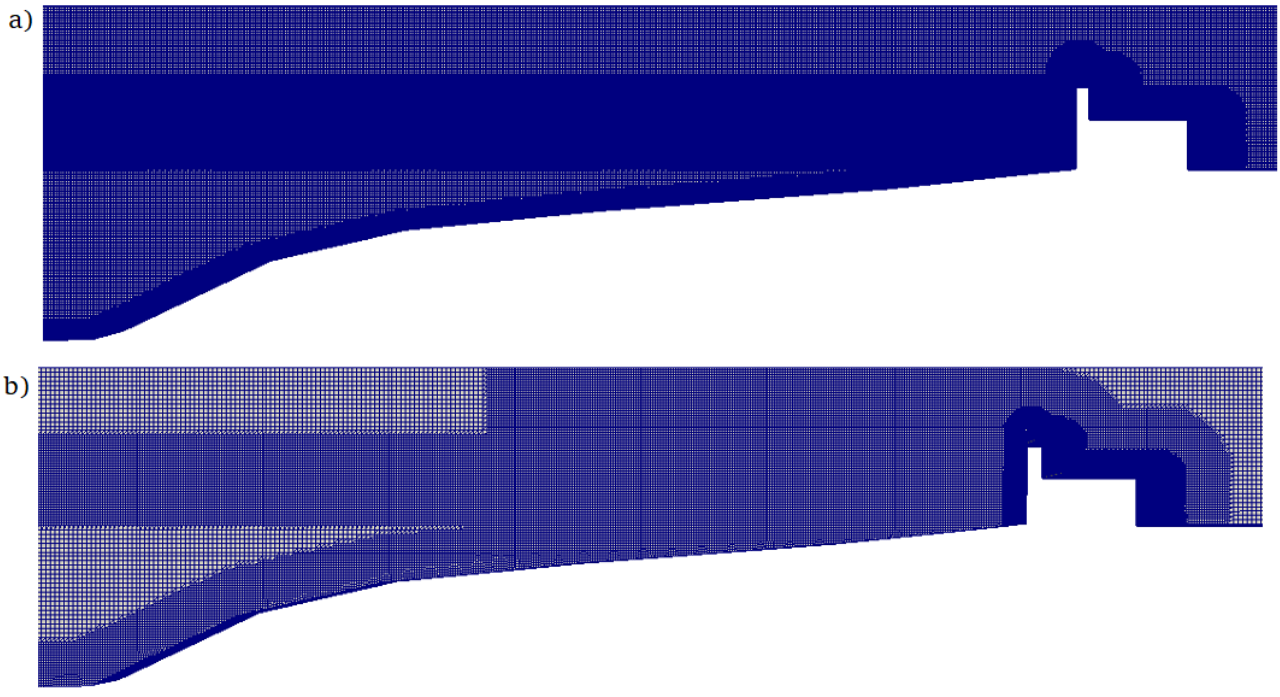

Figure B.1: OpenFOAM grid sensitivity analysis: a) Fine Grid, b) Coarse Grid

Table B.1: Mesh resolution for the fine and coarse grid types

Grid Type	Base Mesh $\Delta x X \Delta y$ [cm X cm]	Refinement regions	Refinement level
Fine	0.4 X 0.4	Near the water surface	1
		At shoaling area	-
		Near the slope surface	1
		Around the crest wall	1
Coarse	1 X 1	Near the water surface	1
		At shoaling area	1
		Near the slope surface	1
		Around the crest wall	2

B.3 Numerical vs Experimental comparison

A comparison was made between the numerical results and the experimental measurements, both for the surface elevation and for the pressure transducers integrated dynamic force (see summary in Table B.2). By reducing the computational effort by almost 90%, a decrease in accuracy of 3% and 5% was obtained for the surface elevation and the dynamic force, respectively. To visualize these results, Figures B.3 and B.2 display the incident water surface elevation recorded at gauge 10, in the time and frequency domain. Figure B.4 compares the dynamic forcing against the wall.

Table B.2: OpenFOAM Mesh comparison

Grid Type	Simulation time [s]	Computational time [h]	ρ Surface Elevation (1)	ρ Dynamic Force
Fine	100	25	0.9407	0.9597
Coarse	100	3	0.9101	0.9163

(1) Incident surface elevation at gauge 10

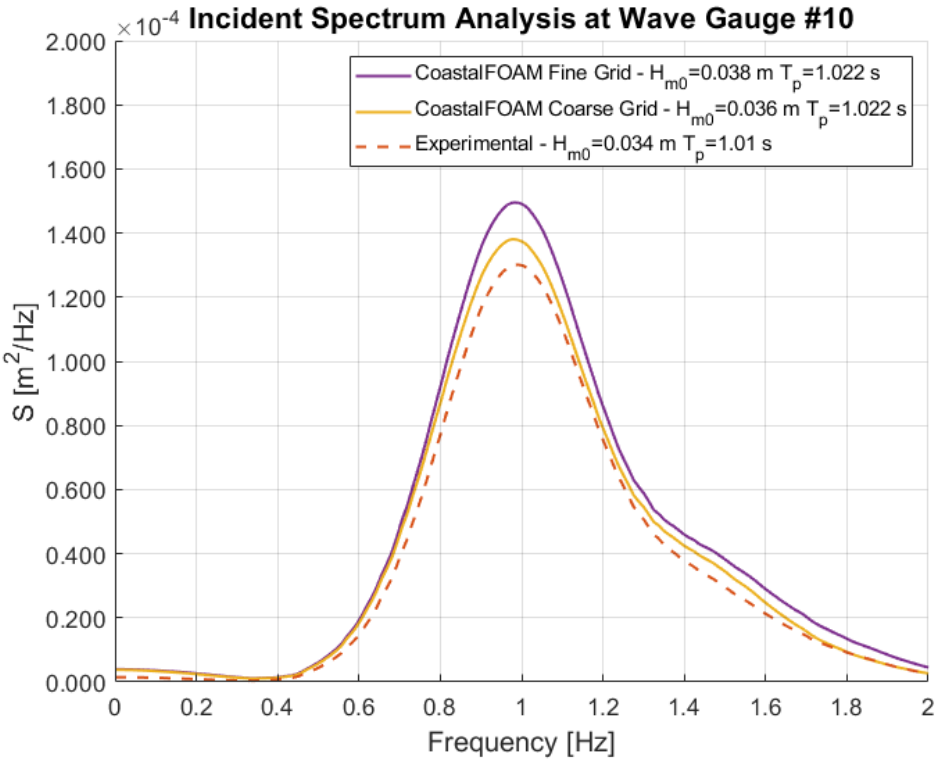

Figure B.2: Incident spectrum analysis at Gauge 10. Wave reflection analysis based on the method by Zelt and Skjelbreia (1993) using the water surface elevation recorded at gauges 6-10

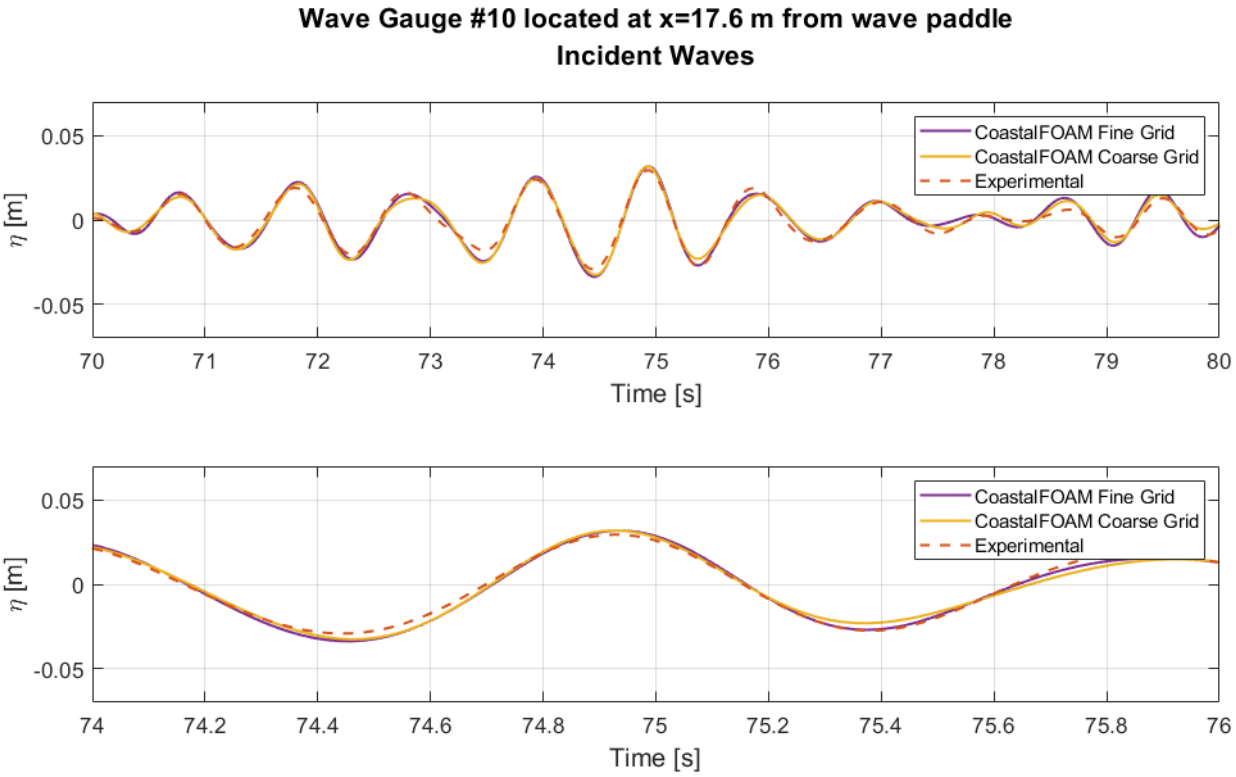

Figure B.3: Surface elevation time series comparison

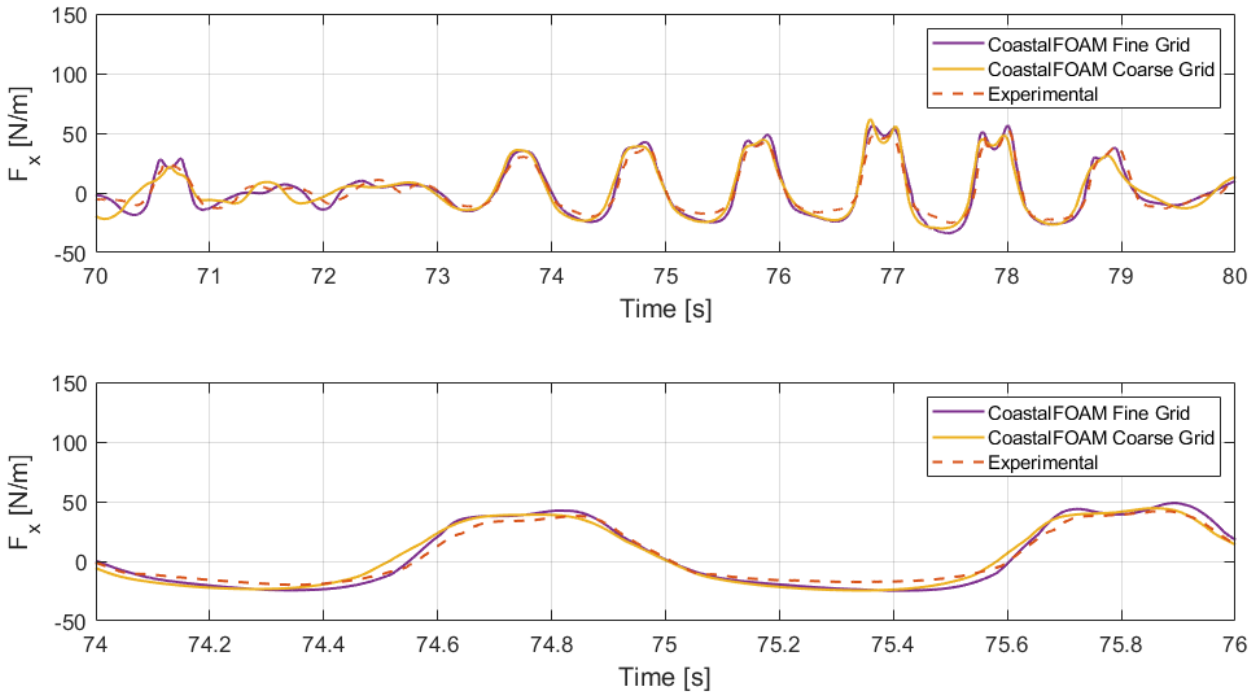

Figure B.4: Dynamic force time series comparison

Appendix C

Simulations summary

Table C.1: Experimental and numerical results of wave conditions for all the simulation cases

Simulation	**Wave climate**	**Bulk wave statistics** (1)			
		$H_{m0,exp}\,[m]$	$T_{p,exp}\,[s]$	$H_{m0,model}\,[m]$	$T_{p,model}\,[s]$
BO01	Operational	0.034	1.010	0.036	1.023
BO02	Operational	0.034	1.010	0.036	1.023
BO03	Operational	0.034	1.010	0.036	1.023
BO04	Operational	0.034	1.010	0.036	1.023
BE01	Extreme	0.108	1.503	0.104	1.521
BE02	Extreme	0.108	1.503	0.105	1.503
BE03	Extreme	0.108	1.503	0.103	1.521
BE04	Extreme	0.108	1.503	0.103	1.521
BE05	Extreme	0.108	1.503	0.105	1.521
BE06	Extreme	0.108	1.503	0.109	1.503
BE07	Extreme	0.108	1.503	0.107	1.503
TT00	Operational	0.034	1.008	0.035	1.021
TT01	Extreme	0.104	1.473	0.101	1.491
TT02	Extreme	0.104	1.473	0.105	1.509
TT03	Extreme	0.104	1.473	0.105	1.509
TT04	Extreme	0.104	1.473	0.104	1.491
TT05	Extreme	0.104	1.473	0.104	1.509
TT06	Extreme	0.104	1.473	0.103	1.491

(1) Measured at Gauge 10

Table C.2: Numerical settings for all the simulation cases: relaxation zones and turbulence modelling

Simulation	Relaxation zones (1)		Turbulence
	Inlet	Outlet	
BO01	Length = 1.64 (13.86 m to 15.50 m)	Length = 0.82 (20.60 m to 21.42 m)	No
BO02	Length = 1.64 (13.86 m to 15.50 m)	Length = 0.82 (20.60 m to 21.42 m)	No
BO03	Length = 1.64 (13.86 m to 15.50 m)	Length = 0.82 (20.60 m to 21.42 m)	No
BO04	Length = 1.64 (13.86 m to 15.50 m)	Length = 0.82 (20.60 m to 21.42 m)	No
BE01	Length = 3.36 (12.14 m to 15.50 m)	Length = 1.68 (20.60 m to 22.28 m)	No
BE02	Length = 3.36 (12.14 m to 15.50 m)	Length = 1.68 (20.60 m to 22.28 m)	No
BE03	Length = 3.36 (12.14 m to 15.50 m)	Length = 1.68 (20.60 m to 22.28 m)	No
BE04	Length = 3.36 (12.14 m to 15.50 m)	Length = 1.68 (20.60 m to 22.28 m)	No
BE05	Length = 3.36 (12.14 m to 15.50 m)	Length = 1.68 (20.60 m to 22.28 m)	No
BE06	Length = 3.36 (12.14 m to 15.50 m)	Length = 1.68 (20.60 m to 22.28 m)	No
BE07	Length = 3.36 (12.14 m to 15.50 m)	Length = 1.68 (20.60 m to 22.28 m)	Yes
TT00	Length = 1.64 (13.86 m to 15.50 m)	Length = 0.82 (20.60 m to 21.42 m)	No
TT01	Length = 3.36 (12.14 m to 15.50 m)	Length = 1.68 (20.60 m to 22.28 m)	No
TT02	Length = 3.36 (12.14 m to 15.50 m)	Length = 1.68 (20.60 m to 22.28 m)	No
TT03	Length = 3.36 (12.14 m to 15.50 m)	Length = 1.68 (20.60 m to 22.28 m)	No
TT04	Length = 3.36 (12.14 m to 15.50 m)	Length = 1.68 (20.60 m to 22.28 m)	No
TT05	Length = 3.36 (12.14 m to 15.50 m)	Length = 1.68 (20.60 m to 22.28 m)	No
TT06	Length = 3.36 (12.14 m to 15.50 m)	Length = 1.68 (20.60 m to 22.28 m)	No

(1) Measures from wave maker

Table C.3: Numerical settings for all the simulation cases: the ventilated boundary condition and the porous media parameters

Simulation	Ventilated boundary condition		Tetrapods layer				
	Degree of openness	**Loss coefficient**	$d_{n50}\,[m]$	$n_p\,[-]$	$\alpha\,[-]$	$\beta\,[-]$	$KC\,[-]$
BO01	None	1.5	-	-	-	-	-
BO02	0.50%	1.5	-	-	-	-	-
BO03	3.00%	1.5	-	-	-	-	-
BO04	6.00%	1.5	-	-	-	-	-
BE01	None	1.5	-	-	-	-	-
BE02	0.001%	1.5	-	-	-	-	-
BE03	0.10%	1.5	-	-	-	-	-
BE04	0.50%	1.5	-	-	-	-	-
BE05	3.00%	1.5	-	-	-	-	-
BE06	6.00%	1.5	-	-	-	-	-
BE07	3.00%	1.5	-	-	-	-	-
TT00	3.00%	1.5	0.08	0.5	200	1.1	2.187
TT01	3.00%	1.5	0.08	0.5	200	0.8	7.407
TT02	3.00%	1.5	0.08	0.5	200	1.1	7.407
TT03	3.00%	1.5	0.08	0.5	200	1.8	7.407
TT04	3.00%	1.5	0.08	0.5	500	1.1	7.407
TT05	3.00%	1.5	0.08	0.5	1000	1.1	7.407
TT06	3.00%	1.5	0.08	0.5	200	1.1	10000

Appendix D

CoastalFOAM typical results

D.1 Introduction

This appendix presents results from the numerical flume for the cases: Baseline layout and Tetrapods layout subjected to extreme conditions. The results include hydrodynamic information with high spatial and temporal resolution, showing the added value of using a numerical flume when studying wave-structure interaction.

D.2 Extreme Conditions

D.2.1 Baseline layout

Two force events of different magnitude are presented below (see Figures D.1 and D.4). The force event captured between 21.1 s and 22.0 has a higher magnitude than the force event captured between 104.2 s and 105.0 s. To visualize the differences between these two events, details of the flow and pressure over both impact events are extracted from the numerical flume. Horizontal velocities, vertical velocities, total pressure and dynamic pressure along the entire domain are displayed, where different stages of the wave are illustrated: the wave approaching the wall, the wave closer to the wall, the wave impacting the wall and the run-down stage (see Figures D.2, D.3, D.5 and D.6).

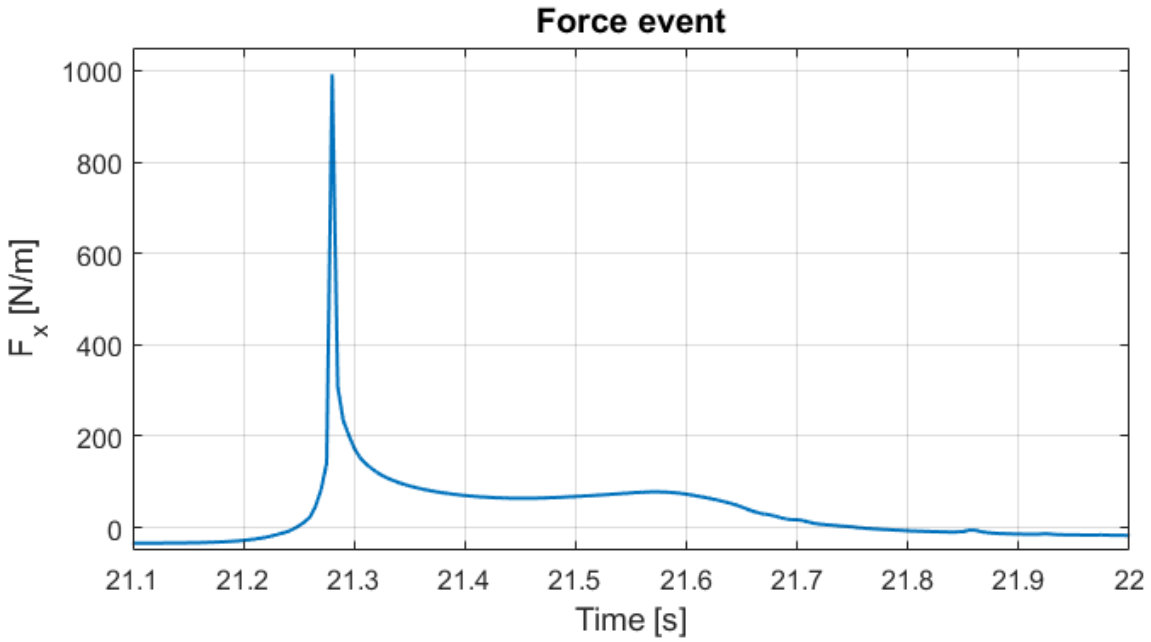

Figure D.1: Force event recorded between 21.1-22.0 s for the baseline layout under extreme conditions

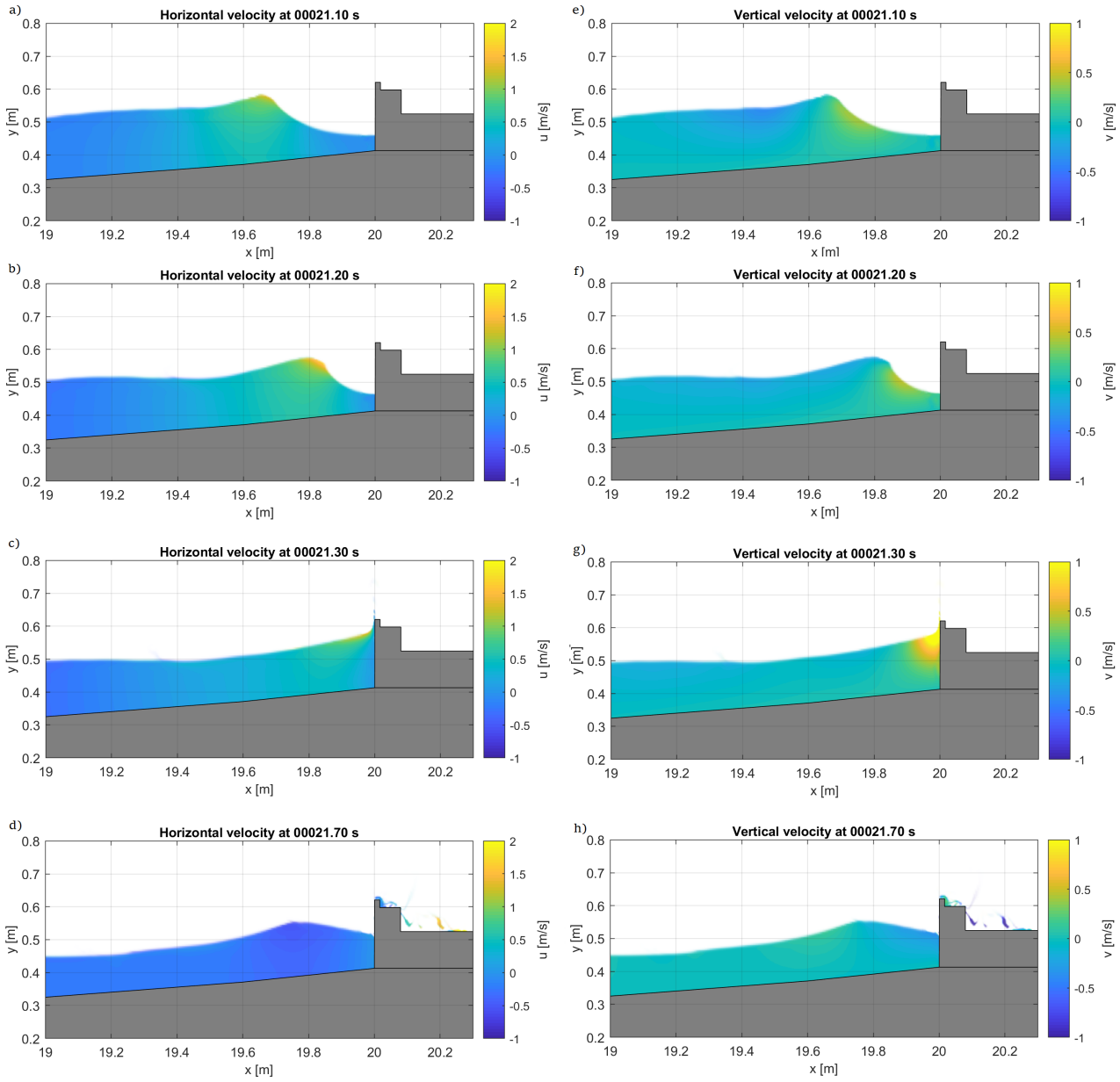

Figure D.2: Visualization of velocities for the impact event on the crown wall recorded between 21.1 s and 22.0 s, for the baseline layout under extreme conditions
Left panel shows the horizontal velocities and the right panel, the vertical velocities. The impact event is represented by the wave approaching the wall (a) and e)), the wave close to the wall (b) and f)), the wave impacting the wall (c) and g)) and the run down stage of the wave (d) and h))

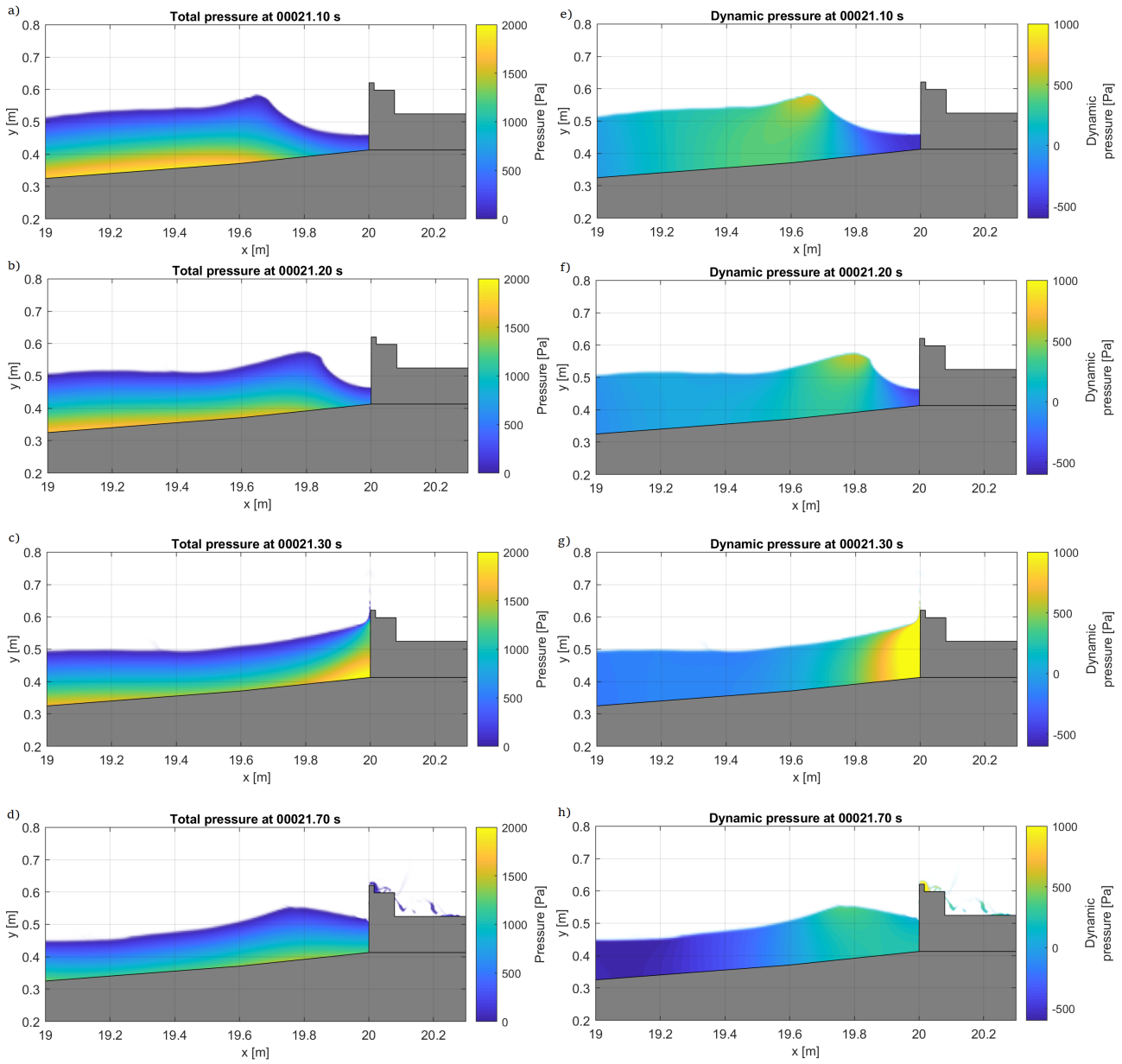

Figure D.3: Visualization of pressures for the impact event on the crown wall recorded between 21.1 s and 22.0 s, for the baseline layout under extreme conditions

Left panel shows the total pressure and the right panel, the dynamic pressure (total pressure minus the hydrostatic pressure). The impact event is represented by the wave approaching the wall (a) and e)), the wave close to the wall (b) and f)), the wave impacting the wall (c) and g)) and the run down stage of the wave (d) and h))

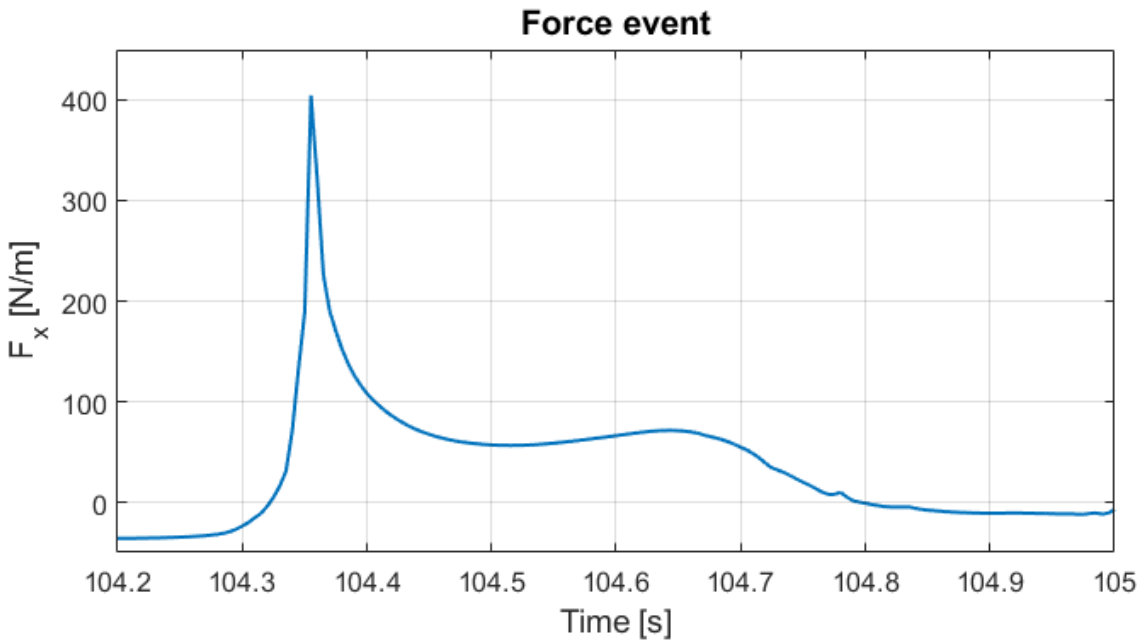

Figure D.4: Force event recorded between 104.2-105.0 s for the baseline layout under extreme conditions

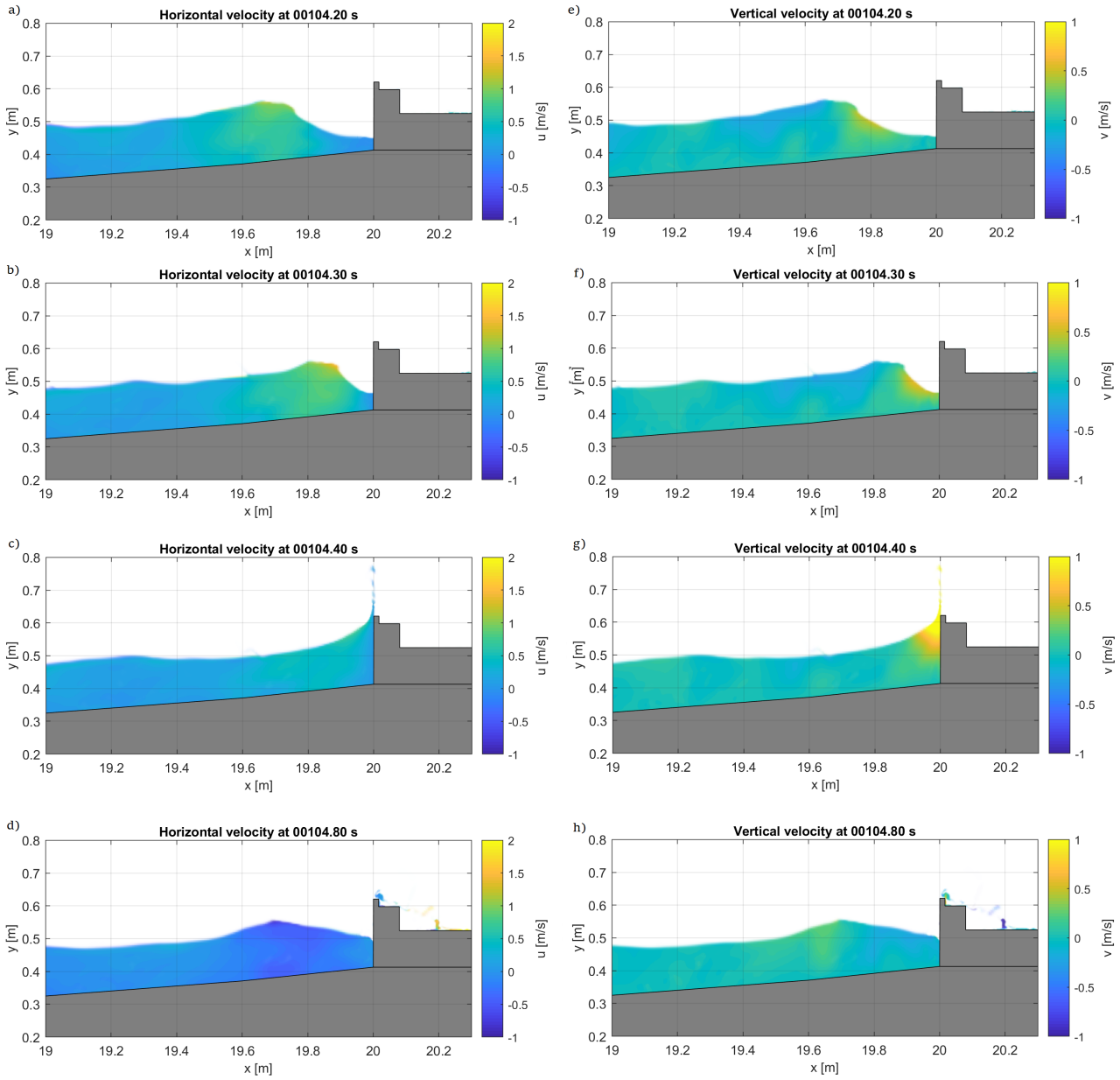

Figure D.5: Visualization of velocities for the impact event on the crown wall recorded between 104.2 s and 105.0 s, for the baseline layout under extreme conditions
Left panel shows the horizontal velocities and the right panel, the vertical velocities. The impact event is represented by the wave approaching the wall (a) and e)), the wave close to the wall (b) and f)), the wave impacting the wall (c) and g)) and the run down stage of the wave (d) and h))

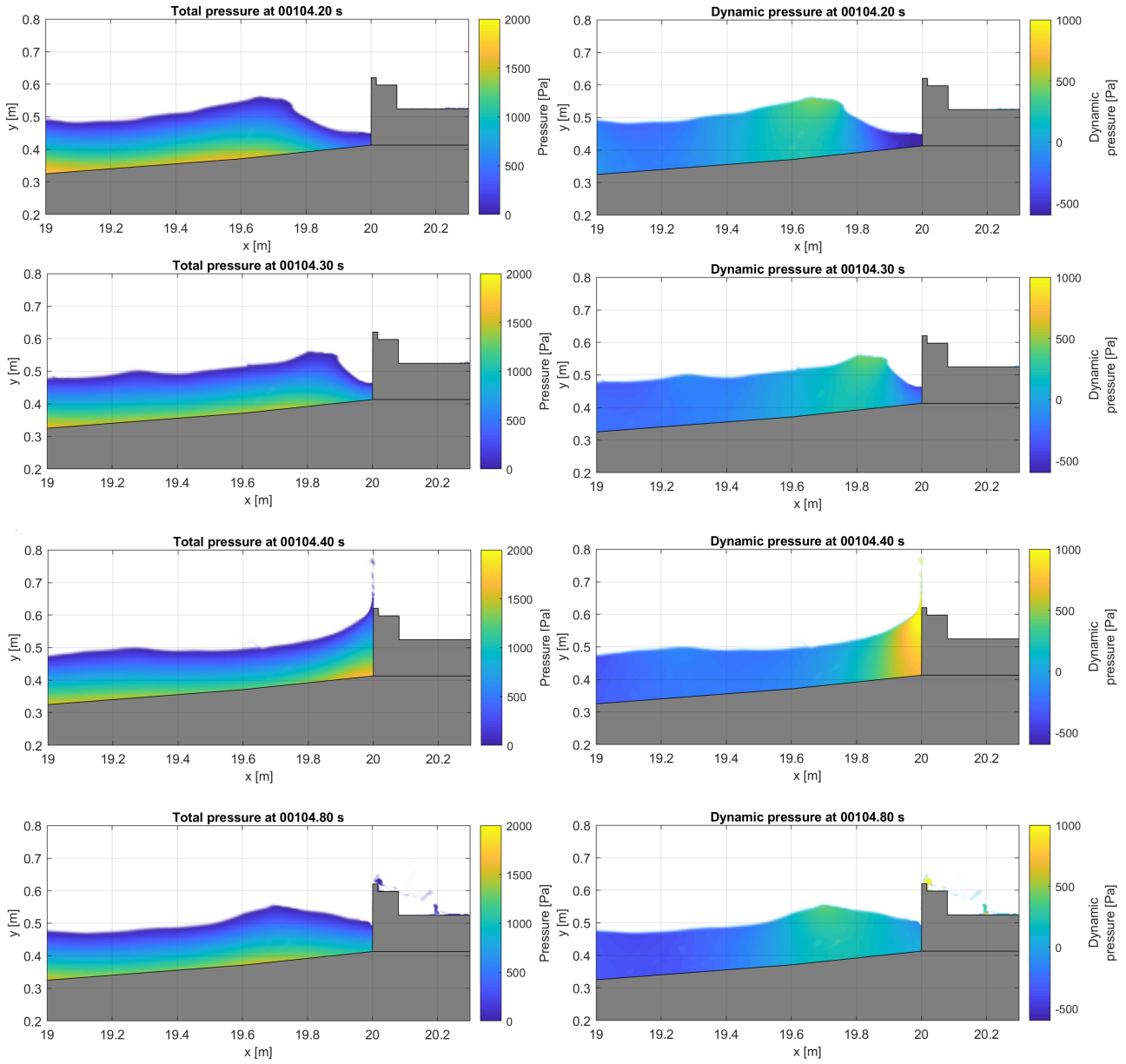

Figure D.6: Visualization of pressures for the impact event on the crown wall recorded between 104.2 s and 105.0 s, for the baseline layout under extreme conditions

Left panel shows the total pressure and the right panel, the dynamic pressure (total pressure minus the hydrostatic pressure). The impact event is represented by the wave approaching the wall (a) and e)), the wave close to the wall (b) and f)), the wave impacting the wall (c) and g)) and the run down stage of the wave (d) and h))

D.2.2 Tetrapods layout

Two force events of different magnitude are presented below (see Figures D.7 and D.10). The force event captured between 21.2 s and 22.4 has a lower magnitude than the force event captured between 148.4 s and 149.2 s. To visualize the differences between these two events, details of the flow and pressure over both impact events are extracted from the numerical flume. Horizontal velocities, vertical velocities, total pressure and dynamic pressure along the entire domain are displayed, where different stages of the wave are illustrated: the wave approaching the wall, the wave closer to the wall, the wave impacting the wall and the run-down stage (see Figures D.9, D.8, D.11 and D.12).

For the Tetrapods layout, the effect of the porous media in the velocity field is notable, resulting in small velocities inside the skeleton during both impact events (see Figures D.9 and D.11).

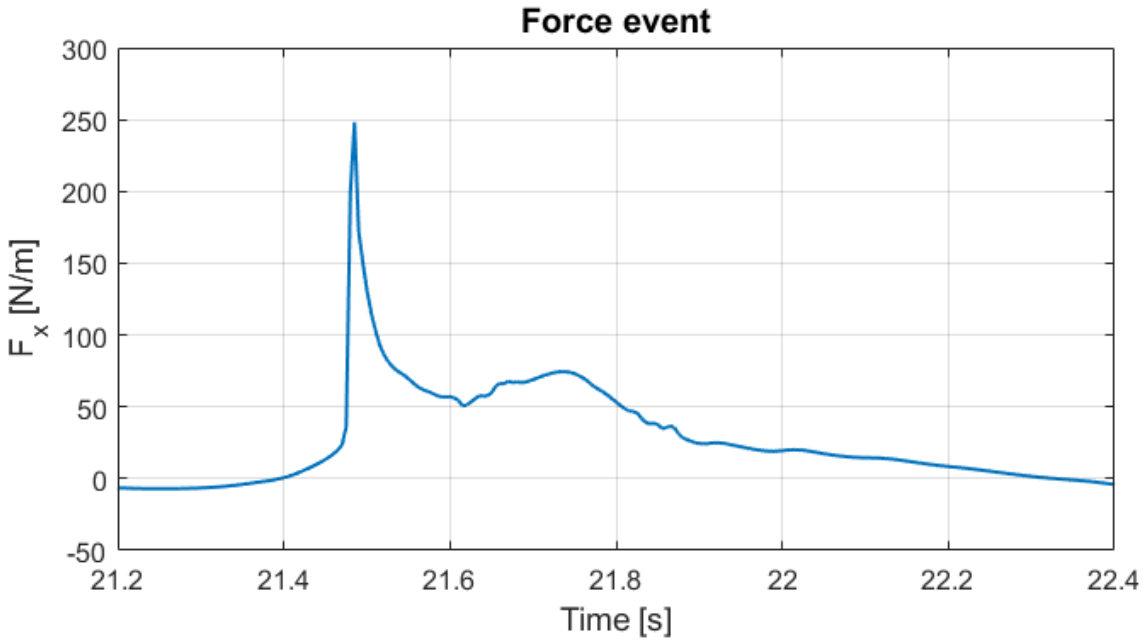

Figure D.7: Force event recorded between 21.2-22.4 s for the Tetrapods layout under extreme conditions

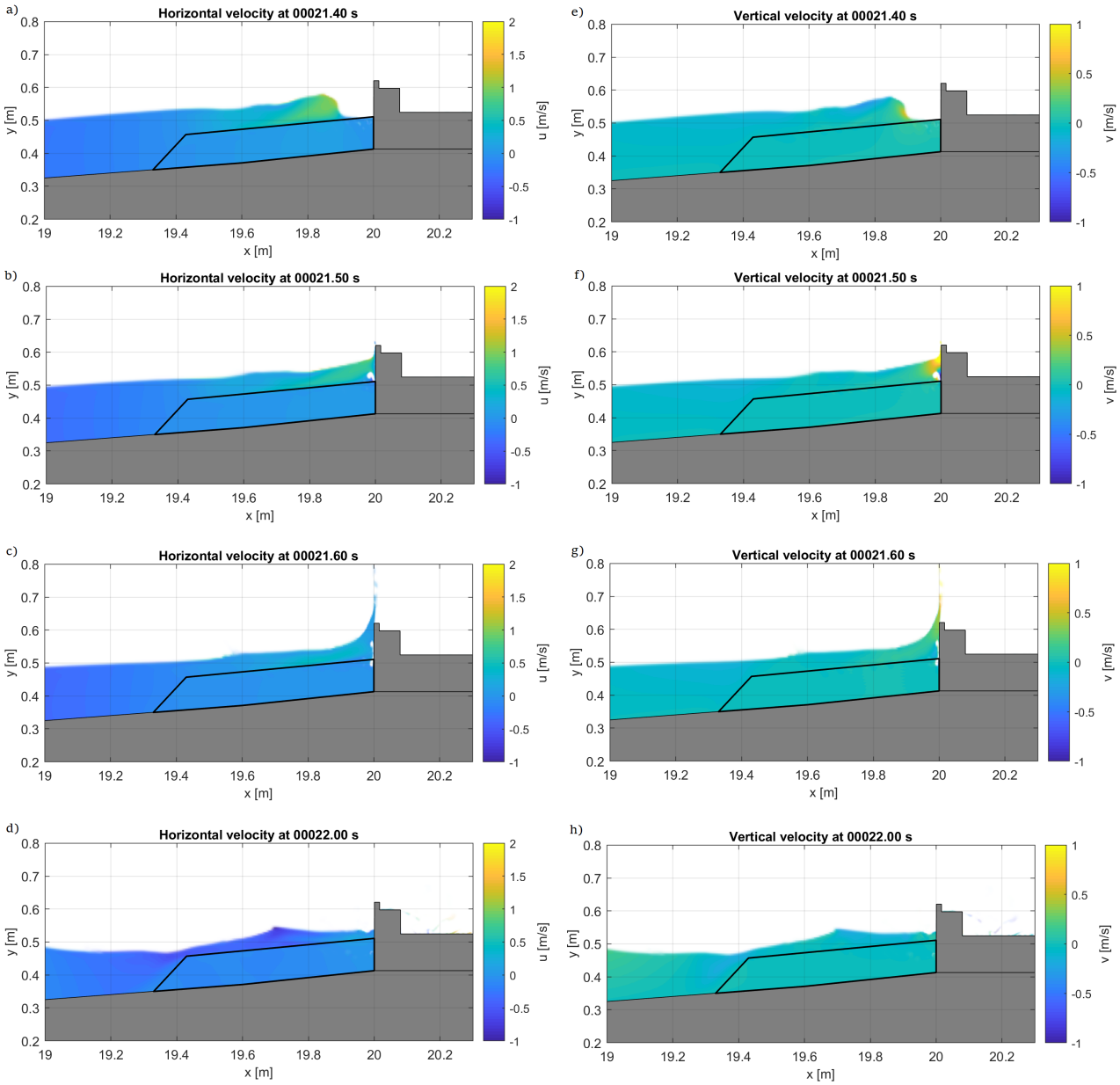

Figure D.8: Visualization of velocities for the impact event on the crown wall recorded between 21.2 s and 22.4 s

Left panel shows the horizontal velocities and the right panel, the vertical velocities. The impact event is represented by the wave approaching the wall (a) and e)), the wave impacting the wall (b) and f)), the run-up stage of the wave (c) and g)) and the run down stage of the wave (d) and h))

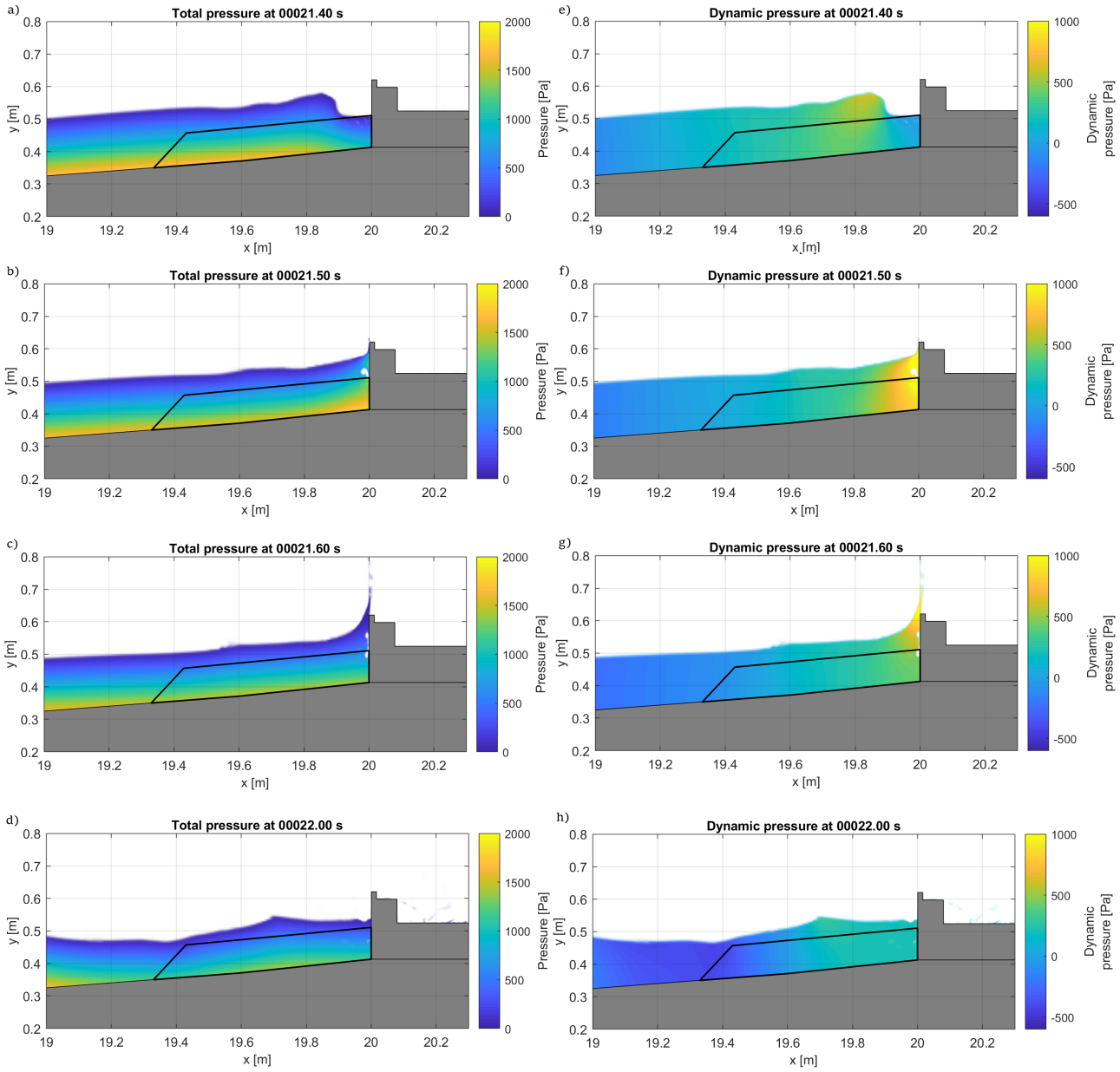

Figure D.9: Visualization of pressures for the impact event on the crown wall recorded between 21.2 s and 22.4 s

Left panel shows the horizontal velocities and the right panel, the vertical velocities. The impact event is represented by the wave approaching the wall (a) and e)), the wave impacting the wall (b) and f)), the run-up stage of the wave (c) and g)) and the run down stage of the wave (d) and h))

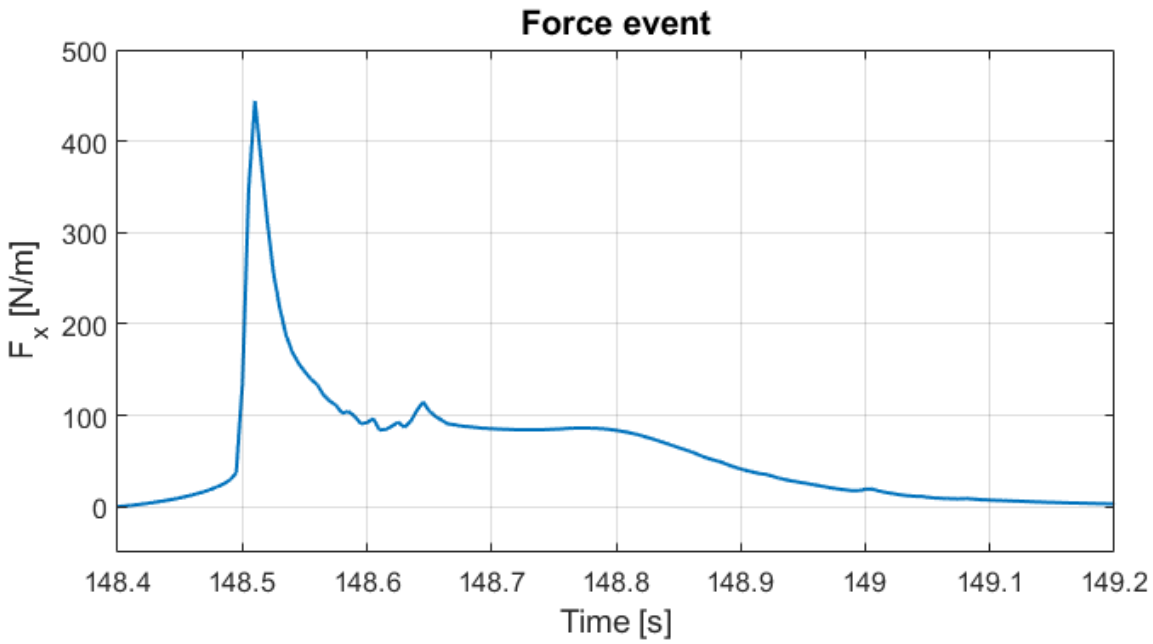

Figure D.10: Force event recorded between 148.4-149.2 s for the Tetrapods layout under extreme conditions

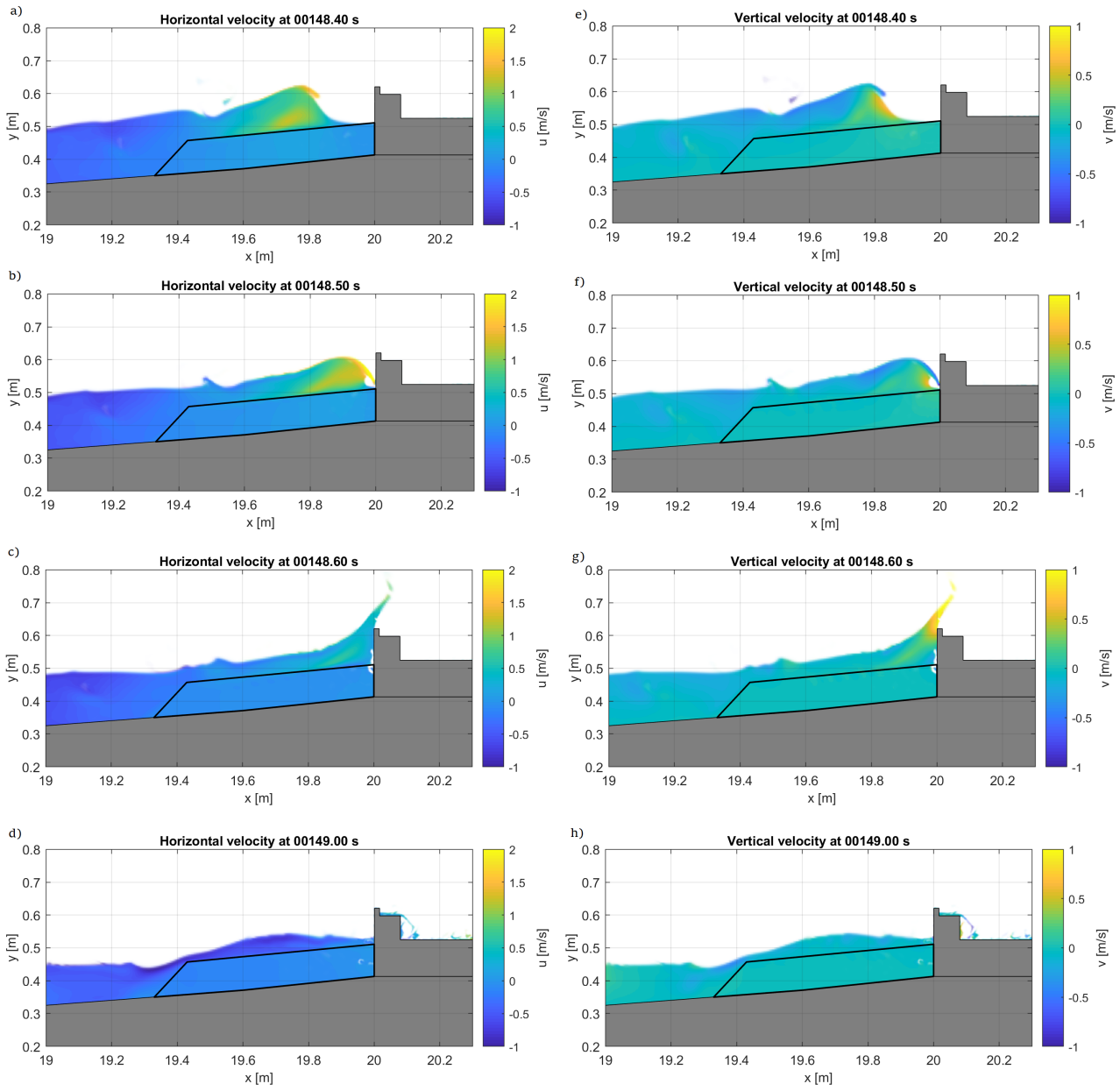

Figure D.11: Visualization of velocities for the impact event on the crown wall recorded between 148.4 s and 149.2 s

Left panel shows the horizontal velocities and the right panel, the vertical velocities. The impact event is represented by the wave approaching the wall (a) and e)), the wave close to the wall (b) and f)), the wave impacting the wall (c) and g)) and the run down stage of the wave (d) and h))

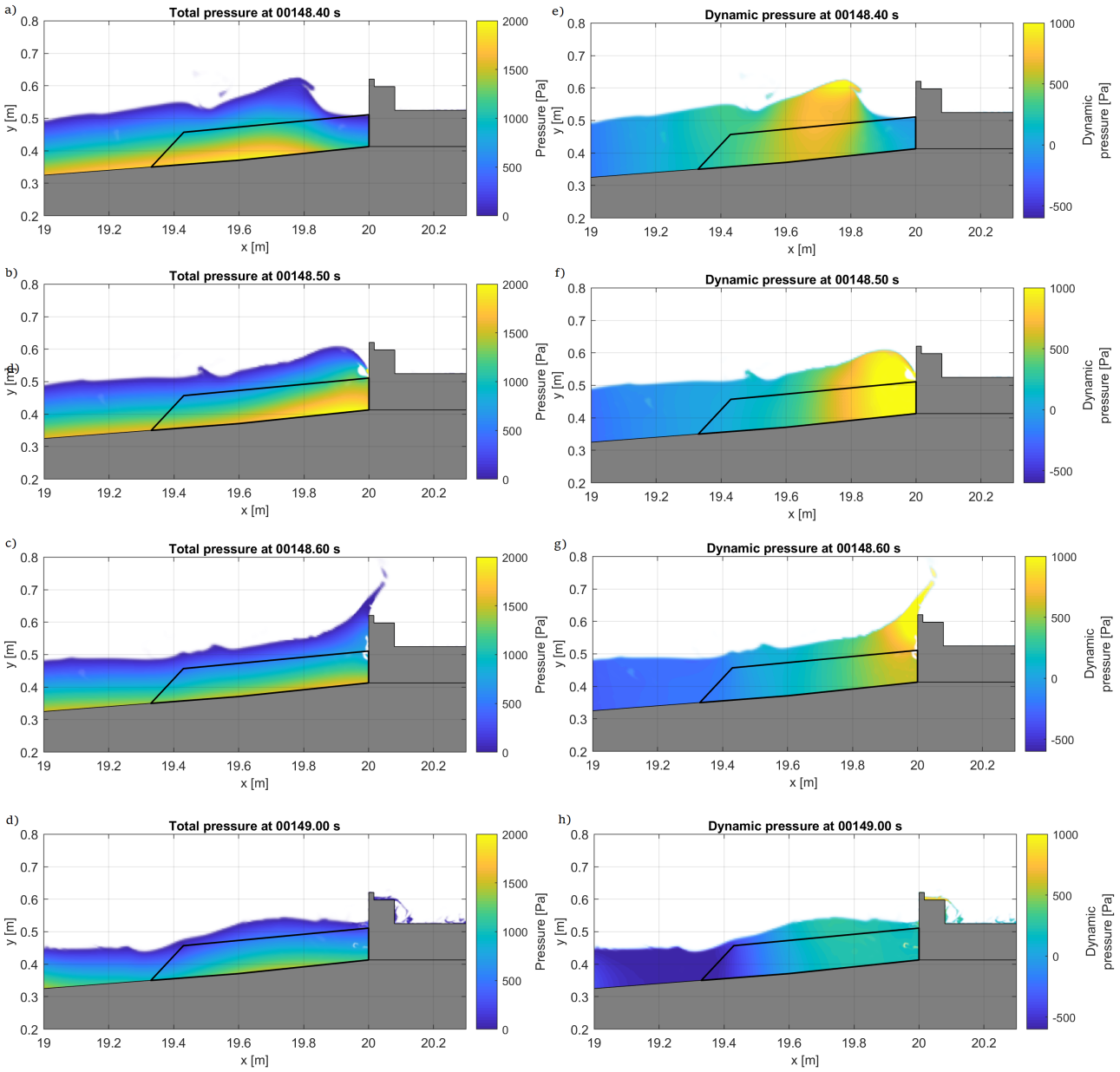

Figure D.12: Visualization of pressures for the impact event on the crown wall recorded between 148.4 s and 149.2 s

Left panel shows the total pressure and the right panel, the dynamic pressure (total pressure minus the hydrostatic pressure). The impact event is represented by the wave approaching the wall (a) and e)), the wave close to the wall (b) and f)), the wave impacting the wall (c) and g)) and the run down stage of the wave (d) and h))